Entanglement in Non-inertial Frames

by

David Cecil Murphy Ostapchuk

A thesis
presented to the University of Waterloo
in fulfillment of the
thesis requirement for the degree of
Master of Science
in
Physics

Waterloo, Ontario, Canada, 2008

I hereby declare that I am the sole author of this thesis. This is a true copy of the thesis, including any required final revisions, as accepted by my examiners.

David Cecil Murphy Ostapchuk

I understand that my thesis may be made electronically available to the public.

David Cecil Murphy Ostapchuk

Abstract

This thesis considers entanglement, an important resource for quantum information processing tasks, while taking into account the theory of relativity. Not only is this a more complete description of quantum information, but it is necessary to fully understand quantum information processing tasks done by systems in arbitrary motion.

It is shown that accelerated measurements on the vacuum of a free Dirac spinor field results in an entangled state for an inertial observer. The physical mechanism at work is the Davies-Unruh effect. The entanglement produced increases as a function of the acceleration, reaching maximal entanglement in the asymptotic limit of infinite acceleration.

The dynamics of entanglement between two Unruh-DeWitt detectors, one stationary and the other undergoing non-uniform acceleration, was studied numerically. In the ultraweak coupling limit, the entanglement decreases as a function of time for the parameters considered and decreases faster than if the moving detector had had a uniform acceleration.

Acknowledgments

First and foremost, I would like to thank Rob Mann. As my supervisor, he not only guided me through my degree, but provided me with much needed support. He has always had time to answer my questions and talk through ideas. For these reasons, and many more, I want to offer him my most sincere appreciation.

I would also like to thank Bei-Lok Hu and Shih-Yuin Lin. Bei-Lok inspired me with his encouragement and words of wisdom and Shih-Yuin's technical expertise, as well as his patience answering my many questions, was invaluable. Together, they provided many stimulating conversations ranging from beer to deep issues about entanglement. It was their guidance that enabled the research in Chapter 6.

I am indebted to Roger Melko for his generous help on the computational aspects of this thesis. I not only learned a lot from him, but had fun doing so as well. It was a pleasure to have had the opportunity to work with him.

I would like to thank my committee members Frank Wilhelm-Mauch and Achim Kempf. The time Frank spent helping me with his course on electromagnetic theory and his guidance and interest in my research was very much appreciated. I am grateful for the time Achim made to answer my questions about the Davies-Unruh effect.

This work was made possible by the facilities of the Shared Hierarchical Academic Research Computing Network (SHARCNET) as well as financial support from the National Science and Engineering Research Council of Canada and the University of Waterloo.

I would like to thank Cozmin Ududec for Fridays at the Grad House, always letting me steal his books, and for being a good friend; my parents for their support; and everyone else whose company I've enjoyed over the past two years.

Finally, I would like to thank Gina Passante. Without her love and support, this thesis would not have been possible.

This the dedicated to my parents and Gina Passante
for always believing in me

Contents

List of Figures

Notation and Conventions

The units used are such that $\hbar = c = 1$

Metric signature: $-+++$

The Minkowski metric is denoted: $\eta_{\mu\nu} = \text{diag}(-1, 1, 1, 1)$

An arbitrary metric is denoted: $g_{\mu\nu}$

Three vector: $\boldsymbol{x}$

Four vector: x

Operator: $\hat{O}$

Greek indices run from 0 to 3

Latin indices run from 1 to 3 (spatial components)

Repeated indices denote summation unless otherwise noted (Einstein summation convention)

Comma denotes partial differentiation: $\partial_\mu x_\nu = x_{\nu,\mu}$

The symmetric part of a tensor is denoted: $T_{(\mu\nu)}$

Fourier transform convention:

$$f(\boldsymbol{k}) = \mathcal{F}[f(\boldsymbol{x})] = \frac{1}{(2\pi)^{3/2}} \int d^3x\, e^{-i\boldsymbol{k}\cdot\boldsymbol{x}} f(\boldsymbol{x})$$
$$f(\boldsymbol{x}) = \mathcal{F}^{-1}[f(\boldsymbol{k})] = \frac{1}{(2\pi)^{3/2}} \int d^3k\, e^{i\boldsymbol{k}\cdot\boldsymbol{x}} f(\boldsymbol{k})$$

Chapter 1

Introduction

The rapidly developing field of quantum information theory exploits the idea that information is physical [1]. While this idea is simple, it has profound consequences. Research in the past several decades has shown that performing information processing using quantum mechanical systems can lead to novel and powerful new computational techniques. Such *quantum computers* are in some cases significantly more powerful than their classical counterparts. In particular, by an algorithm due to Shor, quantum computers can find the prime factorization of an integer exponentially faster than the best known classical algorithms [2]. This has important consequences for the security of certain widely used cryptosystems [3]. Searching unstructured databases is also more efficient on a quantum computer, achieving a quadratic speedup using Grover's algorithm [4]. These algorithms, in addition to many others [5], make the prospect of building a quantum computer very desirable from a practical point of view.

However, all of these results have been within the framework of non-relativistic quantum mechanics. If the notion that information is physical is to be taken seriously, it must be described in the same way that nature is. An indispensable component of any complete theoretical model is the theory of relativity and therefore, understanding information within this context is important from a fundamental point of view. Moreover, it is necessary to fully understand information processing tasks performed by systems in arbitrary motion.

An important resource for quantum communication and computation is entanglement. Entanglement is a property of multipartite quantum systems, each of which could be in a separate frame of reference. It was recently found

that in non-inertial frames, entanglement is a relative quantity [6, 7, 8, 9]. This thesis extends previous work by considering non-uniform accelerations and the generation of entanglement as a result of particle detection by a uniformly accelerating observer.

This thesis is organized as follows. In Chapter 2, several concepts from quantum field theory in curved spacetime are reviewed. While introduced in the context of an arbitrary curved spacetime, these techniques are also required when considering non-inertial frames in flat spacetime, as is done in this thesis. Chapter 3 introduces entanglement in more detail, describing the two methods of quantifying entanglement that are employed in this thesis. The findings of previous studies of relativistic quantum information are summarized in Chapter 4.

Chapter 5 considers entanglement and the Davies-Unruh effect [10, 11], which states that an accelerating observer would perceive a thermal bath in the state that an inertial observer would describe as the vacuum. In particular, it is shown that if the accelerating observer detects one of these particles, the resulting state is entangled in the inertial frame of reference. This effect was known for scalar fields [12] and is generalized to spinor fields here.

Chapter 6 studies the dynamics of entanglement between two model particle detectors called Unruh-DeWitt detectors. One detector is taken to be stationary while the other starts inertial and smoothly transitions to a uniform acceleration. This model was studied in [13] where the non-inertial detector had a uniform acceleration. For the parameters considered, it was found numerically that the entanglement between the detectors decreased faster for the case of non-uniform acceleration than for uniform acceleration. In the uniform acceleration case, a set of parameters is also found where the entanglement between the detectors increases as a function of time. Finally, conclusions and prospects for future work are discussed in Chapter 7.

Chapter 2

Quantum Field Theory

In this chapter, quantum field theory in curved spacetime is introduced. Particular emphasis is placed on the particle interpretation of quantum fields and the additional considerations that curved spacetime bring in this regard. An example is the Davies-Unruh effect, which is used in Chapter 5.

Two types of fields are considered: the Klein-Gordon field, which is used in Chapter 6, and the Dirac field, which is used in Chapter 5. The main reference for this chapter is [14].

2.1 The Klein-Gordon Field

In classical field theory, the Klein-Gordon field $\Phi(x)$ is a (real valued) scalar field governed by the Lagrange density

$$\mathcal{L}_{\mathrm{KG}}(x) = -\frac{1}{2}\sqrt{-g(x)}\left[\nabla_\mu\Phi(x)\nabla^\mu\Phi(x) + m^2\Phi^2(x)\right].$$

The parameter m is interpreted as a mass, as will be seen in Section 2.1.2. This Lagrangian is said to be minimally coupled to the gravitational action because it only couples through the metric. More generally, there could be other couplings to gravity such as $R\Phi^2(x)$ where R is the Ricci scalar. These additional couplings are beyond the scope of this thesis (where only flat spacetimes are considered) and the interested reader is directed to [14].

The action

$$S_{\mathrm{KG}} = \int d^4x\, \mathcal{L}_{\mathrm{KG}}(x) = -\frac{1}{2}\int \sqrt{-g(x)}d^4x\, \left[\nabla_\mu\Phi(x)\nabla^\mu\Phi(x) + m^2\Phi^2(x)\right]$$

gives rise to the equation of motion (free Klein-Gordon equation)

$$\left(\Box^2 - m^2\right)\Phi(x) = 0, \tag{2.1}$$

where $\Box^2 = \nabla_\mu \nabla^\mu$ is the d'Alembertian operator. The Klein-Gordon inner product, defined on the solution space of the Klein-Gordon equation, is

$$\big(\phi_1(x), \phi_2(x)\big) = -i \int d^3\boldsymbol{x} \left[\phi_1(x)\big(n^\mu \partial_\mu \phi_2^*(x)\big) - \big(n^\mu \partial_\mu \phi_1(x)\big)\phi_2^*(x)\right],$$

where the integration is over a spacelike hypersurface with unit normal n^μ. By virtue of Gauss's theorem and the Klein-Gordon equation, this quantity is conserved and independent of the hypersurface chosen.

The energy-momentum tensor can be obtained in the usual way of varying the action with respect to the metric, giving

$$T_{\mu\nu} = \nabla_\mu \Phi(x) \nabla_\nu \Phi(x) - g_{\mu\nu} \frac{1}{2} \left[\nabla^\alpha \Phi(x) \nabla_\alpha \Phi(x) + m^2 \big(\Phi(x)\big)^2\right].$$

The conjugate momentum to the field is given by

$$\Pi(x) = \frac{\partial \mathcal{L}_{\mathrm{KG}}}{\partial\big(n^\mu \Phi_{,\mu}(x)\big)} = \sqrt{-g(x)}\, n^\mu \nabla_\mu \Phi(x), \tag{2.2}$$

where n^μ is a timelike unit vector. The transition to the quantum theory makes use of the Hamiltonian formalism which treats time separately from space. The coordinates used for the remainder of the section will be such that $n^\mu = (1, 0, 0, 0)$ and the timelike coordinate will be denoted by t. In these coordinates, the Hamiltonian is

$$\begin{aligned} H_{\mathrm{KG}} &= \int d^3x \, \sqrt{-g(x)} T_{00} \\ &= \int d^3x \, \sqrt{-g(x)} \Big\{ \nabla_0 \Phi(x) \nabla_0 \Phi(x) \\ &\quad - g_{00} \frac{1}{2} \left[\nabla^\alpha \Phi(x) \nabla_\alpha \Phi(x) + m^2 \big(\Phi(x)\big)^2\right] \Big\}. \end{aligned}$$

2.1.1 Quantum Theory in the Heisenberg Picture

The quantum field theory is constructed by promoting the dynamical variables $\Phi(x)$ and $\Pi(x)$ to be Hermitian operators on a Hilbert space and enforcing the equal time commutation relations

$$\big[\hat{\Phi}(t, \boldsymbol{x}), \hat{\Pi}(t, \boldsymbol{x}')\big] = i\hbar \delta^3(\boldsymbol{x} - \boldsymbol{x}'), \tag{2.3}$$

$$\big[\hat{\Phi}(t, \boldsymbol{x}), \hat{\Phi}(t, \boldsymbol{x}')\big] = \big[\hat{\Pi}(t, \boldsymbol{x}), \hat{\Pi}(t, \boldsymbol{x}')\big] = 0. \tag{2.4}$$

The Hilbert space these operators act on is the space of *quantum states* of the field.

Since the Hamiltonian is a function of $\hat{\Phi}(x)$ and $\hat{\Pi}(x)$, it too becomes an operator. The Hamiltonian is related to the dynamics of an operator $\hat{O}$ through the Heisenberg equation of motion

$$i\hbar\frac{\partial}{\partial_t}\hat{O} = [\hat{O}, \hat{H}].$$

In particular,

$$\frac{\partial}{\partial_t}\hat{\Phi}(x) = \frac{1}{\sqrt{-g(x)}}\hat{\Pi}(x), \tag{2.5}$$

$$\frac{\partial}{\partial_t}\hat{\Pi}(x) = \nabla_i\nabla^i\hat{\Phi}(x) - m^2\hat{\Phi}(x), \tag{2.6}$$

which are the operator valued versions of Equations (2.1) and (2.2). To solve the quantum field theory, $\hat{\Phi}(x)$ must be obtained such that it is Hermitian, satisfies the canonical commutation relations, and solves the operator valued Klein-Gordon equation. This can be simplified by expanding the field as

$$\hat{\Phi}(x) = \int d^3\boldsymbol{k}\left[u_{\boldsymbol{k}}(x)\hat{a}_{\boldsymbol{k}} + u^*_{\boldsymbol{k}}(x)\hat{a}^\dagger_{\boldsymbol{k}}\right].$$

Such an expansion is called a *mode expansion*. The functions $u_{\boldsymbol{k}}(x)$ are called *mode functions* and the operators $\hat{a}_{\boldsymbol{k}}$ are called *mode operators*. The mode operators are further divided into the *annihilation operators* $\hat{a}_{\boldsymbol{k}}$ and the *creation operators* $\hat{a}^\dagger_{\boldsymbol{k}}$. This expansion satisfies Hermiticity by construction. Taking the mode operators to be constant, Equations (2.5) and (2.6) imply that the mode functions must satisfy Equation (2.1). Finally, if the set of mode functions is complete and normalized to

$$\begin{aligned}\big(u_{\boldsymbol{k}}(x), u_{\boldsymbol{k}'}(x)\big) = -\big(u_{\boldsymbol{k}}(x)^*, u_{\boldsymbol{k}'}(x)^*\big) &= \delta^3(\boldsymbol{k}-\boldsymbol{k}'),\\ \big(u_{\boldsymbol{k}}(x), u_{\boldsymbol{k}'}(x)^*\big) &= 0,\end{aligned}$$

then the canonical commutation relations (2.3) are satisfied if the mode operators satisfy

$$[\hat{a}_{\boldsymbol{k}}, \hat{a}^\dagger_{\boldsymbol{k}'}] = \delta^3(\boldsymbol{k}-\boldsymbol{k}'). \tag{2.7}$$

The mode expansion reduces the problem of solving the quantum field theory to finding a complete set of solutions to the complex number valued Klein-Gordon equation.

2.1.2 Particle Interpretation of the Field

A convenient basis for the Hilbert space can be constructed from the mode operators. This basis is called the *Fock basis* and its elements are called *Fock states*. First, there is a vector $|0\rangle$ such that

$$\hat{a}_{\boldsymbol{k}} |0\rangle = 0$$

for all $\boldsymbol{k}$. This vector is called the *vacuum state* of the mode expansion. From this state, the rest of the basis is constructed by successive applications of the creation operators

$$|n_{\boldsymbol{k}}\rangle = \frac{1}{\sqrt{n_{\boldsymbol{k}}!}} (\hat{a}^\dagger_{\boldsymbol{k}})^{n_k} |0\rangle ,$$

where the prefactor is required for normalization. A general Fock state takes the form

$$|n_{\boldsymbol{k}_1}, n_{\boldsymbol{k}_2}, \dots \rangle = \frac{1}{\sqrt{n_{\boldsymbol{k}_1}! n_{\boldsymbol{k}_2}! \cdots}} (\hat{a}^\dagger_{\boldsymbol{k}_1})^{n_{k_1}} (\hat{a}^\dagger_{\boldsymbol{k}_2})^{n_{k_2}} \cdots |0\rangle .$$

The action of the mode operators on a Fock state is

$$\begin{aligned} \hat{a}^\dagger_{\boldsymbol{k}} |n_{\boldsymbol{k}}\rangle &= \sqrt{n_{\boldsymbol{k}} + 1}\, |(n+1)_{\boldsymbol{k}}\rangle , \\ \hat{a}_{\boldsymbol{k}} |n_{\boldsymbol{k}}\rangle &= \sqrt{n_{\boldsymbol{k}}}\, |(n-1)_{\boldsymbol{k}}\rangle . \end{aligned}$$

From the above relations, it can be seen that the Fock states are eigenstates of the Hermitian operators $\hat{n}_{\boldsymbol{k}} = \hat{a}^\dagger_{\boldsymbol{k}} \hat{a}_{\boldsymbol{k}}$ with eigenvalues $n_{\boldsymbol{k}}$. These operators are called the *number operators* and the positive integers $n_{\boldsymbol{k}}$ is called the *occupation numbers* of mode $\boldsymbol{k}$. This justifies classifying the mode operators as either creation or annihilation operators as they create or destroy quanta, respectively.

In spacetimes that possess time translation symmetry, the Fock states have a nice physical interpretation. In this case there exists a timelike solution to Killing's equation[1]

$$2\nabla_{(\mu} K_{\nu)} = 0.$$

The vector K_μ is called a *Killing vector* and can be used to define a preferred set of modes. These modes are the eigenfunctions of K_μ

$$\begin{aligned} K^\mu \partial_\mu u_{\boldsymbol{k}}(x) &= -i\omega_{\boldsymbol{k}} u_{\boldsymbol{k}}(x), \\ K^\mu \partial_\mu u^*_{\boldsymbol{k}}(x) &= i\omega_{\boldsymbol{k}} u^*_{\boldsymbol{k}}(x), \end{aligned}$$

[1] Or, more naturally, $\mathcal{L}_K g_{\mu\nu} = 0$ where $\mathcal{L}_K$ is the Lie derivative with respect to K_μ.

where $\omega_{\boldsymbol{k}} > 0$. The modes whose eigenvalues are $-i\omega_{\boldsymbol{k}}$ are called *positive frequency* modes whereas the ones whose eigenvalues are $i\omega_{\boldsymbol{k}}$ are called *negative frequency* modes. In the coordinate system where $K^\mu \partial_\mu = \partial_t$, the Klein-Gordon equation implies that the $u_{\boldsymbol{k}}(x)$ are eigenfunctions of ∇_i with eigenvalue $i\boldsymbol{k}$, the magnitude of which is

$$|\boldsymbol{k}|^2 = \omega_{\boldsymbol{k}}^2 - m^2.$$

In this mode expansion the momentum operator takes the form

$$\hat{\boldsymbol{P}} = \int d^3x\, \hat{T}_{0i} = \int d^3\boldsymbol{k}\, \boldsymbol{k} \hat{a}_{\boldsymbol{k}}^\dagger \hat{a}_{\boldsymbol{k}},$$

which is a sum of the number operators. As a result, its eigenstates are the Fock states. Their momentum can be read off from the eigenvalue equation

$$\hat{\boldsymbol{P}} \left| n_{\boldsymbol{k}_1}, n_{\boldsymbol{k}_2}, \dots \right\rangle = \left[\sum_i n_{\boldsymbol{k}_i} \boldsymbol{k}_i \right] \left| n_{\boldsymbol{k}_1}, n_{\boldsymbol{k}_2}, \dots \right\rangle .$$

In particular, the vacuum state has no momentum. Now consider the Hamiltonian, which in these modes is expressed as

$$\begin{aligned} \hat{H}_{\mathrm{KG}} &= \int d^3x\, \hat{T}_{00} = \int d^3\boldsymbol{k}\, \frac{\omega_{\boldsymbol{k}}}{2} \left[\hat{a}_{\boldsymbol{k}} \hat{a}_{\boldsymbol{k}}^\dagger + \hat{a}_{\boldsymbol{k}}^\dagger \hat{a}_{\boldsymbol{k}} \right] \\ &= \int d^3\boldsymbol{k}\, \omega_{\boldsymbol{k}} \left[\hat{a}_{\boldsymbol{k}}^\dagger \hat{a}_{\boldsymbol{k}} + \frac{1}{2} [a_{\boldsymbol{k}}, a_{\boldsymbol{k}}^\dagger] \right] . \end{aligned}$$

By Equation (2.7), the second term is divergent. Fortunately, while infinite, this term is constant and since only energy differences can be measured, the energy scale can be shifted so this term is eliminated. This is achieved by subtracting off the divergent term so that the Hamiltonian becomes

$$\hat{H}_{\mathrm{KG}} = \int d^3\boldsymbol{k}\, \omega_{\boldsymbol{k}} \hat{a}_{\boldsymbol{k}}^\dagger \hat{a}_{\boldsymbol{k}}.$$

Again, the presence of the number operator indicates that the Fock states are also eigenstates of the Hamiltonian. Their energy is given by the eigenvalue equation

$$\hat{H}_{\mathrm{KG}} \left| n_{\boldsymbol{k}_1}, n_{\boldsymbol{k}_2}, \dots \right\rangle = \left[\sum_i n_{\boldsymbol{k}_i} \omega_{\boldsymbol{k}_i} \right] \left| n_{\boldsymbol{k}_1}, n_{\boldsymbol{k}_2}, \dots \right\rangle .$$

The ground state is the vacuum, having zero energy.

Notice that the energy and momentum of the Fock states satisfy

$$\omega_{\boldsymbol{k}}^2 = |\boldsymbol{k}|^2 + m^2,$$

which, if m is interpreted as a mass, is the usual relation from classical relativity. With this as motivation, the Fock states are interpreted as describing *particles*. The Fock state $|n_{\boldsymbol{k}}\rangle$ describes a state of $n_{\boldsymbol{k}}$ particles each with energy $\omega_{\boldsymbol{k}}$, momentum $\boldsymbol{k}$, and mass m. However, unlike classical particles, which are localized objects, these particles, being states of definite momentum, are completely de-localized. Each of these particles is identical and since the mode operators commute,

$$|n_{\boldsymbol{k}_1}, n_{\boldsymbol{k}_2}\rangle = |n_{\boldsymbol{k}_2}, n_{\boldsymbol{k}_1}\rangle \,.$$

That is, they obey Bose-Einstein statistics. The Klein-Gordon field describes particles of spin-0.

It is important to note that particles, being an interpretation of field excitations, play a secondary role here. The fundamental objects in quantum field theory are the fields. For example, although the vacuum is interpreted as the state of "no particles" it does not mean that nothing is there. The field is there and in general, a measurement of the field amplitude would not be zero due to quantum fluctuations. This is especially important because the construction of the particle interpretation relies on the spacetime having a time symmetry. In general spacetimes, this is not the case and there will be no preferred set of modes [15].

To see the consequences of this, consider two complete sets of modes $\{u_{\boldsymbol{k}}, u^*_{\boldsymbol{k}}\}$ and $\{v_{\boldsymbol{k}}, v^*_{\boldsymbol{k}}\}$ with associated mode operators $\hat{a}_{\boldsymbol{k}}$ and $\hat{b}_{\boldsymbol{k}}$. By completeness and orthonormality, the two sets of mode functions are related by

$$v_{\boldsymbol{k}}(x) = \int d^3\boldsymbol{k}' \, \left[\alpha_{\boldsymbol{k}\boldsymbol{k}'} u_{\boldsymbol{k}'}(x) + \beta_{\boldsymbol{k}\boldsymbol{k}'} u^*_{\boldsymbol{k}'}(x)\right],$$

where $\alpha_{\boldsymbol{k}\boldsymbol{k}'} = \big(v_{\boldsymbol{k}}(x), u_{\boldsymbol{k}'}(x)\big)$ and $\beta_{\boldsymbol{k}\boldsymbol{k}'} = -\big(v_{\boldsymbol{k}}(x), u^*_{\boldsymbol{k}'}(x)\big)$. This is called a *Bogoliubov transformation* [14] and the complex numbers $\alpha_{\boldsymbol{k}\boldsymbol{k}'}$ and $\beta_{\boldsymbol{k}\boldsymbol{k}'}$ are called *Bogoliubov coefficients*. The inverse transformation is given by

$$u_{\boldsymbol{k}} = \int d^3\boldsymbol{k}' \, \left[\alpha^*_{\boldsymbol{k}'\boldsymbol{k}} v_{\boldsymbol{k}'}(x) - \beta_{\boldsymbol{k}'\boldsymbol{k}} v^*_{\boldsymbol{k}'}(x)\right].$$

These induce the following transformations on the mode operators

$$\hat{a}_{\boldsymbol{k}} = \int d^3\boldsymbol{k}' \, \left[\alpha_{\boldsymbol{k}'\boldsymbol{k}} \hat{b}_{\boldsymbol{k}'} + \beta^*_{\boldsymbol{k}'\boldsymbol{k}} \hat{b}^\dagger_{\boldsymbol{k}'}\right], \tag{2.8}$$

$$\hat{b}_{\boldsymbol{k}} = \int d^3\boldsymbol{k}' \, \left[\alpha^*_{\boldsymbol{k}\boldsymbol{k}'} \hat{a}_{\boldsymbol{k}'} - \beta^*_{\boldsymbol{k}\boldsymbol{k}'} \hat{a}^\dagger_{\boldsymbol{k}'}\right]. \tag{2.9}$$

As a consequence of the commutation relations of the mode operators, the Bogoliubov coefficients must satisfy

$$\begin{pmatrix} \alpha & \beta \\ \beta^* & \alpha^* \end{pmatrix} \begin{pmatrix} \alpha^\dagger & -\beta^{\mathrm{T}} \\ -\beta^\dagger & \alpha^{\mathrm{T}} \end{pmatrix} = \begin{pmatrix} 1 & 0 \\ 0 & 1 \end{pmatrix},$$

where these are to be interpreted as block matrices.

From Equations (2.8) and (2.9), it can be seen that the Fock bases associated with these two mode expansions are different. This leads to two different particle interpretations of the field. In particular, according to the particle interpretation based on the $u_{\boldsymbol{k}}(x)$ modes, particles are present in the vacuum of the $v_{\boldsymbol{k}}(x)$ mode expansion $|0\rangle_v$. The average number of particles present is given by

$${}_v\langle 0|\, a^\dagger_{\boldsymbol{k}} a_{\boldsymbol{k}}\, |0\rangle_v = \int d^3\boldsymbol{k}'\, |\beta_{\boldsymbol{k}\boldsymbol{k}'}|^2.$$

In this sense, there is no absolute notion of particles in quantum field theory. Like simultaneity, a particle interpretation is associated with an observer.

Even in spacetimes that do possess time translation symmetry, the preferred choice of mode functions may still not be uniquely determined. In different regions of the spacetime, there could be different timelike Killing vectors. Observers moving along the orbits of these two different Killing vectors would have different particle interpretations of the field. The simplest example of this is the case of uniformly accelerating observers in Minkowski space. Those observers would detect a thermal bath with a temperature proportional to their acceleration in the state that inertial observers would describe as the vacuum [10, 11]. This is known as the *Davies-Unruh effect* [16] and is discussed in Chapter 5.

If one wants to talk about particles in a general spacetime, an operational notion of particle is needed. This is achieved by considering a quantum system that acts as a *particle detector*. The detector interacts with the field and if it becomes excited, it is said to have detected a particle. In this way, a particle is what a particle detector detects. In general, there is no direct relationship between the number operators of a mode expansion and the number of particles a detector would detect. Only when the spacetime admits a timelike Killing vector do they coincide. The study of particle detectors in the context of quantum field theory in curved spacetime was first undertaken by Unruh [11] and later expanded by DeWitt [17]. The model they considered is called an *Unruh-DeWitt detector* and is introduced in Appendix C. The dynamics of

entanglement between two Unruh-DeWitt detectors interacting with a massless Klein-Gordon field is studied in Chapter 6.

2.2 The Dirac Field

The Dirac field $\Psi(x)$ is a four component spinor valued field described by the Lagrange density (with minimal coupling to the gravitational action)

$$\mathcal{L}_{\mathrm{D}} = \sqrt{-g(x)}\left\{\frac{i}{2}\left[\bar{\Psi}(x)\gamma^{\mu}\big(\nabla_{\mu}\Psi(x)\big) - \big(\nabla^{\mu}\bar{\Psi}(x)\big)\gamma^{\mu}\Psi(x)\right] - m\bar{\Psi}(x)\Psi(x)\right\},$$

where m is interpreted as a mass and γ_{μ} are the *Dirac matrices*. These are 4×4 matrices that satisfy

$$\{\gamma_{\mu}, \gamma_{\nu}\} = 2g_{\mu\nu}.$$

Here, the covariant derivative ∇_{μ} is defined as

$$\nabla_{\mu} = \partial_{\mu} = \Gamma_{\mu},$$

where Γ_{μ} is the *spin connection* given by

$$\Gamma_{\mu} = \frac{1}{4}\gamma_{\nu}(\partial_{\mu}\gamma^{\nu} + \Gamma^{\nu}_{\rho\mu}\gamma^{\rho})$$

and $\Gamma^{\nu}_{\rho\mu}$ are the usual Christoffel symbols. An overbar denotes the Dirac adjoint, defined as

$$\bar{\Psi}(x) = \Psi^{\dagger}(x)\tilde{\gamma}^{0}.$$

Here, $\tilde{\gamma}^{0}$ is the zeroth component of $\tilde{\gamma}^{\mu}$, which are 4×4 matrices defined by

$$\{\tilde{\gamma}_{\mu}, \tilde{\gamma}_{\nu}\} = 2\eta_{\mu\nu}.$$

The $\tilde{\gamma}^{\mu}$ are related to γ^{μ} by $\gamma^{\mu} = V_{\alpha}{}^{\mu}\tilde{\gamma}^{\alpha}$ where $V_{\alpha}{}^{\mu}$ is a vierbein field. The vierbein formalism is natural when describing higher spins in curved spacetime. However, it is beyond the scope of this thesis and the interested reader is directed to [14] for more information.

The equation of motion (free Dirac equation) is

$$\left[i\gamma^{\mu}\nabla_{\mu} - m\right]\Psi(x) = 0,$$

which follows from the action

$$S_{\mathrm{D}} = \int d^{4}x\mathcal{L}_{\mathrm{D}}(x).$$

The Dirac inner product, defined on the solution space of the Dirac equation, is

$$\big(\psi_1(x), \psi_2(x)\big) = \int d^4x\, n_\mu \bar{\psi}_1(x)\gamma^\mu\psi_2(x),$$

where the integration is over a spacelike hypersurface with unit normal n^μ. Varying the action with respect to the metric results in the energy-momentum tensor

$$T_{\mu\nu} = \frac{i}{2}\left[\bar{\Psi}(x)\gamma_{(\mu}\big(\nabla_{\nu)}\Psi(x)\big) - \big(\nabla_{(\mu}\bar{\Psi}(x)\big)\gamma_{\nu)}\Psi(x)\right].$$

2.2.1 Quantum Theory in the Heisenberg Picture

The Dirac field is quantized by promoting the dynamical variable $\Psi(x)$ to be a Hermitian operator on the Hilbert space of the quantum states of the field. Similar to the Klein-Gordon field, the quantum field theory is solved by expanding the field operator in a complete set modes

$$\hat{\Psi}(x) = \sum_s \int d^3\boldsymbol{k}\left[\hat{a}_{\boldsymbol{k},s}\psi^+_{\boldsymbol{k},s}(x) + \hat{b}^\dagger_{\boldsymbol{k},s}\psi^-_{\boldsymbol{k},s}(x)\right],$$

where $s \in \{\uparrow, \downarrow\}$ is an index related to the spinor nature of the field. The mode functions $\psi^\pm_{\boldsymbol{k},s}(x)$ satisfy the spinor valued Dirac equation and are normalized to

$$\begin{aligned}\big(\psi^+_{\boldsymbol{k},s}(x), \psi^+_{\boldsymbol{k}',s'}(x)\big) = -\big(\psi^-_{\boldsymbol{k},s}(x), \psi^-_{\boldsymbol{k}',s'}(x)\big) &= \delta_{ss'}\delta^3(\boldsymbol{k}-\boldsymbol{k}'),\\ \big(\psi^\pm_{\boldsymbol{k},s}(x), \psi^\mp_{\boldsymbol{k}',s'}(x)\big) &= 0.\end{aligned}$$

However, unlike the Klein-Gordon equation, the mode operators must satisfy the anticommutation relations

$$\{\hat{a}_{\boldsymbol{k},s}, \hat{a}^\dagger_{\boldsymbol{k}',s'}\} = \{\hat{b}_{\boldsymbol{k},s}, \hat{b}^\dagger_{\boldsymbol{k}',s'}\} = \delta_{ss'}\delta^3(\boldsymbol{k}-\boldsymbol{k}'),$$

with all other anticommutators vanishing. This ensures that the energy of the field has a lower bound and that causality is obeyed (see §3.5 in [18] for a discussion of this in the context of Minkowski space quantum field theory).

2.2.2 Particle Interpretation of the Field

Constructing the Fock basis of a mode expansion follows the same procedure as for the Klein-Gordon field. The vacuum state is defined by

$$\hat{a}_{\boldsymbol{k},s}\,|0\rangle = \hat{b}_{\boldsymbol{k},s}\,|0\rangle = 0$$

for all $\boldsymbol{k}$ and s. The Dirac field has two different types of quanta. When the mode functions are divided into positive and negative frequency by a timelike Killing vector K_μ, the Fock states created by $a^\dagger_{\boldsymbol{k},s}$ can be interpreted as *particles* and the states created be $b^\dagger_{\boldsymbol{k},s}$ can be interpreted as *antiparticles*. These particles have mass m and spin-1/2. The index s labels the spin state as being up or down with respect to some axis. Since mode operators anticommute,

$$\left(a^\dagger_{\boldsymbol{k},s}\right)^2 = \left(b^\dagger_{\boldsymbol{k},s}\right)^2 = 0$$

and so there is only one excitation per mode. This is known as the *Pauli Exclusion Principle*.

Like the Klein-Gordon field, the Dirac field describes identical particles. However, due to the anticommutation relations of the modes, the Fock states are antisymmetric

$$|1_{\boldsymbol{k}_1,s_1}, 1_{\boldsymbol{k}_2,s_2}\rangle = -\,|1_{\boldsymbol{k}_2,s_2}, 1_{\boldsymbol{k}_1,s_1}\rangle$$

and so the quanta of the Dirac field obey *Fermi-Dirac statistics*.

When the spacetime does not possess a timelike Killing vector, there is no preferred set of modes. However, like the Klein-Gordon field, all possible sets of modes are related by a Bogoliubov transformation. For example, two sets of modes $\{\psi^\pm_{\boldsymbol{k},s}(x)\}$ and $\{\chi^\pm_{\boldsymbol{k},s}(x)\}$ with corresponding mode operators $\{\hat{a}_{\boldsymbol{k},s}, \hat{b}^\dagger_{\boldsymbol{k},s}\}$ and $\{\hat{c}_{\boldsymbol{k},s}, \hat{d}^\dagger_{\boldsymbol{k},s}\}$, are related by

$$\begin{aligned}
\hat{a}_{\boldsymbol{k}} &= \int d^3\boldsymbol{k}' \left[\alpha_{\boldsymbol{k}\boldsymbol{k}'}\hat{c}_{\boldsymbol{k}'} + \beta^*_{\boldsymbol{k}\boldsymbol{k}'}\hat{d}^\dagger_{\boldsymbol{k}'}\right], \\
\hat{b}_{\boldsymbol{k}} &= \int d^3\boldsymbol{k}' \left[\alpha_{\boldsymbol{k}\boldsymbol{k}'}\hat{d}_{\boldsymbol{k}'} + \beta^*_{\boldsymbol{k}\boldsymbol{k}'}\hat{c}^\dagger_{\boldsymbol{k}'}\right], \\
\hat{c}_{\boldsymbol{k}} &= \int d^3\boldsymbol{k}' \left[\alpha^*_{\boldsymbol{k}\boldsymbol{k}'}\hat{a}_{\boldsymbol{k}'} + \beta^*_{\boldsymbol{k}\boldsymbol{k}'}\hat{b}^\dagger_{\boldsymbol{k}'}\right], \\
\hat{d}_{\boldsymbol{k}} &= \int d^3\boldsymbol{k}' \left[\alpha^*_{\boldsymbol{k}\boldsymbol{k}'}\hat{b}_{\boldsymbol{k}'} + \beta^*_{\boldsymbol{k}\boldsymbol{k}'}\hat{a}^\dagger_{\boldsymbol{k}'}\right],
\end{aligned}$$

where $\alpha_{\boldsymbol{k}\boldsymbol{k}'} = \left(\psi^+_{\boldsymbol{k}}(x), \chi^+_{\boldsymbol{k}'}(x)\right)$ and $\beta_{\boldsymbol{k}\boldsymbol{k}'} = \left(\psi^+_{\boldsymbol{k}}(x), \chi^-_{\boldsymbol{k}'}(x)\right)$ and the spin degree of freedom has been suppressed for ease of notation. However, the fermionic Bogoliubov coefficients must satisfy

$$\begin{pmatrix} \alpha & \beta \\ \beta^* & \alpha^* \end{pmatrix} \begin{pmatrix} \alpha^\dagger & \beta^{\mathrm{T}} \\ \beta^\dagger & \alpha^{\mathrm{T}} \end{pmatrix} = \begin{pmatrix} 1 & 0 \\ 0 & 1 \end{pmatrix}$$

to be consistent with the anticommutation relations.

Chapter 3

Entanglement

Given two quantum systems A, whose state space is $\mathcal{H}_A$, and B, whose state space is $\mathcal{H}_B$, the composite system's state space $\mathcal{H}$ is obtained by taking the tensor product of the two individual state spaces

$$\mathcal{H} = \mathcal{H}_A \otimes \mathcal{H}_B.$$

That is, if system A is in state $|\psi_A\rangle$ and B is in state $|\psi_B\rangle$, then the state of the composite system is $|\psi\rangle = |\psi_A\rangle\,|\psi_B\rangle$ where it is understood that the two vectors are multiplied using the tensor product. Such states are called *product states*. However, not all states in $\mathcal{H}$ are of this form. States of the composite system that cannot be written as a tensor product of states in the individual Hilbert spaces are called *entangled states*. Physically, this means that there are global properties of the composite system that are well defined but the corresponding individual properties are not. It is only after one of the subsystems is measured that the properties of both subsystems become well defined. The measurement outcomes of the individual systems will be correlated in a manner consistent with the global properties.

An example of an entangled state is the spin singlet state of two spin-$1/2$ particles

$$\frac{1}{\sqrt{2}}\big(|\uparrow\downarrow\rangle - |\downarrow\uparrow\rangle\big),$$

where $|\uparrow\rangle$ means a spin up state and $|\downarrow\rangle$ means spin down. Here, the spin state of the composite system is well defined (it is zero), while each subsystem is not in a definite spin state. If the first subsystem is measured, it has equal probability of being up or down. With knowledge of the measurement result, it is then possible to predict the state of the other spin without measuring

it because the total spin is zero. The results of spin measurements on the subsystems are always anti-correlated in this case.

These correlations are one of the most interesting properties of entanglement. The ability to predict the measurement outcome is independent of the separation of the two subsystems. So, while the systems might be lightyears apart, after a measurement is made on one subsystem, that experimenter can predict the outcome of measurements on the other. However, such measurements cannot be used to send signals faster than the speed of light since the act of measuring one subsystem cannot change the probabilities of measurement outcomes on the other. It is only after there is classical communication that the correlations will be apparent. This is known as the *no-signaling theorem*. For example, suppose two experimenters, Alice and Bob, shared a spin singlet state. If Alice measured the spin of her system and determined it was spin up, then she would know immediately that a measurement of Bob's system would yield spin down. However, Bob, who is ignorant of Alice's measurement, would still attribute a 50% probability to either outcome of a spin measurement. Regardless, when Alice and Bob compare their measurement results, they would find them anti-correlated.

Entanglement is inherently quantum mechanical and cannot be reproduced in classical physics. It is also of great interest to the field of quantum information and computation because it enables certain tasks that are not possible, or at least not efficient, without quantum mechanics. Examples include quantum state teleportation, superdense coding, and various other quantum information processing tasks [3]. In light of this, entanglement is viewed as a resource, like energy or time, and as such, it is natural to quantify it. Quantifying entanglement is an active field of research with many techniques, only a few of which will be presented here.

3.1 Entanglement Entropy

The simplest type of entanglement is that of a pure bipartite system of finite dimension. This is the type of entanglement encountered in Chapter 5. In this case, when one of the subsystem's degrees of freedom are ignored (traced out) the other subsystem's state is mixed. Since the global state is pure, this mixing must have been due to the entanglement. The amount of mixing in the reduced state of subsystem a, described by the density matrix ρ_a, can be

quantified by the von Neumann entropy[1], defined as

$$S(\rho_a) = -\operatorname{Tr}(\rho_a \log_2 \rho_a).$$

Equivalently, it can be expressed in terms of the eigenvalues λ_i of ρ_a as

$$S(\rho_a) = -\sum_i \lambda_i \log_2 \lambda_i.$$

The more mixed the reduced state is, the more information was lost by neglecting the other subsystem, implying stronger correlations between them. Entanglement can then be quantified by the the von Neumann entropy of the reduced state. This is called the *entanglement entropy*.

If the state is a product state, then the reduced state is pure. In this case, the entanglement entropy is zero, as expected. States where each subsystem is maximally mixed, such as the spin singlet state, are called maximally entangled states. For these states, the entanglement entropy achieves its maximal value of $\log_2(n)$ where n is the dimension of the space.

The entanglement entropy fails to be a good measure of entanglement for mixed states. This is because there are two contributions to the entanglement entropy, one from the mixing and the other from any entanglement present. These two sources of entropy cannot be separated. Similarly, the entanglement entropy is also not appropriate to quantify entanglement in systems made up of more than two subsystems. To see why this is the case, consider a tripartite system. If the first subsystem is traced out, the remaining bipartite system could be mixed. Again, the entropy cannot be solely attributed to the entanglement.

3.2 Sigma

This section introduces the method used to quantify entanglement in Chapter 6. The entanglement encountered there is between two harmonic oscillators in a Gaussian state. Simon proved that a necessary and sufficient condition for a Gaussian state to be entangled is that the the quantity

$$\Sigma(t,\tau) = \det\left(\mathbf{V}^{\mathrm{PT}} + i\frac{\hbar}{2}\mathbf{M}\right)$$

[1]The von Neumann entropy is the quantum mechanical analogue of the Gibbs entropy from classical thermodynamics (or equivalently, the Shannon entropy from information theory).

is negative [19], where

$$\mathbf{M} = \begin{pmatrix} 0 & 1 & 0 & 0 \\ -1 & 0 & 0 & 0 \\ 0 & 0 & 0 & 1 \\ 0 & 0 & -1 & 0 \end{pmatrix},$$

and

$$\mathbf{V} = \langle \mathcal{R}_\mu, \mathcal{R}_\nu \rangle = \frac{1}{2} \langle (\mathcal{R}_\mu \mathcal{R}_\nu + \mathcal{R}_\nu \mathcal{R}_\mu) \rangle .$$

$\mathbf{V}$ is the symmetric two point correlation matrix and $\mathcal{R}_\mu = (\hat{Q}_B, \hat{P}_B, \hat{Q}_A, \hat{P}_A)$. The operators $\hat{Q}$ and $\hat{P}$ are the phase space operators of the subsystem indicated by their subscript. The partial transpose is taken by a time reversal in the phase space [19]. That is, $\mathbf{V}^{\mathrm{PT}} = \mathbf{\Lambda V \Lambda}$ where

$$\mathbf{\Lambda} = \begin{pmatrix} 1 & 0 & 0 & 0 \\ 0 & 1 & 0 & 0 \\ 0 & 0 & 1 & 0 \\ 0 & 0 & 0 & -1 \end{pmatrix}.$$

This is the continuous variable analogue of the Peres-Horodecki separability criterion [20, 21][2]

Entanglement is then quantified by the numerical value of Σ; the smaller the number, the more entangled the state is. This quantity behaves similarly to the logarithmic negativity [22, 23], which is another method that can be used to quantify entanglement. The motivation for using Σ over other methods is that it was used in [13], which studied a similar model to that studied in Chapter 6. It was used in their case because it was possible to get an analytic expression for Σ in the ultraweak coupling limit. To facilitate comparison to those results, the same method is used here.

[2]The Peres-Horodecki criterion is a necessary condition. However, it is also sufficient for Hilbert spaces of dimension 2×2 and 2×3 [21] and, in the continuous variable case, for Gaussian states [19].

Chapter 4

Previous Work

While the study of relativistic quantum information is young, there have been many interesting results [24]. Many of these focus on the relative nature of entanglement. In particular, it has been shown that entanglement can be transferred between different degrees of freedom, such as between spin and momentum, by Lorentz transformations [25, 26, 27, 28, 29]. As a result, the amount of entanglement available for quantum information processing by detectors sensitive to a single degree of freedom can change (for better or worse). Despite this, the overall entanglement of the state remains unchanged and in this sense, entanglement is an invariant quantity for inertial observers [30].

However, in non-inertial frames the situation is quite different. Alsing and Milburn found that the fidelity of teleportation between two observers in relative uniform acceleration decreases as a function of acceleration [6, 7]. From this, they concluded that entanglement is degraded in non-inertial frames due to the Davies-Unruh effect. While their analysis made use of cavities, whose boundary conditions are not compatible with those of the Davies-Unruh effect [31], their general conclusion still holds. This was shown explicitly by Fuentes-Schuller and Mann who considered two entangled modes of a free scalar field as viewed by two observers in relative uniform acceleration [8]. While the state appears maximally entangled in the inertial frame, it is less entangled from the point of view of the accelerating observer. The entanglement in that frame degrades as a function of the acceleration and in the limit of infinite acceleration, completely disappears. This is contrasted to a spinor field where even in the limit of infinite acceleration, the state is still entangled [9]. This loss of entanglement is the result of the communication horizons experienced by the accelerating observer and can be understood as a redistribution of entanglement

between the accessible and inaccessible regions of spacetime [32].

One limitation of the previous studies is that there is no dynamics. In particular, entanglement is always present for finite accelerations in both scalar and spinor fields. It is known that even when there is no relativistic motion, entanglement can experience "sudden death". That is, vacuum fluctuations can cause two quantum systems to disentangle after a finite time [33], even if they are completely isolated from each other. To study this effect in a relativistic framework, Lin, Chou, and Hu considered a model consisting of two Unruh-DeWitt detectors, one inertial and the other uniformly accelerating, interacting with a massless Klein-Gordon field. The detectors are taken to be initially in an entangled Gaussian state while the field is in the Minkowski vacuum state. They find that the interaction with the field does induce disentanglement of the detectors. They also considered the dynamics of entanglement in two different time slicings, the proper times of each detector. In the ultraweak coupling limit, the disentanglement time in Minkowski slicing is insensitive to the acceleration of the other detector to leading order. In Rindler slicing however, they find that the disentanglement time is proportional to the reciprocal of the magnitude of the acceleration. The same model is studied in Chapter 6 except that a more realistic non-inertial trajectory is considered where the detector starts inertial and smoothly transitions to a uniform acceleration.

On the other hand, non-inertial frames are one way to access the entanglement naturally present in the vacuum. Reznik provided an operational notion of vacuum entanglement by considering two Unruh-DeWitt detectors interacting with a field in its vacuum state. He found that while the detectors remained causally disconnected, they can become entangled due to their interaction with the field. Since their interaction is local, the entanglement must have been extracted from the vacuum. This is a feature of both Klein-Gordon fields [34] and Dirac fields [35] and was demonstrated not only for detectors undergoing uniform acceleration but also for inertial detectors. Taking this further, van Enk and Rudolph [36] considered what types of quantum information protocols were possible using the vacuum as a resource. They considered two causally disconnected, uniformly accelerating observers moving through the vacuum of a Klein-Gordon field. Using only the entanglement present in the vacuum, they concluded that in general, protocols that resulted in classical information such as coin tossing and key distribution were possible, but noise due to the Davies-Unruh effect hinders protocols where the goal is quantum information, such as teleportation.

Along the same lines, Han, Olson, and Dowling considered the effects of projective measurements on the vacuum of a Klein-Gordon field by a uniformly accelerating observer [12]. Due to the Davies-Unruh effect, this observer has a nonzero probability of detecting a particle and after such a detection, the field is left in a state that is entangled in an inertial frame of reference. With further processing, the inertial observer can extract a Bell state. Recently, an experimental setup to generate entangled photons using the Davies-Unruh effect was proposed by Schültzhold, Schaller, and Habs [37]. Their process involves shooting electrons at ultra-relativistic speeds into an oscillating electric field, such as a laser. Chapter 5 of this thesis extends the work of extracting entanglement from the vacuum by generalizing the effect of Han *et al* to Dirac fields.

Chapter 5

Generation of Entanglement in the Fermionic Unruh Effect

In this chapter, the generation of entanglement between different modes of a Dirac spinor field due to measurements on the vacuum by an accelerating observer is studied. As a result of the Davies-Unruh effect [10, 11], the accelerating observer will perceive a Fermi-Dirac distribution of particles and antiparticles in what an inertial observer would describe as the vacuum state. It is shown here that if one of these particles is detected, an entangled state is produced in the inertial reference frame. It is found that entanglement is always produced and that larger accelerations produce more entanglement as quantified by the entanglement entropy. In the asymptotic limit of infinite acceleration, a maximally entangled Bell state is produced. A similar effect holds for scalar fields [12]; however, further processing is required to extract a Bell state, even in the asymptotic limit of infinite acceleration.

5.1 The Davies-Unruh Effect

The Davies-Unruh effect for a Dirac spinor field $\Psi(x)$ of mass m is a consequence of two inequivalent quantization schemes [15]. For an inertial observer in flat spacetime, the appropriate metric is the Minkowski metric $g_{\mu\nu} = \eta_{\mu\nu} = \text{diag}(1, -1, -1, -1)$. Since this metric is static, the field can be quantized in a straightforward manner by expanding it in terms of a complete set of positive and negative frequency modes (suppressing henceforth the spin degree

of freedom for ease of notation)

$$\hat{\Psi}(x) = \int dk \left(\hat{a}_k \, \psi_k^+(x) + \hat{b}_k^\dagger \, \psi_k^-(x) \right),$$

and imposing the canonical anticommutation relations on the mode operators $\{\hat{a}_k, \hat{a}_{k'}^\dagger\} = \{\hat{b}_k, \hat{b}_{k'}^\dagger\} = \delta(k - k')$, with all other anticommutators vanishing. Here, the modes are labelled by k, which is shorthand for the wavevector $\boldsymbol{k}$.

The key element here is the division of the modes into positive and negative frequency, which is done according to the Minkowski timelike Killing vector ∂_t. The operators $\hat{a}_k$ and $\hat{b}_k^\dagger$ are then interpreted as particle annihilation operators and antiparticle creation operators, respectively. With this interpretation, a Fock space can be constructed in the usual manner.

Now consider an observer moving through flat spacetime with uniform acceleration a in the z direction. This observer will experience communication horizons that divide the spacetime into four regions denoted I, II, F, and P (see Fig. 5.1). The observer will be confined to region I, which is causally disconnected from region II. The appropriate coordinates to describe his motion are the Rindler coordinates η and ξ (see Appendix A). In these coordinates, their trajectory is the line $\xi = 0$, which can be expressed in Minkowski coordinates as

$$at = \sinh(a\eta), \qquad\qquad az = \cosh(a\eta),$$

where η is the observer's proper time.

The quantum field theory for the Rindler observer is constructed by expanding the field in terms of the complete set of positive and negative frequency Rindler modes

$$\hat{\Psi}(x) = \int dk \left(\hat{c}_k^I \, \psi_k^{I+}(x) + \hat{d}_k^{I\dagger} \, \psi_k^{I-}(x) + \hat{c}_k^{II} \, \psi_k^{II+} + \hat{d}_k^{II\dagger} \, \psi_k^{II-}(x) \right),$$

and imposing the canonical anticommutation relations on the mode operators

$$\{\hat{c}_k^I, \hat{c}_{k'}^{I\dagger}\} = \{\hat{d}_k^I, \hat{d}_{k'}^{I\dagger}\} = \delta(k - k'),$$
$$\{\hat{c}_k^{II}, \hat{c}_{k'}^{II\dagger}\} = \{\hat{d}_k^{II}, \hat{d}_{k'}^{II\dagger}\} = \delta(k - k'),$$

with all other anticommutators vanishing.

There are two types of Rindler modes that reflect the causal structure of Rindler spacetime: the modes $\psi_k^{I\pm}(x)$ have support in region I, whereas the modes $\psi_k^{II\pm}(x)$ have support in region II. Each type is divided into positive

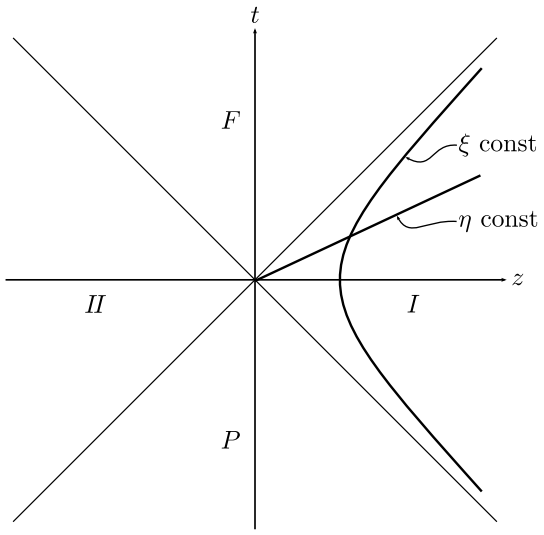

Figure 5.1: Spacetime is naturally divided into four regions denoted I, F, II, P for a uniformly accelerating observer. The line $\xi = 0$ is the worldline of the observer and η is his proper time.

and negative frequency according to the Rindler timelike Killing vector in the appropriate region. In region I this is given by ∂_η, however, in region II it is $\partial_{-\eta}$ where the minus sign ensures it is future pointing. The operators $\hat{c}_k^I$ and $\hat{d}_k^{I\dagger}$ respectively annihilate a particle and create an antiparticle in region I while $\hat{c}_k^{II}$ and $\hat{d}_k^{II\dagger}$ respectively annihilate and create particles and antiparticles in region II.

5.1.1 The Bogoliubov Transformation

These two quantizations are not equivalent [15]. Making the single mode approximation, in which the Rindler observer's particle detector is sensitive to a narrow bandwidth centered about the perpendicular components of the wavevector $\boldsymbol{k}_\perp$ (which is the same for a Minkowski observer) [6, 7, 9], the mode operators are related by the following Bogoliubov transformation

$$\begin{pmatrix} \hat{a}_k \\ \hat{b}_{-k}^\dagger \end{pmatrix} = \begin{pmatrix} \cos r_k & -e^{-i\phi_k} \sin r_k \\ e^{i\phi_k} \sin r_k & \cos r_k \end{pmatrix} \begin{pmatrix} \hat{c}_k^I \\ \hat{d}_{-k}^{II\dagger} \end{pmatrix}. \tag{5.1}$$

The parameter r_k is defined by

$$\cos r_k = [2\cosh(\pi\omega_k/a)]^{-1/2} \exp(\pi\omega_k/2a), \tag{5.2}$$

and $\omega_k = \sqrt{k^2 + m^2}$ is the frequency of the mode. This transformation can also be expressed as

$$\begin{pmatrix} \hat{a}_k \\ \hat{b}^\dagger_{-k} \end{pmatrix} = S_+(r_k) \begin{pmatrix} \hat{c}^I_k \\ \hat{d}^{II\dagger}_{-k} \end{pmatrix} S^\dagger_+(r_k), \tag{5.3}$$

where the unitary operator $S_+(r_k)$ is the *two mode squeezing operator* [38]

$$S_+(r_k) = \exp\left[r_k\big(\hat{c}^{I\dagger}_k\, \hat{d}^{II\dagger}_{-k} e^{-i\phi_k} + \hat{c}^I_k\, \hat{d}^{II}_{-k} e^{i\phi_k}\big)\right].$$

Similarly, if the Rindler observer's antiparticle detector is sensitive to a narrow bandwidth centered about the wavevector $-\boldsymbol{k}_\perp$ then

$$\begin{pmatrix} \hat{b}_k \\ \hat{a}^\dagger_{-k} \end{pmatrix} = \begin{pmatrix} \cos r_k & e^{-i\phi_k} \sin r_k \\ -e^{i\phi_k} \sin r_k & \cos r_k \end{pmatrix} \begin{pmatrix} \hat{d}^I_k \\ \hat{c}^{II\dagger}_{-k} \end{pmatrix}. \tag{5.4}$$

This can also be expressed as a squeezing transformation

$$\begin{pmatrix} \hat{b}_k \\ \hat{a}^\dagger_{-k} \end{pmatrix} = S_-(r_k) \begin{pmatrix} \hat{d}^I_k \\ \hat{c}^{II\dagger}_{-k} \end{pmatrix} S^\dagger_-(r_k), \tag{5.5}$$

where in this case, the squeezing operator is given by

$$S_-(r_k) = \exp\left[-r_k\big(\hat{d}^{I\dagger}_k\, \hat{c}^{II\dagger}_{-k} e^{-i\phi_k} + \hat{d}^I_k\, \hat{c}^{II}_{-k} e^{i\phi_k}\big)\right].$$

In all the above transformations, the phase ϕ_k can be absorbed into the definitions of the mode operators and will be done so from now on using the sign conventions of [9].

5.1.2 Transformation of the Vacuum

The Minkowski particle vacuum in mode k is defined by

$$\hat{a}_k \left|0_k\right\rangle^+ = 0.$$

Applying the Bogoliubov transformation in the form of Equation (5.3) to the mode operator and then acting with S_+ on both sides yields

$$\hat{c}^I_k \left(S_+(r_k) \left|0\right\rangle^+\right) = 0.$$

Therefore, the state in the brackets is the Rindler vacuum $\left|0\right\rangle_R$. As a result, the Minkowski vacuum, expressed in the Rindler Fock basis, is

$$\left|0_k\right\rangle^+ = S^\dagger_+ \left|0\right\rangle_R = \cos r_k \, \exp\big(\tan(r_k)\, \hat{c}^{I\dagger}_k\, \hat{d}^{II\dagger}_{-k}\big) \left|0_k\right\rangle^+_I \left|0_{-k}\right\rangle^-_{II}, \tag{5.6}$$

where the $+/-$ superscripts denote particle/antiparticle. A formal expression for the total Minkowski particle vacuum is obtained by using Eq. (5.6) for each mode

$$|0\rangle^{+} = N \prod_{k} \exp\big(\tan(r_k)\, \hat{c}_k^{I\dagger}\, \hat{d}_{-k}^{II\dagger}\big)\, |0_k\rangle_I^{+}\, |0_{-k}\rangle_{II}^{-}\,, \tag{5.7}$$

where $N = \prod_k \cos r_k$. By an analogous argument, the Minkowski antiparticle vacuum in mode k can be expressed in the Rindler Fock basis as

$$|0_k\rangle^{-} = \cos r_k\, \exp\big(-\tan(r_k)\, \hat{d}_k^{I\dagger}\, \hat{c}_{-k}^{II\dagger}\big)\, |0_k\rangle_I^{-}\, |0_{-k}\rangle_{II}^{+}\,.$$

Formally, the total Minkowski antiparticle vacuum is then

$$|0\rangle^{-} = N \prod_{k} \exp\big(-\tan(r_k)\, \hat{d}_k^{I\dagger}\, \hat{c}_{-k}^{II\dagger},\big)\, |0_k\rangle_I^{-}\, |0_{-k}\rangle_{II}^{+}\,.$$

While the Minkowski observer would say the field is in the vacuum state, the state according to the Rindler observer is

$$\rho_k^I = \mathrm{Tr}_{II}\big(|0\rangle^{++}\langle 0|\big),$$

where region II has been traced out since it is causally disconnected from the observer. The expectation value of the particle number operator is then

$$\mathrm{Tr}_I\big(\hat{c}_k^{I\dagger}\hat{c}_k^I\rho_k^I\big) = \sin^2(r_k) = \frac{1}{1+e^{\omega_k/k_BT}},$$

which is a Fermi-Dirac distribution at temperature

$$T = \frac{a}{2\pi k_B}$$

and k_B is Boltzmann's constant. This is the phenomenon known as the Davies-Unruh effect.

5.2 Detection of a Single Particle

What are the consequences of detecting one of these particles? Suppose two observers, Alice, an inertial observer, and Rob, a uniformly accelerating observer, are moving through the field $\hat{\Psi}(x)$. When the field is in the vacuum state as described by Alice, Rob would describe the state as the thermal state (5.7) due to the Davies-Unruh effect. Now suppose Rob performs the measurement represented by the Hermitian operator $\hat{c}_k^{I\dagger}\hat{c}_k^I$ and detects one

particle. Immediately after his measurement, the state will be the projection of (5.7) onto the single particle state in region I. This can be written succinctly as

$$|\psi_+(k)\rangle = P_k N \prod_{k'} \exp\big(\tan(r_{k'})\, \hat{c}^{I\dagger}_{k'}\, \hat{d}^{II\dagger}_{-k'}\big)\, |0_{k'}\rangle^+_I\, |0_{-k'}\rangle^-_{II}\,,$$

where the operator P_k is defined as

$$P_k = \sec(r_k) \hat{c}^{I\dagger}_k\, \hat{d}^{II\dagger}_{-k} \exp\big(-\tan(r_k)\, \hat{c}^{I\dagger}_k\, \hat{d}^{II\dagger}_{-k}\big).$$

Applying the Bogoliubov transformation (5.1), the state can be simplified to

$$|\psi_+(k)\rangle = \big(\sin(r_k) + \cos(r_k)\, \hat{a}^\dagger_k\, \hat{b}^\dagger_{-k}\big)\, |0\rangle\,, \tag{5.8}$$

from which it is seen that from Alice's perspective, the state is a superposition of the vacuum (i.e., no particle emission) and pair production at energy ω_k. This state is entangled in the occupation number of the particle mode k and the antiparticle mode $-k$.

5.2.1 Entanglement

To study the entanglement properties of this state it is convenient to work in the basis

$$\Big\{ \big|\tilde{0}\big\rangle^+, \big|\tilde{1}\big\rangle^+, \big|\tilde{0}\big\rangle^-, \big|\tilde{1}\big\rangle^- \Big\},$$

where $\big|\tilde{0}\big\rangle^\pm = |0_{\pm k}\rangle^\pm$ and $\big|\tilde{1}\big\rangle^\pm = |1_{\pm k}\rangle^\pm$. The state can then be represented by the density matrix

$$\rho(k) = \begin{pmatrix} \sin^2(r_k) & 0 & 0 & \sin(r_k)\,\cos(r_k) \\ 0 & 0 & 0 & 0 \\ 0 & 0 & 0 & 0 \\ \sin(r_k)\,\cos(r_k) & 0 & 0 & \cos^2(r_k) \end{pmatrix}.$$

The entanglement of this state is quantified by the entanglement entropy, defined in Chapter 3. To find the entanglement entropy of (5.8), the particle states are traced out resulting in the the reduced density matrix

$$\rho_-(k) = \mathrm{Tr}_+\, \rho(k) = \begin{pmatrix} \sin^2(r_k) & 0 \\ 0 & \cos^2(r_k) \end{pmatrix}.$$

From which the entropy is calculated to be

$$S\big(\rho_-(k)\big) = \log_2\big(\csc^2(r_k)\big) + \cos^2(r_k) \log_2\big(\tan^2(r_k)\big).$$

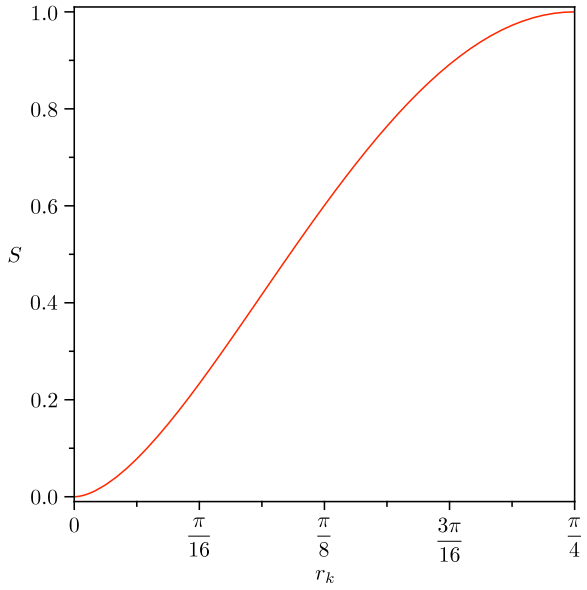

Figure 5.2: Entanglement entropy of the produced state (5.8) as a function of r_k. Larger accelerations produce more entanglement reaching the maximum of 1 when $r_k = \pi/4$.

Recalling that r_k is defined by Equation (5.2), it can be seen that the entanglement entropy is nonzero regardless of the frequency detected or the (nonzero) acceleration of the observer. Therefore, the state always contains distillable entanglement with larger accelerations producing more entanglement, as illustrated in Figure 5.2. Expressed in terms of the acceleration of the observer and energy of the particle, the entanglement entropy is

$$S(a, \omega_k) = \log_2 \left[2 \cosh \left(\frac{\pi\omega}{a} \right) \right] - \frac{\pi\omega_k}{a} \tanh \left(\frac{\pi\omega_k}{a} \right),$$

which is plotted in Figure 5.3.

Note that in order for Alice to use this state in a quantum information processing task, she must know Rob's acceleration and the momentum of the particle detected. Rob can communicate these parameters to Alice classically since he can always signal to her despite there being a point where he can no longer receive signals from her. It is interesting to note that if Alice does not know Rob's acceleration, she may be able to deduce it from the resulting quantum state. Studying exactly what information can be extracted from these states would make for an interesting future problem.

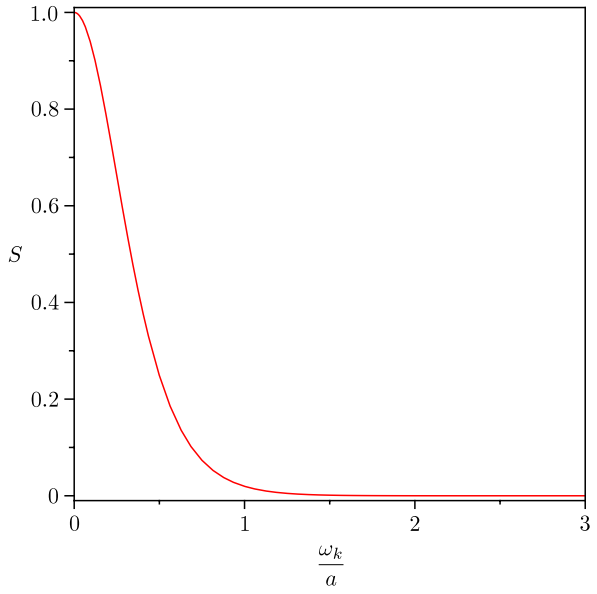

Figure 5.3: Entanglement entropy of the produced state (5.8) as a function of ω_k/a. Entanglement arbitrarily close to maximal can be generated for finite acceleration by detecting sufficiently low energy modes.

In the limit $\omega_k/a \to 0$, $r_k = \pi/4$ and the state approaches the maximally entangled Bell state

$$\lim_{\omega_k/a \to 0} |\psi_+(k)\rangle = \frac{1}{\sqrt{2}}(|\tilde{0}\rangle^+ |\tilde{0}\rangle^- + |\tilde{1}\rangle^+ |\tilde{1}\rangle^-),$$

which has an entanglement entropy of 1. This limit corresponds physically to the asymptotic limit of infinite acceleration. However, whenever $\omega_k \ll a$, the state is approximately

$$|\psi_+(k)\rangle \approx \sqrt{2}\left[\left(\frac{1}{2} - \frac{\pi\omega_k}{4a} - \frac{\pi^2\omega_k^2}{16a^2}\right)|\tilde{0}\rangle^+ |\tilde{0}\rangle^- + \left(\frac{1}{2} + \frac{\pi\omega_k}{4a} - \frac{\pi^2\omega_k^2}{16a^2}\right)|\tilde{1}\rangle^+ |\tilde{1}\rangle^-\right],$$

which has an entanglement entropy of

$$S(a,\omega_k) \approx 1 - \frac{\pi^2}{2\ln(2)}\frac{\omega_k^2}{a^2} + O\left(\frac{\omega_k^4}{a^4}\right).$$

In the case of massless fermions, entanglement arbitrarily close to maximal can be generated for finite acceleration by detecting sufficiently low energy modes.

However, this is not true in the massive case where the rest mass energy is a lower bound to the energy that can be detected. In this case, accelerations at least much greater than the rest mass energy are required to approximate a Bell state.

5.3 Detecting Many Particles

While the above analysis is conditioned on Rob detecting a single particle in mode k, it generalizes to other measurement outcomes. If he had instead detected an antiparticle in mode k, the resulting state would be

$$|\psi_-(k)\rangle = A_k N \prod_{k'} \exp\big(-\tan(r_{k'})\, \hat{d}^{I\dagger}_{k'}\, \hat{c}^{II\dagger}_{-k'}\big)\, |0_{k'}\rangle^-_I\, |0_{-k'}\rangle^+_{II}\,,$$

where the operator A_k is defined as

$$A_k = -\sec(r_k) \hat{d}^{I\dagger}_{r_k}\, \hat{c}^{II\dagger}_{r_-k} \exp\big(\tan(r_k) \hat{d}^{I\dagger}_{r_k}\, \hat{c}^{II\dagger}_{r_{-k}}\big).$$

Upon applying the Bogoliubov transformation (5.4) this simplifies to

$$|\psi_-(k)\rangle = \big(\sin(r_k) - \cos(r_k) \hat{b}^\dagger_k\, \hat{a}^\dagger_{-k}\big)\, |0\rangle\,,$$

which also approaches a Bell state in the asymptotic limit of infinite acceleration.

Noting that the operators P_k and $A_{k'}$ only contain an even number of mode operators, they will commute. Therefore, the state after the detection of an arbitrary number of particles or antiparticles will be the product of the states $|\psi_\pm(k)\rangle$ for each mode detected. Physically, this would be a superposition of all possible pair productions including no pair production; in the asymptotic limit of infinite acceleration, this approaches a product of Bell states. Regardless of the acceleration, given this state, Alice could use it as a resource in quantum information processing tasks.

Chapter 6

Entanglement of Non-inertial Detectors

In this chapter the dynamics of two entangled Unruh-Dewitt detectors interacting with a massless Klein-Gordon field are investigated. One detector is taken to be stationary while the other is undergoing non-uniform acceleration. The trajectory of the moving detector is initially inertial and smoothly transitions to a uniform acceleration, thus offering a more physical situation than the previous studies of entanglement in non-inertial frames. This model was studied in [13], where one detector was taken to have uniform acceleration.

The dynamics of the entanglement between the detectors is described in the time slicings of each observer. The calculations involved in quantifying the entanglement were performed numerically using the techniques described in Appendix D. It is found that in the ultraweak coupling limit, the entanglement decreases as a function of time for all parameters considered. In the case where one detector is uniformly accelerating, there are parameters where the entanglement can increase or decrease as a function of the accelerating detector's proper time. It is observed that in the parameter range considered, entanglement decreases more rapidly for the detector with non-uniform acceleration than one with uniform acceleration, however, it is not as rapid as two inertial detectors.

An overview of Unruh-DeWitt detector theory is given in Appendix C. The trajectory with non-uniform acceleration is naturally described in Costa-Villalba coordinates, which are introduced in Appendix B. To facilitate comparison between this trajectory and one with a uniform acceleration, Rindler coordinates are also used and their definition can be found in Appendix A.

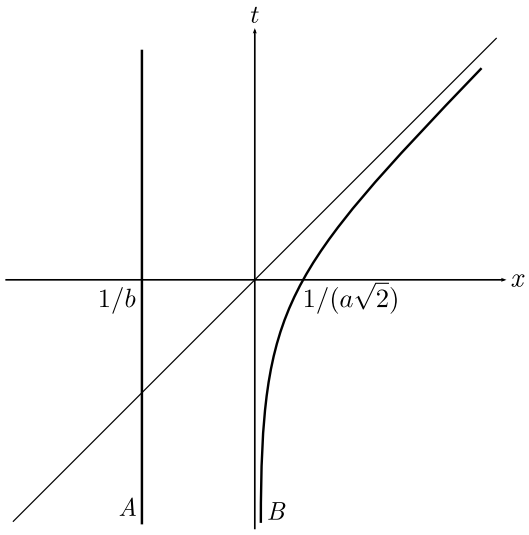

Figure 6.1: The trajectories of the two detectors. Detector A is carried by Alice who is stationary at position $1/b$ while detector B is carried by Rob, who has a non-uniform acceleration.

6.1 Two Unruh-DeWitt Detectors

The model considered here consists of two Unruh-Dewitt detectors, each interacting with the field through the Lagrangian (C.2) but not directly interacting with each other. The first detector is carried by "Alice" and its variables are denoted with the subscript A. The second is carried by "Rob" and its variables are denoted with the subscript B. Both detectors are considered to be identical (same mass, natural frequency, etc.) and the same cutoffs are performed for each so that they have the same renormalized frequency and damping coefficient. Alice is taken to be on the trajectory

$$z_A^\mu(t) = \left[t, \frac{1}{b}, 0, 0\right],$$

while Rob's trajectory is taken to be

$$\begin{aligned} z_B^\mu(\tau_\psi) = \Bigg[&\frac{1}{a}\sinh(a\tau_\psi) - \frac{\psi}{2a}\exp(-a\tau_\psi), \\ &\frac{1}{a}\cosh(a\tau_\psi) - \frac{\psi}{2a}\exp(-a\tau_\psi), 0, 0\Bigg]. \end{aligned} \tag{6.1}$$

If $\psi = 1$, then Rob's trajectory is that of a Costa-Villalba observer with $\zeta = 0$ and $w = a$. This observer is inertial in the asymptotic past but smoothly

accelerates to an asymptotic acceleration of a as can be seen in Figure 6.1. The evolution is parameterized by $\tau_\psi = \upsilon$ which can be related to the observer's proper time through Equation (B.3). Studying the dynamics of entanglement for this observer is the primary interest in this chapter. To highlight the differences due to the non-uniform acceleration it is useful to compare the Costa-Villalba trajectory to a Rindler trajectory. This is accomplished by setting $\psi = 0$, in which case the trajectory reduces to the Rindler trajectory given by $\xi = 0$. In this situation, $\tau_\psi = \eta$ is the proper time of the observer who has a uniform acceleration of a.

To distill the physics of the non-uniform acceleration, the interaction starts on the Minkowski time slice t_0 and terminates at time t_f. These times are chosen such that the Costa-Villalba trajectory is approximately inertial at the initial time and approximately Rindler at the final time.

At the start of the interaction the state of the system is taken to be

$$|\psi\rangle = |0\rangle \otimes |AB\rangle\,, \tag{6.2}$$

where the field is in the Minkowski vacuum state $|0\rangle$ and the detectors are in a Gaussian state $|AB\rangle$ described by the Wigner function

$$\begin{aligned} W(Q_B, P_B, Q_A, P_A) = \frac{1}{\pi^2} \exp\Bigg(&\beta^2 (Q_A + Q_B)^2 + \frac{1}{\alpha^2}(Q_A - Q_B)^2 \\ &+ \alpha^2 (P_A - P_B)^2 + \frac{1}{\beta^2}(P_A + P_B)^2\Bigg)\,. \end{aligned}$$

This is an entangled state for all $\alpha^2\beta^2 \neq 1$, however, regardless of the values of α and β, the detectors are not entangled with the field at the initial time.

6.1.1 Equations of Motion and Mode Decomposition

Since the system is linear, the results of Section C.1.1 can be summed to obtain the following equations of motion

$$\begin{aligned} (\partial_t^2 - \nabla^2)\hat{\Phi}(x) = \lambda_0 \Bigg\{ &\int_{\tau_A(t_0)}^{\infty} d\tau_A\, \hat{Q}_A(\tau_A)\delta^4\big(x - z_A(\tau_A)\big) \\ &+ \int_{\tau_\psi(t_0)}^{\infty} d\tau_B\, \hat{Q}_B(\tau_B)\delta^4\big(x - z_B(\tau_\psi)\big)\Bigg\}\,, \end{aligned} \tag{6.3}$$

$$(\partial_{\tau_i}^2 + \Omega_0^2)\hat{Q}_i(\tau_i) = \frac{\lambda_0}{m_0}\hat{\Phi}(z_i(\tau_i)), \tag{6.4}$$

where $i \in \{A, B\}$ and τ_i being the proper time of detector i. By performing the analogous mode decomposition as in Section C.2, these operators can be expressed as

$$\begin{aligned}\hat{\Phi}(x) = &\sqrt{\frac{1}{2\Omega_r m_0}} \sum_{j\in\{A,B\}} \left(f^{(j)}(x)\hat{a}_j + f^{(j)^*}(x)\hat{a}_j^\dagger\right) \\ &+ \frac{1}{(2\pi)^{3/2}} \int_{-\infty}^{\infty} d^3k \sqrt{\frac{1}{2\omega}} \left(f^{(+)}(x,\boldsymbol{k})\hat{b}_{\boldsymbol{k}} + f^{(-)}(x,\boldsymbol{k})\hat{b}_{\boldsymbol{k}}^\dagger\right),\end{aligned} \tag{6.5}$$

$$\begin{aligned}\hat{Q}_i(\tau_i) = &\sqrt{\frac{1}{2\Omega_r m_0}} \sum_{j\in\{A,B\}} \left(q_i^{(j)}(\tau_i)\hat{a}_j + q_i^{(j)^*}(\tau_i)\hat{a}_j^\dagger\right) \\ &+ \frac{1}{(2\pi)^{3/2}} \int_{-\infty}^{\infty} d^3k \sqrt{\frac{1}{2\omega}} \left(q_i^{(+)}(\tau_i,\boldsymbol{k})\hat{b}_{\boldsymbol{k}} + q_i^{(-)}(\tau_i,\boldsymbol{k})\hat{b}_{\boldsymbol{k}}^\dagger\right).\end{aligned} \tag{6.6}$$

The canonical equal time commutation relations on $\hat{\Phi}(x)$ and $\hat{\Pi}(x)$ (Equation (C.3)) impose the following commutation relations on the mode operators

$$[\hat{b}_{\boldsymbol{k}}, \hat{b}_{\boldsymbol{k}'}^\dagger] = \delta^3(\boldsymbol{k} - \boldsymbol{k}') \qquad \text{and} \qquad [\hat{a}_i, \hat{a}_j^\dagger] = \delta_{ij}.$$

The mode decompositions of the conjugate momentum operators can be obtained from Equations (6.5) and (6.6) by differentiation with respect to proper time. Due to the Hermiticity of $\hat{\Phi}(x)$ and $\hat{Q}_i$, it is sufficient to solve for the modes $f^{(j)}(x)$, $f^{(+)}(x,\boldsymbol{k})$, $q_i^{(j)}(\tau_i)$, and $q^{(+)}(\tau_i,\boldsymbol{k})$. Equations (6.3) and (6.4) as well as the linear independence of the operators $\hat{b}_{\boldsymbol{k}}$, $\hat{b}_{\boldsymbol{k}}^\dagger$, $\hat{a}_i$, and $\hat{a}_i^\dagger$ yield the following equations of motion for the mode functions

$$\begin{aligned}(\partial_t^2 - \nabla^2) f^{(j)}(x) = \lambda_0 \Bigg\{ &\int_{\tau_A(t_0)}^{\infty} d\tau_A \, q_A^{(j)}(\tau_A) \delta^4\big(x - z_A(\tau_A)\big) \\ &+ \int_{\tau_\psi(t_0)}^{\infty} d\tau_\psi \, q_B^{(j)}(\tau_\psi) \delta^4\big(x - z_B(\tau_\psi)\big) \Bigg\},\end{aligned} \tag{6.7}$$

$$\begin{aligned}(\partial_t^2 - \nabla^2) f^{(+)}(x,\boldsymbol{k}) = \lambda_0 \Bigg\{ &\int_{\tau_A(t_0)}^{\infty} d\tau_A \, q_A^{(+)}(\tau_A,\boldsymbol{k}) \delta^4\big(x - z_A(\tau_A)\big) \\ &+ \int_{\tau_\psi(t_0)}^{\infty} d\tau_\psi \, q_B^{(+)}(\tau_\psi,\boldsymbol{k}) \delta^4\big(x - z_B(\tau_\psi)\big) \Bigg\},\end{aligned} \tag{6.8}$$

$$(\partial_{\tau_i}^2 + \Omega_0) q_i^{(j)}(\tau_i) = \frac{\lambda_0}{m_0} f^{(j)}\big(z_i(\tau_i)\big), \tag{6.9}$$

$$(\partial_{\tau_i}^2 + \Omega_0) q_i^{(+)}(\tau_i,\boldsymbol{k}) = \frac{\lambda_0}{m_0} f^{(+)}\big(z_i(\tau_i),\boldsymbol{k}\big). \tag{6.10}$$

Since the field and detectors are free before the interaction, the modes must obey the following initial conditions

$$\begin{aligned}
q_i^{(i)}\big(\tau_i(t_0)\big) &= e^{-i\Omega_r\tau_i(t_0)},\\
\partial_{\tau_i} q_i^{(i)}\big(\tau_i(t_0)\big) &= -i\Omega_r e^{-i\Omega_r\tau_i(t_0)},\\
f^{(+)}(t_0,\boldsymbol{x},\boldsymbol{k}) &= e^{i\boldsymbol{k}\cdot\boldsymbol{x}-i\omega t_0},\\
\partial_t f^{(+)}(t_0,\boldsymbol{x},\boldsymbol{k}) &= -i\omega e^{i\boldsymbol{k}\cdot\boldsymbol{x}-i\omega t_0},\\
q_i^{(+)}\big(\tau_i(t_0),\boldsymbol{k}\big) &= \partial_{\tau_i} q_i^{(+)}\big(\tau_i(t_0),\boldsymbol{k}\big) = 0,\\
f^{(i)}(t_0,\boldsymbol{x}) &= \partial_t f^{(a)}(t_0,\boldsymbol{x}) = 0,\\
q_A^{(B)}(t_0) &= \partial_t q_A^{(B)}(t_0) = 0,\\
q_B^{(A)}\big(\tau_\psi(t_0)\big) &= \partial_{\tau_\psi} q_B^{(A)}\big(\tau_\psi(t_0)\big) = 0.
\end{aligned}$$

Due to the presence of the point sources in Equations (6.7) and (6.8), the field amplitude diverges at the location of the detectors. As a result, Equations (6.9) and (6.10) need to be regularized as in Section C.3.1. However, before this procedure can be applied, the retarded times and distances for the trajectories must be obtained.

6.1.2 Retarded Times and Distances

The *retarded time* associated with a field point x is the time at which the trajectory intercepts the past light cone of x. It is given by the solution to $\sigma = 0$ where

$$\sigma = -\frac{1}{2}\big(x_\mu - z_\mu(t)\big)\big(x^\mu - z^\mu(t)\big)$$

and $z^\mu(t)$ is the trajectory of interest. The spatial distance between the field point and the location of the detector at the retarded time is the *retarded distance*. This is obtained by evaluating

$$\left.\frac{\partial\sigma}{\partial t}\right|_{\sigma=0}. \tag{6.11}$$

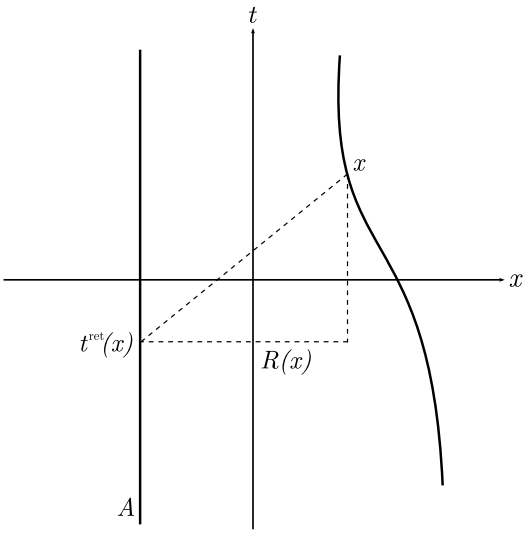

Figure 6.2: The retarded Minkowski time for point x is $t^{\text{ret}}(x)$ and the retarded distance $R(x)$ is the spatial distance between the field point and the detector at the retarded time.

Minkowski $\boldsymbol{\sigma}$

Inserting the trajectory of the Minkowski observer, Alice, into the definition of σ results in

$$\begin{aligned}\sigma_M &= -\frac{1}{2}\big(x_\mu - z_{A\mu}(\tau_A)\big)\big(x^\mu - z_A{}^\mu(\tau_A)\big) \\ &= -\frac{1}{2}\big(R(x)^2 - (t - x^0)^2\big),\end{aligned}$$

where $R(x) = \sqrt{(x^1 - 1/b)^2 + \rho^2}$ and $\rho^2 = y^2 + z^2$. Setting $\sigma_M = 0$, the retarded time is found to be

$$t^{\text{ret}}(x) = x^0 - R(x).$$

Similarly,

$$\left.\frac{\partial \sigma_M}{\partial t}\right|_{\sigma_M = 0} = -R(x),$$

and so the retarded distance is given by $R(x)$, as can be seen in Figure 6.2. Evaluating on the accelerating observer's trajectory yields

$$t^{\text{ret}}(\tau_\psi) = t^{\text{ret}}\big(z_B(\tau_\psi)\big) = \frac{1}{b} - \frac{1}{a}e^{-a\tau_\psi}.$$

Since this is independent of ψ, it is true for both the Costa-Villalba and Rindler trajectories.

Costa-Villalba and Rindler σ

Inserting Rob's trajectory (6.1) into the definition of σ results in

$$\begin{aligned}\sigma_B &= -\frac{1}{2}\big(x_\mu - z_{B\mu}(\tau_\psi)\big)\big(x^\mu - z_B{}^\mu(\tau_\psi)\big) \\ &= -\frac{1}{2}\left[\rho^2 - UV + \frac{U}{a}e^{a\upsilon} - \frac{V}{a}e^{-a\upsilon} + \frac{1}{a^2} - \psi\left(\frac{U}{a}e^{-a\upsilon} + \frac{1}{a^2}e^{-2a\upsilon}\right)\right],\end{aligned}$$

where $U = x^0 - x^1$ and $V = x^0 + x^1$. The Costa-Villalba result is obtained by setting $\psi = 1$

$$\sigma_V = -\frac{1}{2}\left[\rho^2 - UV - \frac{V}{a}e^{-a\upsilon} + \frac{1}{a^2} + \left(\frac{2U}{a} + \frac{1}{a^2}e^{-a\upsilon}\right)\sinh(a\upsilon)\right],$$

while setting $\psi = 0$ gives the Rindler result

$$\sigma_R = -\frac{1}{2}\left(\rho^2 - UV - \frac{V}{a}e^{-a\eta} + \frac{1}{a^2} + \frac{U}{a}e^{a\eta}\right).$$

The retarded times can be obtained by solving the equations $\sigma_V = 0$ and $\sigma_R = 0$. However, to avoid the complicated expressions of the Costa-Villalba trajectory (a cubic equation), the retarded times will be found geometrically instead of solving $\sigma_B = 0$ directly. To simplify this, the analysis will be restricted to the t-x plane. This will not be a problem for the purposes of this chapter since the primary interest is calculating quantities related to the detectors as opposed to the field.

The equation of the null line that passes through the trajectory (6.1) at τ_ψ and intercepts the inertial trajectory in the future is given by

$$t' = -x' + \frac{1}{a}\cosh(a\tau_\psi) + \frac{1}{a}\sinh(a\tau_\psi) - \frac{\psi}{a}e^{-a\tau_\psi}.$$

The retarded time is obtained by evaluating this at the point $(t, 1/b)$ on the inertial trajectory and solving for τ_ψ. The result is

$$\tau_\psi^{\text{ret}}(t) = \frac{1}{a}\ln\left[\frac{a}{2}\left(t + \frac{1}{b}\right) + \sqrt{\frac{a^2}{4}\left(t + \frac{1}{b}\right)^2 + \psi}\right].$$

This can be shown to satisfy $\sigma_B = 0$. The Rindler retarded time, obtained by setting $\psi = 0$, is

$$\eta^{\text{ret}}(t) = \frac{1}{a}\ln\left[a\left(t + \frac{1}{b}\right)\right],$$

while the Costa-Villalba retarded time

$$v^{\rm ret}(t) = \frac{1}{a}\,\mathrm{arcsinh}\left[\frac{a}{2}\left(t+\frac{1}{b}\right)\right],$$

is found by setting $\psi = 1$. The Costa-Villalba retarded proper time is then obtained from Equation (B.3).

The retarded distance is given by

$$\left.\frac{\partial\sigma_B}{\partial\tau_\psi}\right|_{\sigma_B=0} = -\frac{U}{2}e^{a\tau_\psi^{\rm ret}} - \frac{V}{2}e^{-a\tau_\psi^{\rm ret}} - \frac{\psi}{2}\left(Ue^{-a\tau_\psi^{\rm ret}} + \frac{2}{a^2}e^{-2a\tau_\psi^{\rm ret}}\right).$$

Setting $\psi = 0$ results in

$$\left.\frac{\partial\sigma_R}{\partial\tau_\psi}\right|_{\sigma_R=0} \equiv -\frac{a}{2}X(x) = -\frac{a}{2}\left(UV + \frac{1}{a^2}\right),$$

which, when evaluated on the inertial trajectory equals

$$X\big(z_A(t)\big) = t^2 - \frac{1}{b^2} + \frac{1}{a^2}.$$

For the Costa-Villalba trajectory,

$$\begin{aligned}\left.\frac{\partial\sigma_V}{\partial\tau}\right|_{\sigma_V=0} &= \frac{\partial\tau}{\partial\upsilon}\left.\frac{\partial\sigma_V}{\partial\upsilon}\right|_{\sigma_V=0} \equiv D(x)\\ &= \frac{1}{d^2}\sqrt{1+\frac{1}{d^2}}\left[\left(\frac{1}{2b}-\frac{t}{2}\right)d^3 - td - \frac{1}{a}\right],\end{aligned}$$

where $d = aV/2 + \sqrt{1+a^2V^2/4}$.

6.1.3 Regularized Equations of Motion and Solutions

Using the retarded times found in the previous section and applying the results from Section C.3.1, the regularized equations of motion for the Costa-Villalba

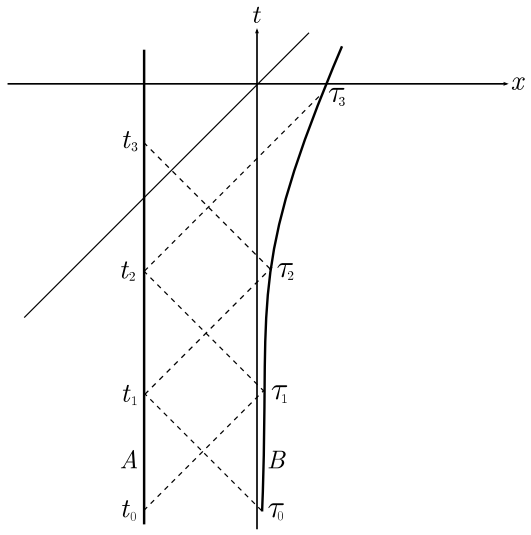

Figure 6.3: The retarded mutual influences between the detectors. The detectors start interacting with the field at t_0 and τ_0 but do not influence each other until after the times t_1 and τ_1.

observer are

$$(\partial_t^2 + 2\gamma\partial_t + \Omega_r^2)q_A^{(j)}(t) = \frac{\lambda_0^2}{4\pi}\frac{\theta\big[\tau^{\rm ret}\big(z_A(t)\big)\big]}{|D\big(z_A(t)\big)|}q_B^{(j)}\left[\tau^{\rm ret}\big(z_A(t)\big)\right], \tag{6.12}$$

$$(\partial_\tau^2 + 2\gamma\partial_\tau + \Omega_r^2)q_B^{(j)}(\tau) = \frac{\lambda_0^2}{4\pi}\frac{\theta\big[t^{\rm ret}\big(z_B(\tau)\big)\big]}{R\big(z_B(\tau)\big)}q_A^{(j)}\left[t^{\rm ret}\big(z_B(\tau)\big)\right], \tag{6.13}$$

$$\begin{aligned}(\partial_t^2 + 2\gamma\partial_t + \Omega_r^2)q_A^{(+)}(t,\boldsymbol{k}) &= \lambda_0 f_0^{(+)}\big(z_a(t),\boldsymbol{k}\big) \\ &\quad + \frac{\lambda_0^2}{4\pi}\frac{\theta\big[\big(\tau^{\rm ret}\big(z_A(t)\big)\big]}{|D\big(z_A(t)\big)|}q_B^{(+)}\left[\tau^{\rm ret}\big(z_A(t)\big),\boldsymbol{k}\right],\end{aligned} \tag{6.14}$$

$$\begin{aligned}(\partial_\tau^2 + 2\gamma\partial_\tau + \Omega_r^2)q_B^{(+)}(\tau,\boldsymbol{k}) &= \lambda_0 f_0^{(+)}\big(z_B(\tau),\boldsymbol{k}\big) \\ &\quad + \frac{\lambda_0^2}{4\pi}\frac{\theta\big[t^{\rm ret}\big(z_B(\tau)\big)\big]}{R\big(z_B(\tau)\big)}q_A^{(+)}\left[t^{\rm ret}\big(z_B(\tau)\big),\boldsymbol{k}\right].\end{aligned} \tag{6.15}$$

The modes are driven damped harmonic oscillators with natural frequency Ω_r and damping coefficient $\gamma = \lambda_0^2/8\pi m_0$. The equations of motion for the Rindler detector can be found in [13][1].

[1] Alternatively, one can simply set $\psi = 0$ in z_B and exchange $D(x)$ for $-aX(x)/2$, τ for η, and $\tau^{\rm ret}(x)$ for $\eta^{\rm ret}(x)$.

The causal connection between the detectors as a result of their mutual interaction with the field is now explicit in the above equations. Since these equations are linear, their solution can be built up iteratively by considering the causal structure of the two detector system.

In particular, consider Equations (6.14) and (6.15). Due to retardation, before time t_1 (see Figure 6.3), B has no causal influence on A and so the only source is the field amplitude at the position of the detector. During this time the solution consistent with the boundary conditions is

$$\Big[q_A^{(+)}(t)\Big]_0 = \lambda_0 \int_{t_0}^{t} dt'\, K(t-t') f_0^{(+)}\big(z_A(t'), \boldsymbol{k}\big), \tag{6.16}$$

where

$$K(t-t') = \frac{1}{\Omega}\theta(t-t') e^{-\gamma(t-t')} \sin\big(\Omega(t-t')\big)$$

is the retarded Green's function for a damped harmonic oscillator and $\Omega = \sqrt{\Omega_r - \gamma^2}$. Similarly, before time τ_1, A has no influence on B and so the solution is

$$\Big[q_B^{(+)}(\tau)\Big]_0 = \lambda_0 \int_{\tau_0}^{\tau} d\tau'\, K(\tau-\tau') f_0^{(+)}\big(z_B(\tau'), \boldsymbol{k}\big), \tag{6.17}$$

where $\tau_0 = \tau(t_0)$. After time t_1 however, the influence of B on A must be taken into account. This influence is obtained by including the solution for $q_B^{(+)}(\tau)$ as a source in Equation (6.14). Before time t_2, this solution is given by Equation (6.17). The correction to $q_A^{(+)}(t)$ is then a term of order λ_0^3

$$\begin{aligned}\Big[q_A^{(+)}(t)\Big]_1 = \theta(t-t_1)\frac{\lambda_0^3}{4\pi}\int_{t_1}^{t} dt'\, \frac{K(t-t')}{|D\big(z_A(t')\big)|} \\ \times \int_{\tau_0}^{\tau^{\mathrm{ret}}(t')} d\tau'\, K(\tau^{\mathrm{ret}}(t')-\tau') f_0^{(+)}\big(z_B(\tau'), \boldsymbol{k}\big).\end{aligned}$$

Similarly, inserting Equation (6.16) into Equation (6.15) yields the correction on B due to the influence of A after time τ_1

$$\begin{aligned}\Big[q_B^{(+)}(\tau)\Big]_1 = \theta(\tau-\tau_1)\frac{\lambda_0^3}{4\pi}\int_{\tau_1}^{\tau} d\tau'\, \frac{K(\tau-\tau')}{R\big(z_B(\tau')\big)} \\ \times \int_{t_0}^{t^{\mathrm{ret}(\tau')}} dt'\, K\big(t^{\mathrm{ret}}(\tau')-t'\big) f_0^{(+)}\big(z_A(t'), \boldsymbol{k}\big).\end{aligned}$$

The next order corrections, which are of order λ_0^5, come into effect at times t_2 and τ_2 and are obtained by substituting these results back into the equations

of motion. The full solution is obtained by repeating this process for the entire duration of the interaction. It can be written succinctly as a recurrence relation in the following way

$$\begin{aligned}\Big[q_A^{(+)}(t)\Big]_i &= \frac{\lambda_0^2}{4\pi}\int_{t_i}^{t} dt' \frac{K(t-t')}{|D\big(z_A(t')\big)|}\Big[q_B^{(+)}\big(\tau^{\rm ret}(t')\big)\Big]_{i-1},\\ \Big[q_B^{(+)}(\tau)\Big]_i &= \frac{\lambda_0^2}{4\pi}\int_{\tau_i}^{\tau} d\tau' \frac{K(\tau-\tau')}{R\big(z_B(\tau')\big)}\Big[q_A^{(+)}\big(t^{\rm ret}(\tau')\big)\Big]_{i-1},\end{aligned}$$

with

$$\begin{aligned}\Big[q_A^{(+)}(t)\Big]_0 &= \lambda_0\int_{t_0}^{t} dt'\, K(t-t') f_0^{(+)}\big(z_A(t'),\boldsymbol{k}\big),\\ \Big[q_B^{(+)}(\tau)\Big]_0 &= \lambda_0\int_{\tau_0}^{\tau} d\tau'\, K(\tau-\tau') f_0^{(+)}\big(z_B(\tau'),\boldsymbol{k}\big).\end{aligned}$$

The solution is given by

$$\begin{aligned}q_A^{(+)}(t) &= \sum_i \theta(t-t_i)\Big[q_A^{(+)}(t)\Big]_i,\\ q_B^{(+)}(\tau) &= \sum_i \theta(\tau-\tau_i)\Big[q_B^{(+)}(\tau)\Big]_i.\end{aligned}$$

Equations (6.12) and (6.13) can be solved in the analogous manner. The solution is the the sum of the retarded mutual influences given by a similar recurrence relation

$$\begin{aligned}\Big[q_A^{(j)}(t)\Big]_i &= \frac{\lambda_0^2}{4\pi}\int_{t_i}^{t} dt' \frac{K(t-t')}{|D\big(z_A(t')\big)|}\Big[q_B^{(j)}\big(\tau^{\rm ret}(t')\big)\Big]_{i-1},\\ \Big[q_B^{(j)}(\tau)\Big]_i &= \frac{\lambda_0^2}{4\pi}\int_{\tau_i}^{\tau} d\tau' \frac{K(\tau-\tau')}{R\big(z_B(\tau')\big)}\Big[q_A^{(j)}\big(t^{\rm ret}(\tau')\big)\Big]_{i-1},\end{aligned}$$

where in this case,

$$\begin{aligned}\Big[q_A^{(A)}(t)\Big]_0 &= \frac{1}{2}e^{-\gamma(t-t_0)}\left[W_+ e^{-i\Omega(t-t_0)} + W_- e^{i\Omega(t-t_0)}\right],\\ \Big[q_B^{(B)}(\tau)\Big]_0 &= \frac{1}{2}e^{-\gamma(\tau-\tau_0)}\left[W_+ e^{-i\Omega(\tau-\tau_0)} + W_- e^{i\Omega(\tau-\tau_0)}\right],\\ \Big[q_A^{(B)}(t)\Big]_0 &= \Big[q_B^{(A)}(\tau)\Big]_0 = 0.\end{aligned}$$

To study the dynamics of the entanglement as quantified by Σ, the two-point functions of the detectors must be obtained.

6.2 The Two-Point Correlation Matrix in the Ultraweak Coupling Limit

With the initial state (6.2), the two-point correlation matrix splits into

$$\langle \mathcal{R}_\mu, \mathcal{R}_\nu \rangle = \langle \mathcal{R}_\mu, \mathcal{R}_\nu \rangle_v + \langle \mathcal{R}_\mu, \mathcal{R}_\nu \rangle_a ,$$

where $\langle \mathcal{R}_\mu, \mathcal{R}_\nu \rangle_v = \langle 0 | \, \mathcal{R}_\mu, \mathcal{R}_\nu \, | 0 \rangle$ is the contribution from the vacuum fluctuations and $\langle \mathcal{R}_\mu, \mathcal{R}_\nu \rangle_a = \langle AB | \, \mathcal{R}_\mu, \mathcal{R}_\nu \, | AB \rangle$ is the contribution from the state of the detectors.

These will be calculated in the ultraweak coupling limit where $\gamma \ll a, \Omega$. In this regime, all terms $O(\lambda_0^2)$ are dropped from the mode functions. It is further assumed that the detectors are very far apart such that there is significant retardation of the mutual influences. This will mean that there will be little correlation between the oscillators due to the vacuum fluctuations.

6.2.1 Vacuum Fluctuations

The contribution to the two-point function due to the vacuum fluctuations can be evaluated as

$$\begin{aligned} \langle \mathcal{R}_\mu, \mathcal{R}_\nu \rangle_v &= \frac{1}{2}\big(\langle 0 | \, \mathcal{R}_\mu \mathcal{R}_\nu \, | 0 \rangle + \langle 0 | \, \mathcal{R}_\nu \mathcal{R}_\mu \, | 0 \rangle \big) \\ &= \frac{1}{2}\left(\langle 0 | \, \mathcal{R}_\mu \mathcal{R}_\nu \, | 0 \rangle + \big[\langle 0 | \, \mathcal{R}_\mu \mathcal{R}_\nu \, | 0 \rangle \big]^* \right) \\ &= \Re\big(\langle 0 | \, \mathcal{R}_\mu \mathcal{R}_\nu \, | 0 \rangle \big). \end{aligned}$$

After inserting the mode expansions of the operators, the only terms that contribute are those that contain $b_{\boldsymbol{k}} b^\dagger_{\boldsymbol{k}}$, thus

$$\langle \mathcal{R}_\mu, \mathcal{R}_\nu \rangle_v = \Re \left\{ \frac{1}{(2\pi)^3} \int \frac{d^3k}{2\omega} r_\mu^{(+)}(t_\mu, \boldsymbol{k}) r_\nu^{(-)}(t_\nu, \boldsymbol{k}) \right\}, \tag{6.18}$$

where $r_\mu^{(\pm)} = (q_B^{(\pm)}, p_B^{(\pm)}, q_A^{(\pm)}, p_A^{(\pm)})$.

Calculating $\langle Q_i(\tau_i)^2\rangle_v$

In the ultraweak coupling approximation, $q_i^{(+)}(\tau_i)$ is given by Equation (6.17). Inserting this into Equation (6.18) and applying Equation (E.1) results in

$$\begin{aligned}\langle Q_B(\tau)Q_B(\tau')\rangle = \theta(\tau-\tau_0)\theta(\tau'-\tau_0')\frac{\lambda_0^2}{m_0^2\Omega^2}\int_{\tau_0}^{\tau}d\tilde{\tau}\int_{\tau_0'}^{\tau'}d\tilde{\tau}'\,e^{-\gamma(\tau-\tilde{\tau})}e^{-\gamma(\tau'-\tilde{\tau}')}\\ \times\sin\big(\Omega(\tau-\tilde{\tau})\big)\sin\big(\Omega(\tau'-\tilde{\tau}')\big)\frac{1}{\sqrt{2\pi}}\left(\frac{1}{\Delta x^2-\Delta t^2}\right),\end{aligned}$$

where

$$\Delta x^2-\Delta t^2=\frac{1}{a^2}\left[2-2\cosh\big(a(\upsilon-\upsilon')\big)-(e^{-a\upsilon}-e^{-a\upsilon'})^2\right]$$

for the Costa-Villalba trajectory. Changing variables to Costa-Villalba coordinates,

$$\begin{aligned}\langle Q_B(\tau)Q_B(\tau')\rangle_v = \theta(\tau-\tau_0)\theta(\tau'-\tau_0')\frac{a^2\lambda_0^2}{8\pi^2m_0^2\Omega^2}\int_{\upsilon_0}^{\upsilon}d\tilde{\upsilon}\int_{\upsilon_0'}^{\upsilon'}d\tilde{\upsilon}'\\ \times\sqrt{1+e^{-2a\tilde{\upsilon}}}\sqrt{1+e^{-2a\tilde{\upsilon}'}}e^{-\gamma[\tau-\tau(\tilde{\upsilon})]}e^{-\gamma[\tau'-\tau(\tilde{\upsilon}')]}\\ \times\sin\left[\Omega\big(\tau-\tau(\tilde{\upsilon})\big)\right]\sin\left[\Omega\big(\tau'-\tau(\tilde{\upsilon}')\big)\right]\\ \times\left[1-\cosh\big(a(\tilde{\upsilon}-\tilde{\upsilon}')\big)-\frac{1}{2}(e^{-a\tilde{\upsilon}}-e^{-a\tilde{\upsilon}'})^2\right]^{-1},\end{aligned}$$

where $\upsilon_0=\upsilon(\tau_0)$, $\upsilon=\upsilon(\tau)$, $\upsilon_0'=\upsilon(\tau_0')$, and $\upsilon'=\upsilon(\tau')$. Note that the integrand diverges when $\tilde{\upsilon}=\tilde{\upsilon}'$, which is a generic feature regardless of the trajectory [39]. This will be handled by subtracting off the divergent piece of the integrand. To simplify this process, the coordinates are changed to

$$T=\tilde{\upsilon}+\tilde{\upsilon}',\qquad\qquad \Delta=\frac{\tilde{\upsilon}-\tilde{\upsilon}'}{2}.$$

In these coordinates the two-point function is

$$\begin{aligned}\langle Q_B(\tau)Q_B(\tau')\rangle_v = -\theta(\tau-\tau_0)\theta(\tau'-\tau_0')\frac{a^2\gamma}{\pi m_0\Omega^2}\iint_{\text{diamond}}dTd\Delta\\ \times\sqrt{1+e^{-2T}+2e^{-T}\cosh(2\Delta)}e^{-\gamma[\tau+\tau'-\tau(T/2+\Delta)-\tau(T/2-\Delta)]}\\ \times\sin\left[\Omega\big(\tau-\tau(T/2+\Delta)\big)\right]\sin\left[\Omega\big(\tau'-\tau(T/2-\Delta)\big)\right]\\ \times[(1+e^{-T})\sinh^2(\Delta)]^{-1}.\end{aligned}$$

The region of integration ("diamond") becomes

$$\begin{aligned}
\Delta \in \left[\frac{\upsilon_0 - \upsilon'}{2}, \frac{\upsilon - \upsilon'}{2}\right] \qquad &\Longrightarrow \qquad T \in [-2(\Delta - \upsilon_0), 2(\Delta + \upsilon')]\,, \\
\Delta \in \left[\frac{\upsilon - \upsilon'}{2}, \frac{\upsilon_0 - \upsilon_0'}{2}\right] \qquad &\Longrightarrow \qquad T \in [-2(\Delta - \upsilon_0), -2(\Delta - \upsilon)]\,, \\
\Delta \in \left[\frac{\upsilon_0 - \upsilon_0'}{2}, \frac{\upsilon - \upsilon_0'}{2}\right] \qquad &\Longrightarrow \qquad T \in [2(\Delta + \upsilon_0), -2(\Delta - \upsilon)]\,.
\end{aligned}$$

The integrand can be expanded in the series

$$\frac{f(T,\Delta)}{\sinh^2(\Delta)} \approx \frac{f(T,0)}{\Delta^2} + \frac{\partial_\Delta f(T,0)}{\Delta} + \frac{1}{2}\partial_\Delta^2 f(T,0) - \frac{1}{3} f(T,0) + \cdots$$

where it can be seen that the first two terms are responsible for the divergence at $\Delta = 0$ and will be subtracted off. The resulting regularized two-point function is then

$$\begin{aligned}
\langle Q_B(\tau) Q_B(\tau') \rangle_v = -\theta(\tau - \tau_0)\theta(\tau' - \tau_0') \frac{a^2\gamma}{\pi m_0 \Omega^2} e^{-\gamma(\tau+\tau')} \iint\limits_{\text{diamond}} dT d\Delta \\
\times \left\{ \frac{\sqrt{1 + e^{-2T} + 2e^{-T}\cosh(2\Delta)}}{(1+e^{-T})\sinh^2(\Delta)} e^{\gamma[\tau(T/2+\Delta)+\tau(T/2-\Delta)]} \right. \\
\times \sin\big[\Omega\big(\tau - \tau(T/2+\Delta)\big)\big] \sin\big[\Omega\big(\tau' - \tau(T/2-\Delta)\big)\big] \\
- e^{2\gamma\tau(T/2)} \left[\frac{1}{\Delta^2} \sin\big[\Omega\big(\tau - \tau(T/2)\big)\big] \sin\big[\Omega\big(\tau' - \tau(T/2)\big)\big] \right. \\
\left. \left. + \frac{\Omega}{a\Delta} \left(\frac{e^{T/2}}{\sqrt{1+e^T}} + \frac{e^{-T}}{1+e^T} \right) \sin\big(\Omega(\tau - \tau')\big) \right] \right\}.
\end{aligned} \tag{6.19}$$

The analogous procedure can be applied to the Rindler trajectory except that in this case

$$\Delta x^2 - \Delta t^2 = \frac{2}{a^2}\left[1 - \cosh\big(a(\tilde\eta - \tilde\eta')\big)\right].$$

The regularized two-point function is then

$$\langle Q_B(\eta)Q_B(\eta')\rangle_v = -\theta(\eta-\eta_0)\theta(\eta'-\eta_0')\frac{a^2\gamma}{\pi m_0\Omega^2}e^{-\gamma(\eta+\eta')}\iint\limits_{\text{diamond}} dTd\Delta$$
$$\left\{\frac{1}{2\sinh^2(\Delta)}\sin\big(\Omega(\eta-T/2-\Delta)\big)\sin\big(\Omega(\eta'-T/2+\Delta)\big)\right.$$
$$-\frac{1}{\Delta^2}\left[\sin\big(\Omega(\eta-T/2)\big)\sin\big(\Omega(\eta'-T/2)\big)\right]$$
$$\left.+\frac{\Omega}{a\Delta}\sin\big(\Omega(\eta-\eta')\big)\right\}.$$

Similarly, for the Minkowski trajectory

$$\Delta x^2-\Delta t^2 = -(\tilde{t}-\tilde{t}')^2,$$

and so the the regularized two-point function is

$$\langle Q_A(t)Q_A(t')\rangle_v = -\theta(t-t')\theta(t'-t_0')\frac{2\gamma}{\pi m_0\Omega^2}e^{-\gamma(\eta+\eta')}\iint\limits_{\text{diamond}} dTd\Delta$$
$$\times e^{\gamma T}\left\{\frac{1}{\Delta^2}\sin\big(\Omega(t-T/2-\Delta)\big)\sin\big(\Omega(t'-T/2+\Delta)\big)\right.$$
$$-\frac{1}{\Delta^2}\left[\sin\big(\Omega(t-T/2)\big)\sin\big(\Omega(t'-T/2)\big)\right]$$
$$\left.+\frac{2\Omega}{a\Delta}\sin\big(\Omega(t-t')\big)\right\}.$$

The Minkowski and Rindler $\langle Q_i(\tau_i)^2\rangle_v$ can be evaluated analytically. In the weak coupling limit they are [13]

$$\big\langle Q_A(t)^2\big\rangle_v \approx \frac{1}{2\Omega}(1-e^{-2\gamma t}), \tag{6.20}$$

$$\big\langle Q_B(\eta)^2\big\rangle_v \approx \frac{1}{2\Omega}\coth\left(\frac{\pi\Omega}{a}\right)(1-e^{-2\gamma\eta}). \tag{6.21}$$

However, for the Costa-Villalba trajectory the two-point function is much more complicated. In this analysis, Equation (6.19) was evaluated numerically using Simpson's rule, and when required, Newton's method for root finding. These are summarized in Appendix D.

Calculating $\langle \boldsymbol{P_i(\tau_i)^2}\rangle$

In the weak coupling limit,

$$p_i^{(+)}(\tau_i) = \partial_{\tau_i}q_i^{(+)}(\tau_i) \approx \Omega\lambda_0\int_{\tau_0}^{\tau} d\tau'\, e^{-\gamma(\tau_i-\tau_i')}\cos\big(\Omega(\tau_i-\tau_i')\big)f_0^{(+)}\big(z_i(\tau_i'),\boldsymbol{k}\big)$$

where the derivative of the exponential has been dropped since it is $O(\gamma/\Omega)$. The two-point function is then

$$\langle P_i(\tau_i)P_i(\tau_i')\rangle \approx \theta(\tau_i-\tau_{i_0})\theta(\tau_i'-\tau_{i_0}')\frac{\lambda_0^2}{m_0^2}\int_{\tau_{i_0}}^{\tau_i} d\tilde{\tau}_i \int_{\tau_{i_0}'}^{\tau_i'} d\tilde{\tau}_i'\, e^{-\gamma(\tau_i-\tilde{\tau}_i)}e^{-\gamma(\tau_i'-\tilde{\tau}_i')} \\ \times \cos\big(\Omega(\tau_i-\tilde{\tau}_i)\big)\cos\big(\Omega(\tau_i'-\tilde{\tau}_i')\big)\frac{1}{\sqrt{2\pi}}\left(\frac{1}{\Delta x^2-\Delta t^2}\right).$$

However, since $\gamma \ll \Omega$, the integration will be over many oscillations of the cosines and there will be little difference than if they were sines as in $\langle Q_i(\tau_i)Q_i(\tau_i')\rangle$. Therefore,

$$\langle P_B(\tau)P_B(\tau')\rangle \approx \Omega^2 \langle Q_B(\tau)Q_B(\tau')\rangle .$$

Calculating $\langle \boldsymbol{Q_i(\tau_i), P_i(\tau_i)}\rangle$

By definition,

$$\begin{aligned}\langle Q_i(\tau_i), P_i(\tau_i)\rangle &= \frac{1}{2}\langle Q_i(\tau_i)P_i(\tau_i) + P_i(\tau_i)Q_i(\tau_i)\rangle \\ &= \frac{1}{2}\partial_{\tau_i}\langle Q_i(\tau_i)^2\rangle .\end{aligned}$$

Applying this to the analytical results for the Minkowski and Rindler trajectories (Equations (6.20) and (6.21)), it can be seen that these two-point functions are $O(\gamma)$. In the ultraweak coupling limit, this is dropped and so

$$\langle Q_i(\tau_i), P_i(\tau_i)\rangle \approx 0.$$

Based on this, the Costa-Villalba $\langle Q_B(\tau), P_B(\tau)\rangle$ is also taken to be negligible in the ultraweak coupling limit. In future work, it would be interesting to include this term to see if it has significant effects on the dynamics of entanglement.

Calculating the Cross Correlations

The origin of the cross correlations between A and B is in their indirect interaction through the field. This is expressed in the mode functions as higher order terms in λ_0. In the ultraweak coupling limit, these higher order terms can be neglected. Additionally, if the detectors are far apart there will be significant retardation of the mutual influences and there will be little correlation between the detectors. In the analysis here, it is assumed that the detectors are sufficiently far apart that the cross correlations can be neglected.

6.2.2 State

The contribution to the two-point function due to the state of the detector can be calculated directly to be [13]

$$\begin{aligned}\langle \mathcal{R}_\mu, \mathcal{R}_\nu \rangle_a = \frac{1}{4}\Bigg\{ &\frac{1}{\beta^2}\Re\left(r_\mu^{(A)} + r_\mu^{(B)}\right)\Re\left(r_\nu^{(A)} + r_\nu^{(B)}\right) \\ &+ \alpha^2 \Re\left(r_\mu^{(A)} - r_\mu^{(B)}\right)\Re\left(r_\nu^{(A)} - r_\nu^{(B)}\right) \\ &+ \frac{1}{\Omega_r^2}\Big[\beta^2 \Im\left(r_\mu^{(A)} + r_\mu^{(B)}\right)\Im\left(r_\nu^{(A)} + r_\nu^{(B)}\right) \\ &+ \frac{1}{\alpha^2}\Im\left(r_\mu^{(A)} - r_\mu^{(B)}\right)\Im\left(r_\nu^{(A)} - r_\nu^{(B)}\right)\Big]\Bigg\}.\end{aligned}$$

Inserting the zeroth order expressions for the mode functions, the zeroth order variances are found to be

$$\begin{aligned}\left\langle Q_i^2(\tau_i)\right\rangle_a &= e^{-2\gamma\tau_i}\left[\frac{c_1^+}{\Omega^2}\big(\gamma\sin(\Omega\tau_i) + \Omega\cos(\Omega\tau_i)\big)^2 + c_2^+\sin^2(\Omega\tau_i)\right], \\ \left\langle P_i^2(\tau_i)\right\rangle_a &= e^{-2\gamma\tau_i}\left[\frac{c_1^+}{\Omega^2}(\Omega^2+\gamma^2)^2\sin^2(\Omega\tau_i)\right. \\ &\quad \left. + c_2^+\big(\gamma\sin(\Omega\tau_i) - \Omega\cos(\Omega\tau_i)\big)^2\right], \\ \langle Q_i(\tau_i)P_i(\tau_i)\rangle_a &= e^{-2\gamma\tau_i}\sin(\Omega\tau_i)\left[c_2^+\big(\Omega\cos(\Omega\tau_i) - \gamma\sin(\Omega\tau_i)\big)\right. \\ &\quad \left. - c_1^+\left(1+\frac{\gamma^2}{\Omega^2}\right)\big(\Omega\cos(\Omega\tau_i) + \gamma\sin(\Omega\tau_i)\big)\right], \\ \langle Q_A(t)Q_B(\tau)\rangle_a &= e^{-\gamma(t+\tau)}\left[c_1^-\frac{\gamma}{\Omega}\sin\big(\Omega(t+\tau)\big) + \left(c_1^-\frac{\gamma^2}{\Omega^2} + c_2^-\right)\sin(\Omega t)\sin(\Omega\tau)\right. \\ &\quad \left. + c_1^-\cos(\Omega t)\cos(\Omega\tau)\right], \\ \langle Q_A(t)P_B(\tau)\rangle_a &= e^{-\gamma(t+\tau)}\left[c_2^-\sin(\Omega t)\big(\Omega\cos(\Omega\tau) - \gamma\sin(\Omega\tau)\big)\right. \\ &\quad \left. - c_1^-\sin(\Omega\tau)\left(1+\frac{\gamma^2}{\Omega^2}\right)\big(\Omega\cos(\Omega t) + \gamma\sin(\Omega t)\big)\right], \\ \langle P_A(t)Q_B(\tau)\rangle_a &= e^{-\gamma(t+\tau)}\left[c_2^-\sin(\Omega\tau)\big(\Omega\cos(\Omega t) - \gamma\sin(\Omega t)\big)\right. \\ &\quad \left. - c_1^-\sin(\Omega t)\left(1+\frac{\gamma^2}{\Omega^2}\right)\big(\Omega\cos(\Omega\tau) + \gamma\sin(\Omega\tau)\big)\right],\end{aligned}$$

$$\langle P_A(t)P_B(\tau)\rangle_a = e^{-\gamma(t+\tau)}\left[\left(c_1^-\Omega^2\left(1+\frac{\gamma^2}{\Omega^2}\right)^2 + c_2^-\gamma^2\right)\sin(\Omega t)\sin(\Omega\tau)\right.$$
$$\left. + c_2^-\Omega^2\cos(\Omega t)\cos(\Omega\tau) - \gamma\Omega c_2^-\sin\big(\Omega(t+\tau)\big)\right],$$

where

$$c_1^\pm = \frac{1}{4}\left(\frac{1}{\beta^2}\pm\alpha^2\right), \qquad \text{and} \qquad c_2^\pm = \frac{1}{4\Omega^2}\left(\beta^2\pm\frac{1}{\alpha^2}\right).$$

6.3 Entanglement Dynamics

In this section, the results of a numerical study of the entanglement dynamics between the two detectors in the ultraweak coupling limit is presented. The entanglement was quantified using Σ, as defined in Section 3.2. The only quantity that was calculated numerically was $\langle Q^2\rangle_v$ for the Rindler and Costa-Villalba trajectories, which was done using the extended Simpson's rule with 50001 samples of the integrand. This offered a reasonable balance between accuracy and computational effort. The integration limits of Equation (6.19) required solving the transcendental Equation (B.3), which was done numerically using Newton's method. All other quantities were calculated analytically. Details on these numerical techniques are presented in Appendix D.

The parameters used for the detectors were $m_0 = 1$, $\gamma = 0.00001$, and $\Omega = 2.3$. This, along with the choice of accelerations considered, ensured the system was in the ultraweak coupling regime. The initial state of the detectors was taken to be the entangled Gaussian state (6.1) with $\alpha = 1.1$ and $\beta = 4.5$. The Minkowski detector was taken to be at $b = -0.001$. This distance makes it reasonable to drop the mutual influences. Sigma was calculated as a function of time for various accelerations, and in the Rindler case, an additional position of the Minkowski detector was considered.

The interaction was activated on the Minkowski time slice

$$at_0 = \sinh(-10) - \frac{1}{2}e^{10} \approx -22026.465772106751636,$$

and terminated at

$$at_f = \sinh(10) - \frac{1}{2}e^{-10} \approx 11013.232852003428496.$$

This covers 10 e-folds on both sides of the turnover from inertial to uniform acceleration of the Costa-Villalba trajectory and thus offers a good opportunity to examine the effects of the non-uniform acceleration on entanglement.

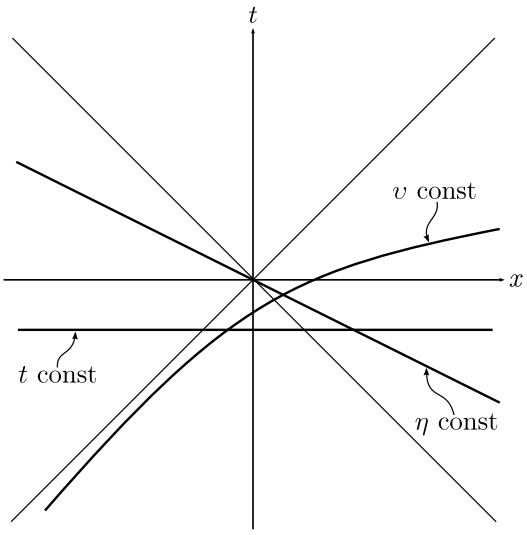

Figure 6.4: The time slicings associated with the detectors. The Costa-Villalba detector measures proper time τ, which is related to υ by Equation (B.3); the Rindler detector η; and the Minkowski detector t.

The evolution of the entanglement between the detectors is described in the time slicings of each observer. The different time slicing schemes are summarized in Figure 6.4. It is important to note that considering different time slicings is not the same as describing entanglement from the point of view of different observers. This is because entanglement is not an observable quantity. Only after they perform a measurement on the state and communicate could they tell if their state was entangled. Furthermore, to estimate the degree in which their state was entangled, they would need to repeat their experiment many times.

6.3.1 Minkowski and Costa-Villalba detectors

In Minkowski time slicing, $\Sigma = \Sigma(t, \tau(\upsilon(t)))$ where $\tau(\upsilon)$ is given by Equation (B.3) and

$$\upsilon(t) = \frac{1}{a}\,\mathrm{arcsinh}\left[\frac{at}{\sqrt{2}}\right] + \frac{1}{a}\ln(\sqrt{2}).$$

The results for several values of a are plotted in Figure 6.5. For the parameters considered, the entanglement present in the initial state decreases as a function of time, regardless of the asymptotic acceleration.

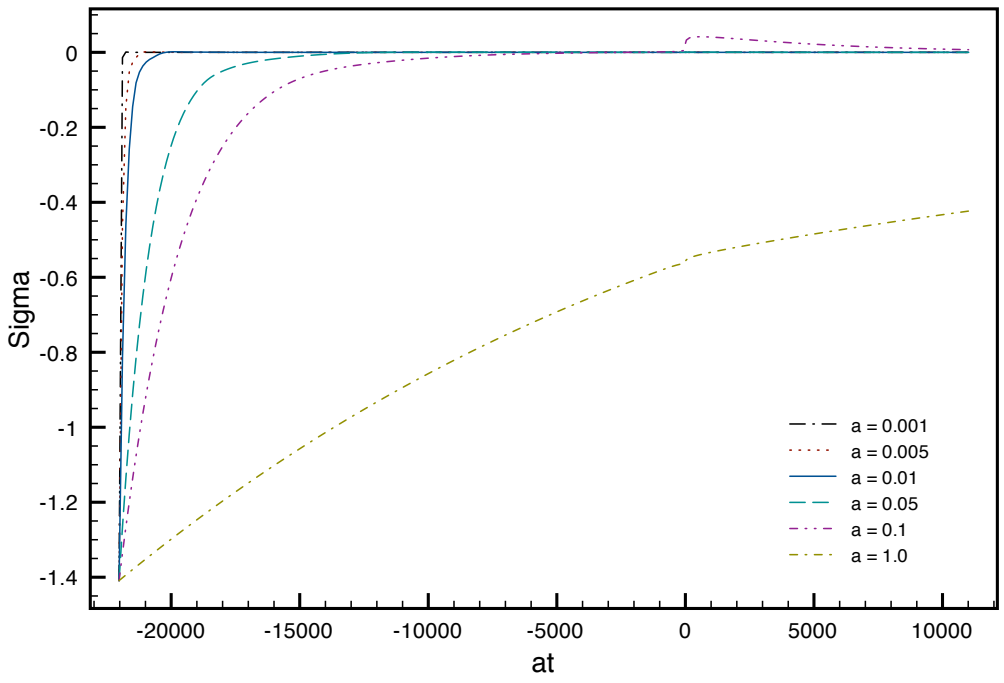

Figure 6.5: Σ in Minkowski time slicing for entanglement between a Minkowski and a Costa-Villalba detector. The horizontal axis is scaled by the asymptotic acceleration and covers 10 e-folds on either side of the transition from inertial to uniform acceleration. The peaks present are likely numerical artifacts.

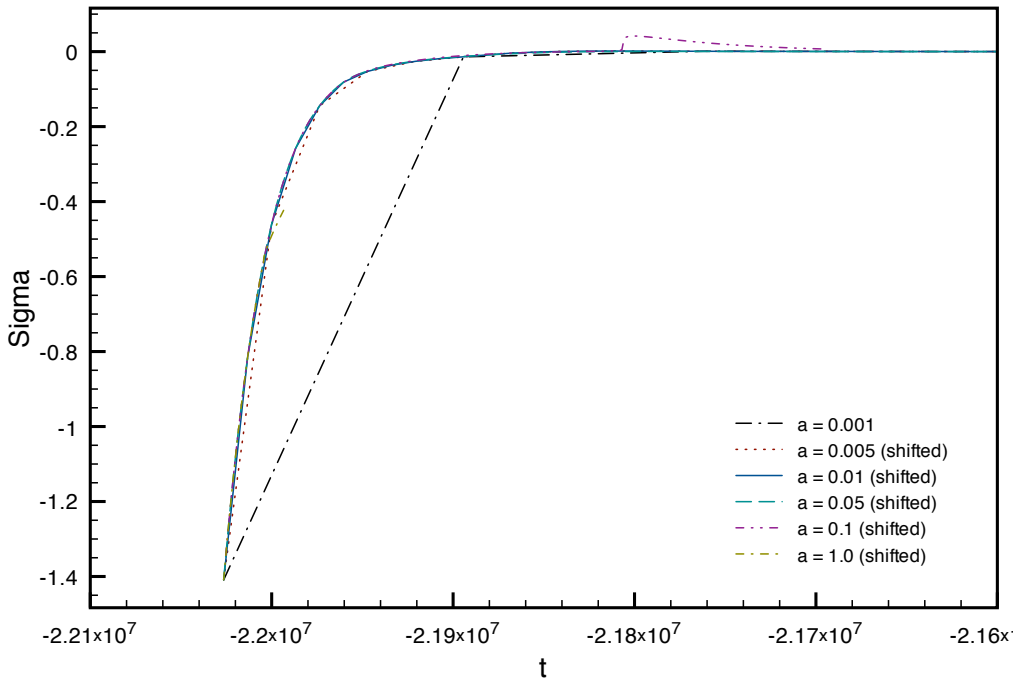

Figure 6.6: Σ in Minkowski time slicing for entanglement between a Minkowski and a Costa-Villalba detector. It is plotted in Minkowski proper time and, for the purposes of comparison, the curves have been shifted so that they all start at the same time. There is little acceleration dependence in this parameter range.

While each curve looks different, this is a result of the scale. Even though each curve covers 10 e-folds of the turnover, the duration of the interaction is different for each value of a. Rescaling the curves to Minkowski proper time shows that in fact, the entanglement dynamics are not sensitive to the asymptotic acceleration of the Costa-Villalba observer. This is expected since most of the change in entanglement occurs before the Rindler regime of the Costa-Villalba trajectory. To facilitate the comparison, the curves in Figure 6.6 are shifted such that they start at the same time.

There are several small peaks in the sigma curves. The peaks occur at $at \approx 44.0529$ and $at \approx 157.3319$ for the $a = 1$ and $a = 0.1$ curves, respectively. There are similar peaks in the other curves, however they cannot be seen on the scale of Figure 6.5; see Figure 6.7 for a close up. Since these peaks do not occur at the same time, and more significantly, not near $t = 0$ where the

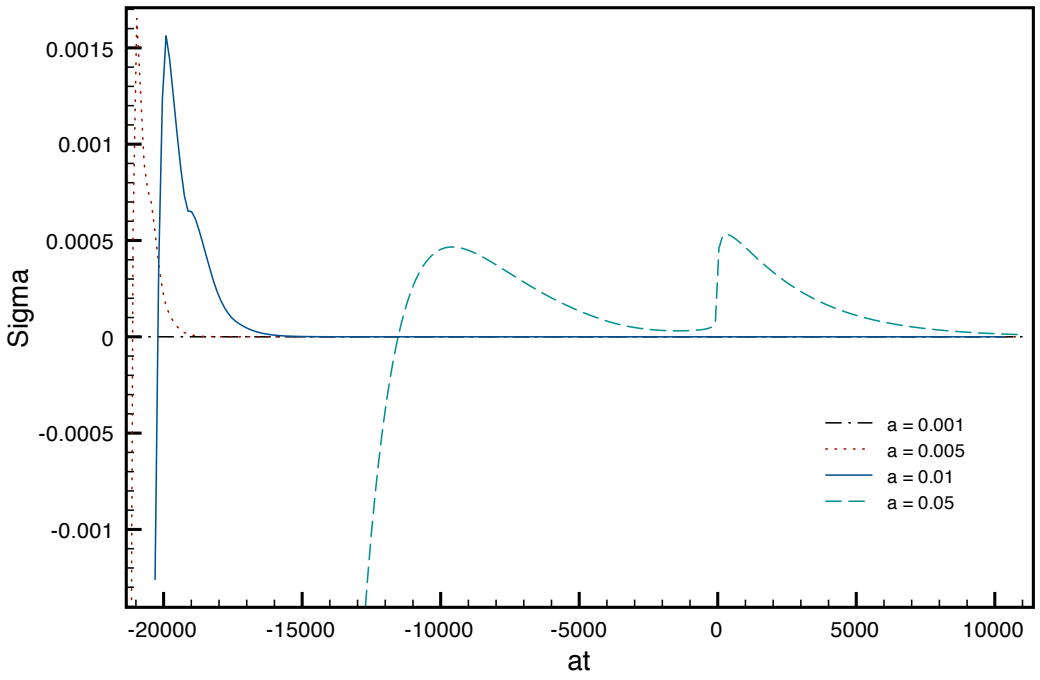

Figure 6.7: The peaks present in Σ in Minkowski time slicing. They are likely a numerical artifact.

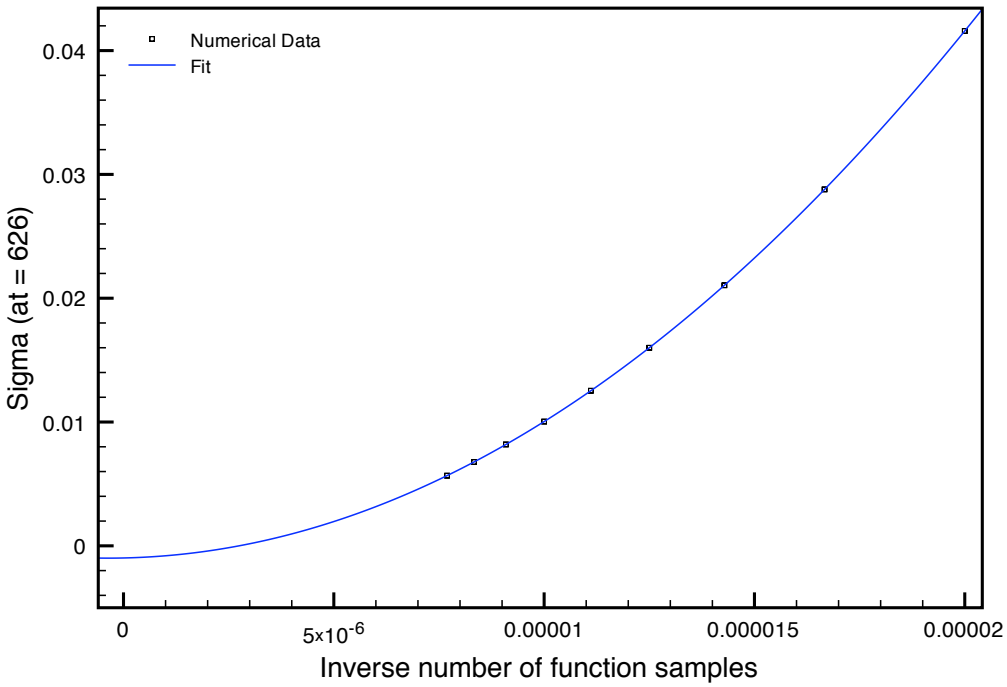

Figure 6.8: Finite size scaling analysis of the peak in Σ with $a = 0.1$. The data was fit to $Ax^2 + Bx + C$ where $A = 1.02668 \times 10^8$, $B = 75.0742$, $C = -0.00098042$. In the continuum limit (infinite number of function samples), $\Sigma = -0.00098042$.

most dramatic changes occur in the trajectory, it is likely they are numerical artifacts. To test if this is the case, a finite size scaling analysis is performed. This involves calculating Σ at a single point for several different numbers of function samples. The resulting values are then plotted against the reciprocal of the number of function samples. This shows how the calculation depends on the size of the finite sampling in the numerical integration. A better estimate of the true value can then be obtained by extrapolating to an infinite number of function samples (continuum limit). As can be seen in Figure 6.8, for $a = 0.1$ the peak was reduced and the estimated true value is approximately -9.8042×10^{-4}. Since this value is negative, the detectors are entangled. This strengthens the argument that this is a numerical artifact but does not settle it. While unlikely, there could still be a small peak and further analysis would be needed to completely determine if the peak is a physical effect.

Disentanglement was not observed for any values of a except for $a = 0.1$

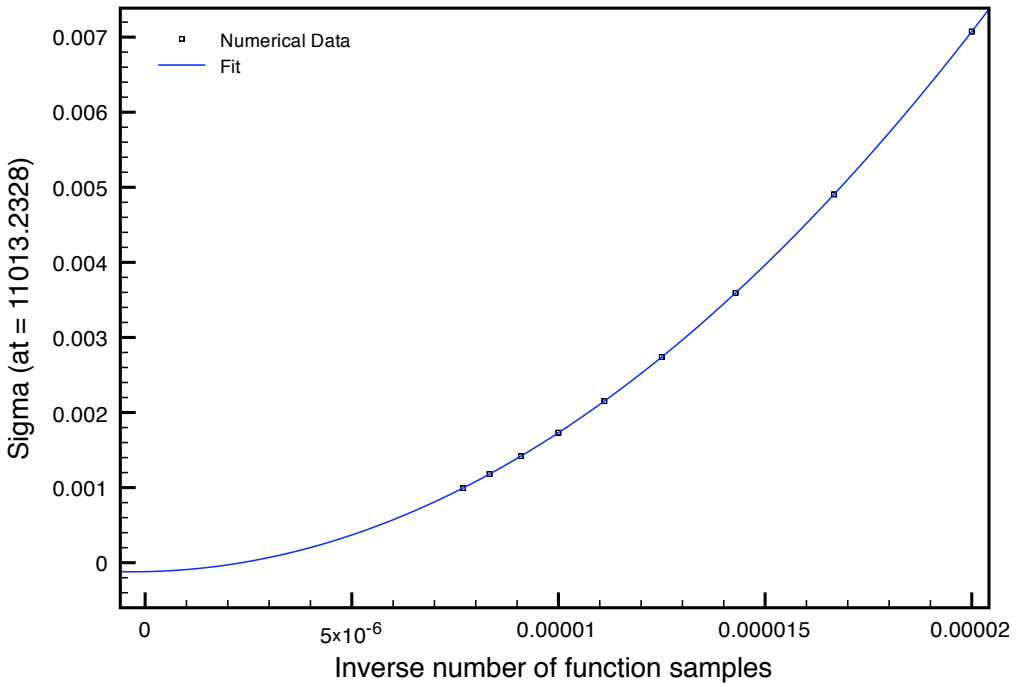

Figure 6.9: Finite size scaling analysis of the last data point of Σ with $a = 0.1$. The data was fit to $Ax^2 + Bx + C$ where $A = 1.74609 \times 10^7$, $B = 10.4737$, $C = -0.00011937$. In the continuum limit (infinite function samples), $\Sigma = -0.00011937$.

and $a = 0.05$. In those cases, Σ remained positive after the artificial peak. This again is due to numerical accuracy and to see that that was the case, another finite size scaling analysis was performed on the last data point of the $a = 0.1$ curve. As can be seen in Figure 6.9, the estimated true value is approximately -1.1937×10^{-4}. This indicates that the detectors remained entangled for the entire duration of the interaction. Furthermore, the similarity of the curves suggests that disentanglement does not occur for any acceleration considered. This is expected based on the results of [13]. In their analysis, they found that to zeroth order, no disentanglement occurs for the Rindler trajectory. However, the first order correction causes Σ to become positive. It is expected that the same behavior would happen here and it would be interesting to see the effect of the higher order corrections.

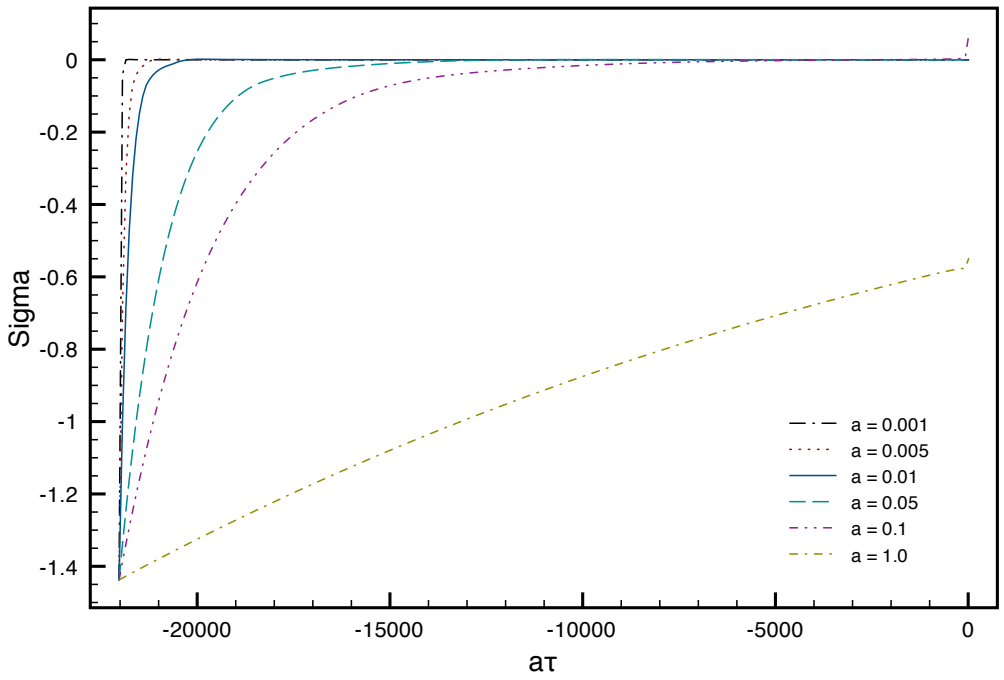

Figure 6.10: Σ in Costa-Villalba time slicing for entanglement between a Minkowski and a Costa-Villalba detector. The horizontal axis is scaled by the asymptotic acceleration and covers 10 e-folds on either side of the transition from inertial to uniform acceleration.

In Costa-Villalba time slicing, $\Sigma = \Sigma(t(\tau), \tau)$ where

$$t(\tau) = \frac{1}{b} - \frac{1}{a} e^{-a\upsilon},$$

and υ is obtained by inverting Equation (B.3). In Figure 6.10, it can be seen that for early times, there is little difference between the two slicings. This is expected since τ is approximately t for early times. However, after $t = 0$ there is significant time dilation due to the rapid change in acceleration. Overall, the dynamics of entanglement are very similar in both time slicings.

6.3.2 Minkowski and Rindler detectors

For a system consisting of a Minkowski detector and a Rindler detector analyzed in Minkowski time slicing, $\Sigma = \Sigma(t, \eta(t))$ where

$$\eta(t) = \frac{1}{a} \operatorname{arcsinh}(at).$$

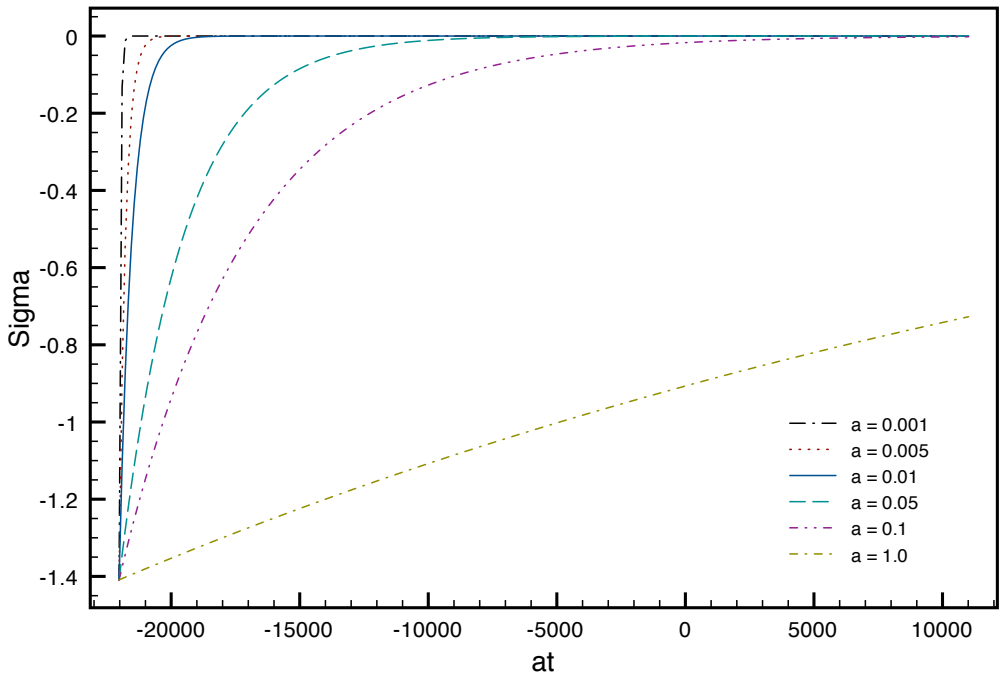

Figure 6.11: Σ in Minkowski time slicing for entanglement between a Minkowski and Rindler detector. Here, the Minkowski observer is in the left Rindler wedge at $b = -0.001$.

The evolution of the entanglement as quantified by Σ is depicted in Figure 6.11 for several different accelerations. The entanglement decreases as a function of time for all the parameters considered. The curves approach zero, but no disentanglement occurs to this order. It is expected that the next order correction would cause disentanglement to occur as found in [13]. Again, in Minkowski time slicing the dynamics of the entanglement are not sensitive to a. This can be seen in Figure 6.12 where Σ is plotted as a function of Minkowski proper time and each curve has been shifted to allow for comparison. This agrees with the findings of [13] where it was also found that there was no acceleration dependence to zeroth order. This suggests that, at least to zeroth order, the Davies-Unruh effect plays a minor role in the dynamics of the entanglement in Minkowski slicing.

In Rindler time slicing

$$t(\eta) = \frac{1}{b}\tanh(a\eta).$$

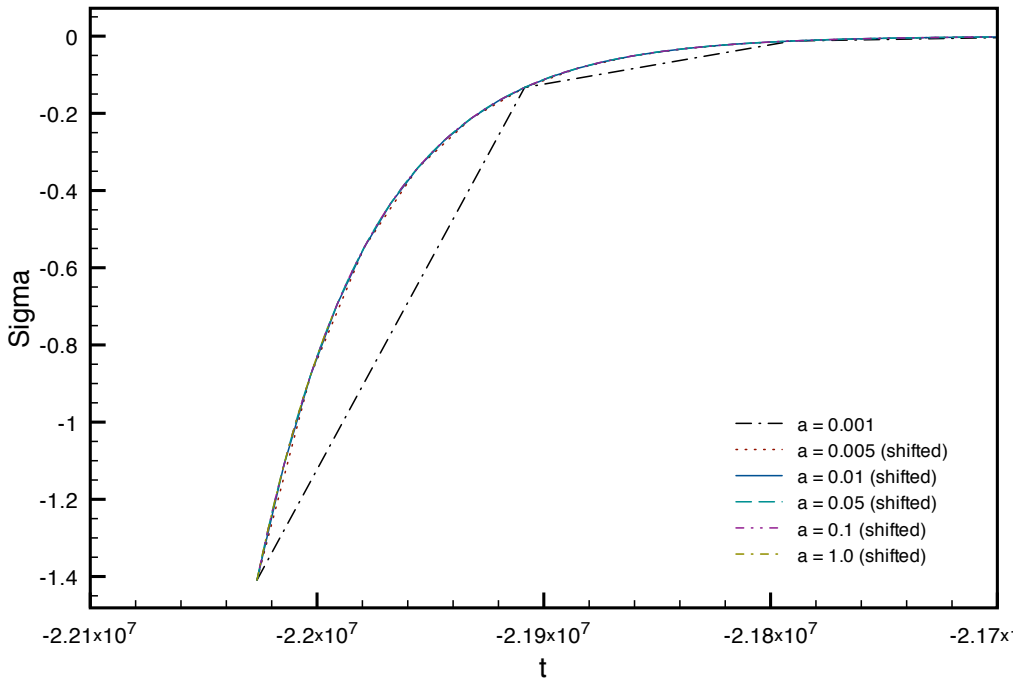

Figure 6.12: Σ in Minkowski time slicing for entanglement between a Minkowski and a Rindler detector. It is plotted in Minkowski proper time and, for the purposes of comparison, the curves have been shifted so they start at the same time. The Minkowski detector is located in the left Rindler wedge at $b = -0.001$.

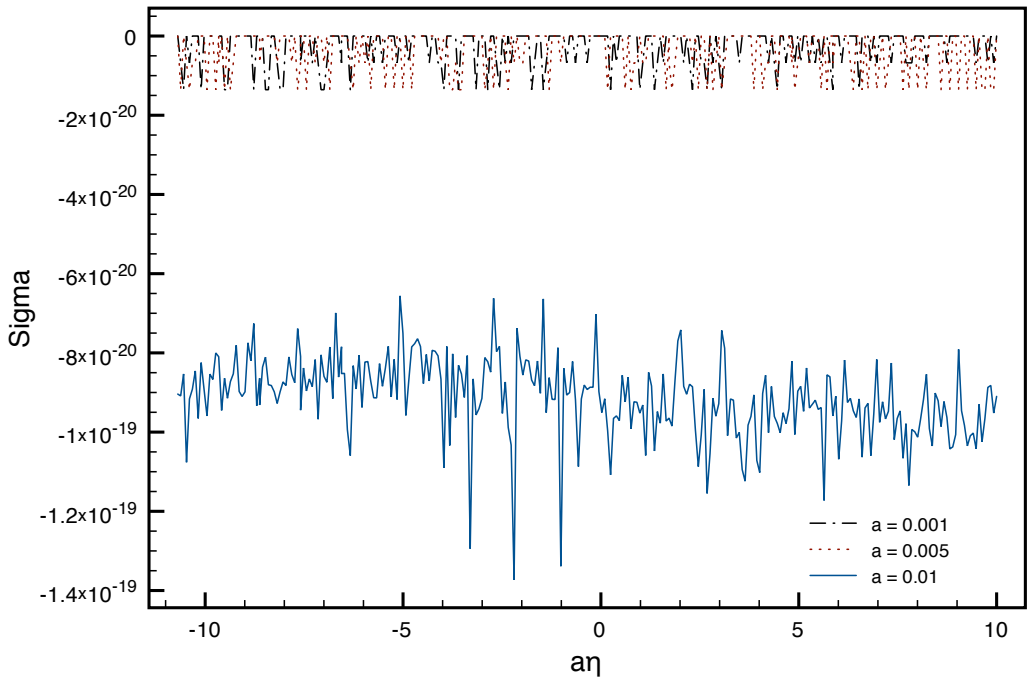

Figure 6.13: Σ in Rindler time slicing for entanglement between a Minkowski and a Rindler detector. The Minkowski detector is in the left Rindler wedge with $b = -0.001$. The noise present is round off error.

Note that if the Minkowski observer is in the left Rindler wedge ($b < 0$), then t is a decreasing function of η. In this case, the time evolution of the Minkowski detector proceeds in the opposite direction relative to that of Minkowski time slicing or if the detector was in the right wedge. This has a qualitative difference on the evolution of entanglement between the detectors.

When $b = -0.001$, the entanglement is found to increase as a function of time. While there is essentially no entanglement for the duration of the interaction for the smallest accelerations considered (Figure 6.13), larger accelerations generated more entanglement as can be seen in Figures 6.14, 6.15, and 6.16. This is similar to the results of [34, 35] where they found that two Unruh-DeWitt detectors interacting with a field in causally disconnected regions of spacetime could become entangled. Their conclusion was that since the interaction was local, the entanglement must have been extracted from the vacuum itself.

In contrast, entanglement was found to decrease as a function of time

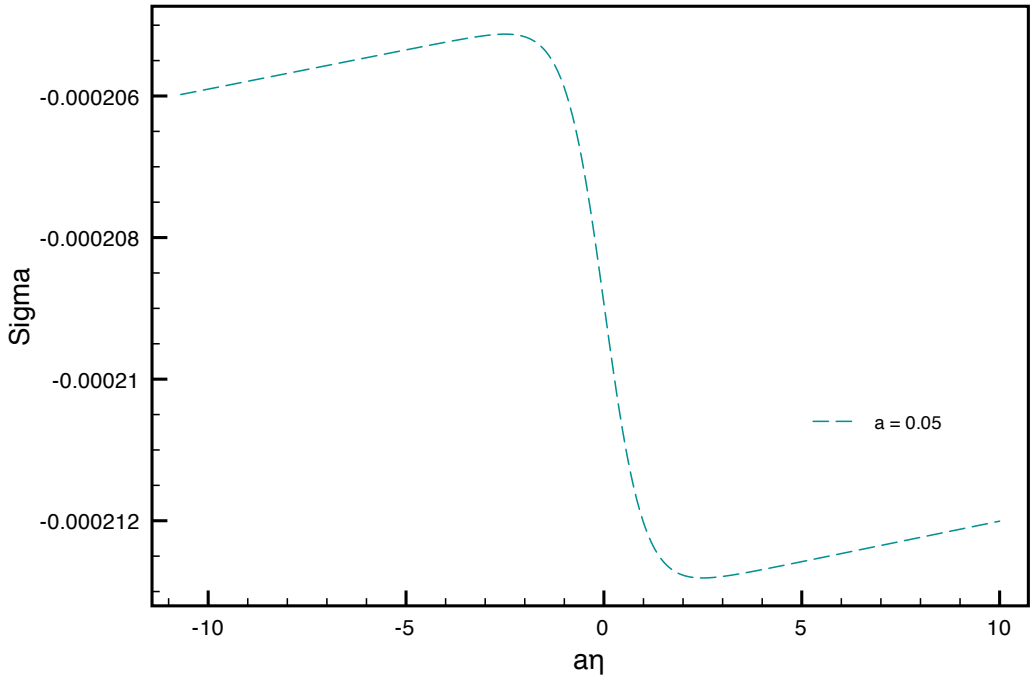

Figure 6.14: Σ in Rindler time slicing for entanglement between a Minkowski and a Rindler detector with $a = 0.05$. The Minkowski detector is located in the left Rindler wedge at $b = -0.001$.

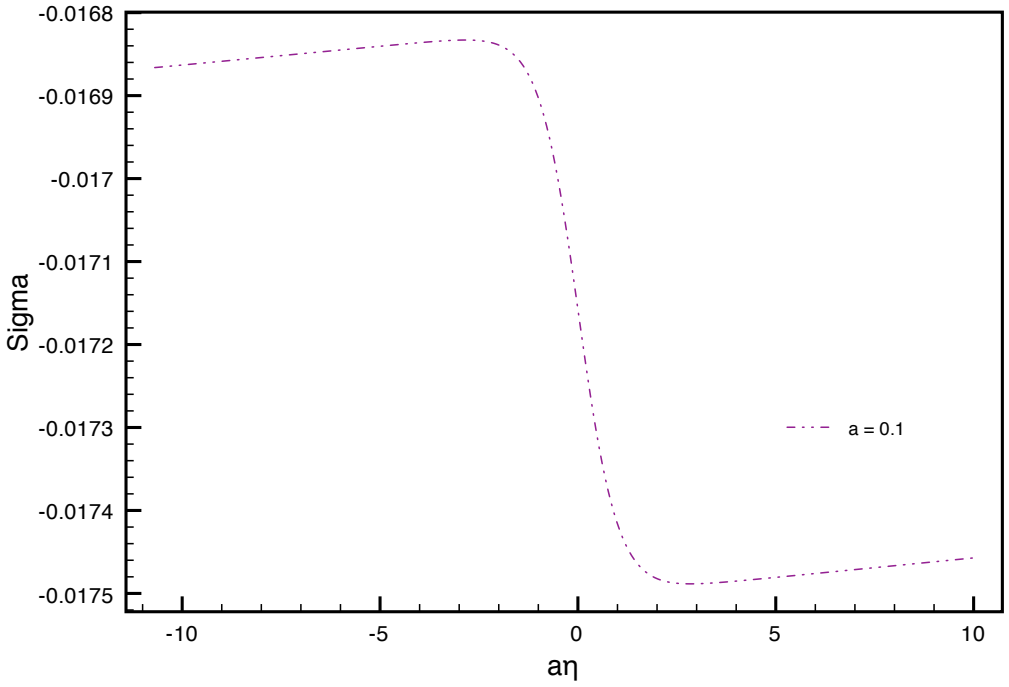

Figure 6.15: Σ in Rindler time slicing for entanglement between a Minkowski and a Rindler detector with $a = 0.1$. The Minkowski detector is located in the left Rindler wedge at $b = -0.001$.

when $b = 1$. Since this is the only parameter that changed, it suggests that the time reversal associated with the left Rindler wedge plays a role in the increase of entanglement observed there. The larger the acceleration, the more entanglement there is throughout the interaction. This is shown in Figures 6.18, 6.19, and 6.20. For the smallest accelerations considered, there was essentially no entanglement during the interaction as can be seen in Figure 6.17. This is likely due to the increased interaction time for small accelerations. The system could have disentangled within the first few data points and if the interaction time was extended for the higher accelerations, they would eventually show similar behavior. However, further numerical calculations would be needed to verify this.

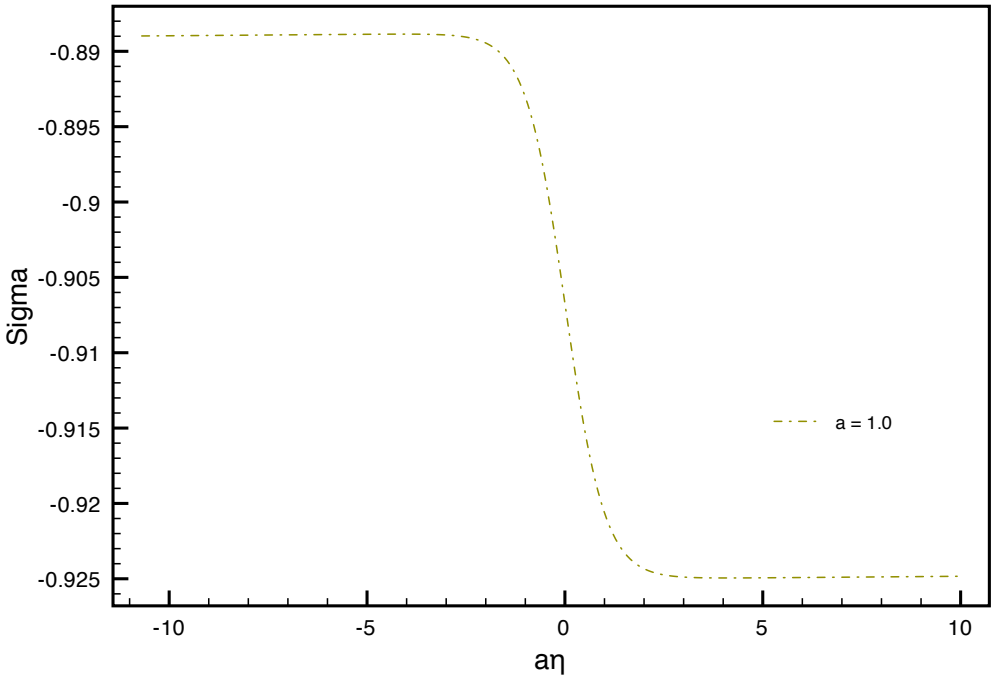

Figure 6.16: Σ in Rindler time slicing for entanglement between a Minkowski and a Rindler detector with $a = 1$. The Minkowski detector is located in the left Rindler wedge at $b = -0.001$.

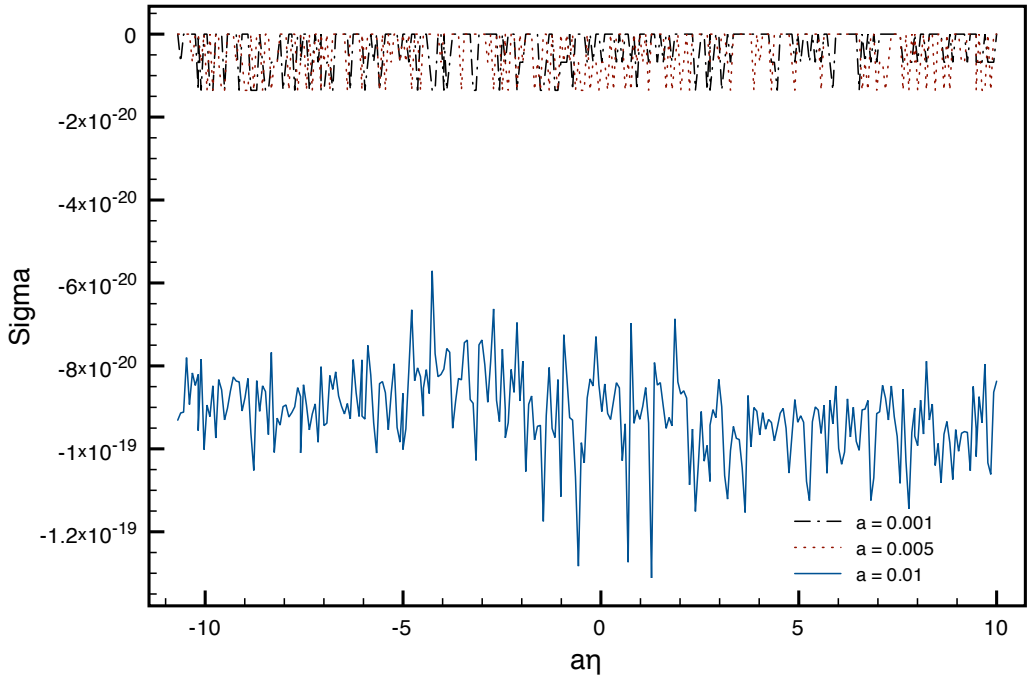

Figure 6.17: Σ in Rindler time slicing for entanglement between a Minkowski and a Rindler detector. The Minkowski detector is located in the right Rindler wedge at $b = 1$. The noise present is round off error.

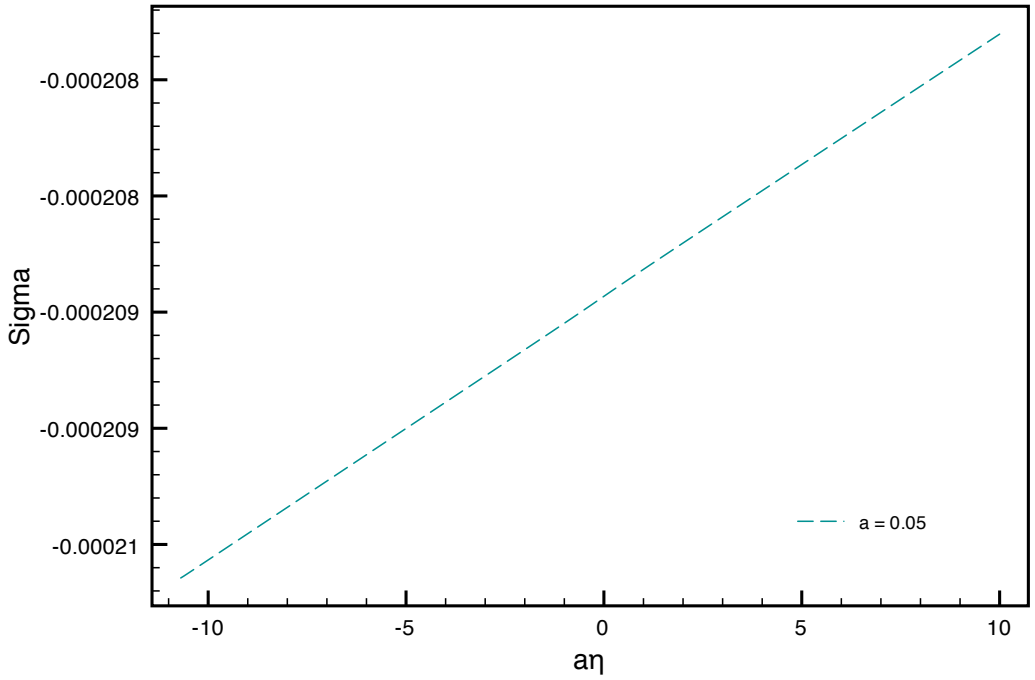

Figure 6.18: Σ in Rindler time slicing for entanglement between a Minkowski and a Rindler detector with $a = 0.05$. The Minkowski detector is located in the right Rindler wedge at $b = 1$.

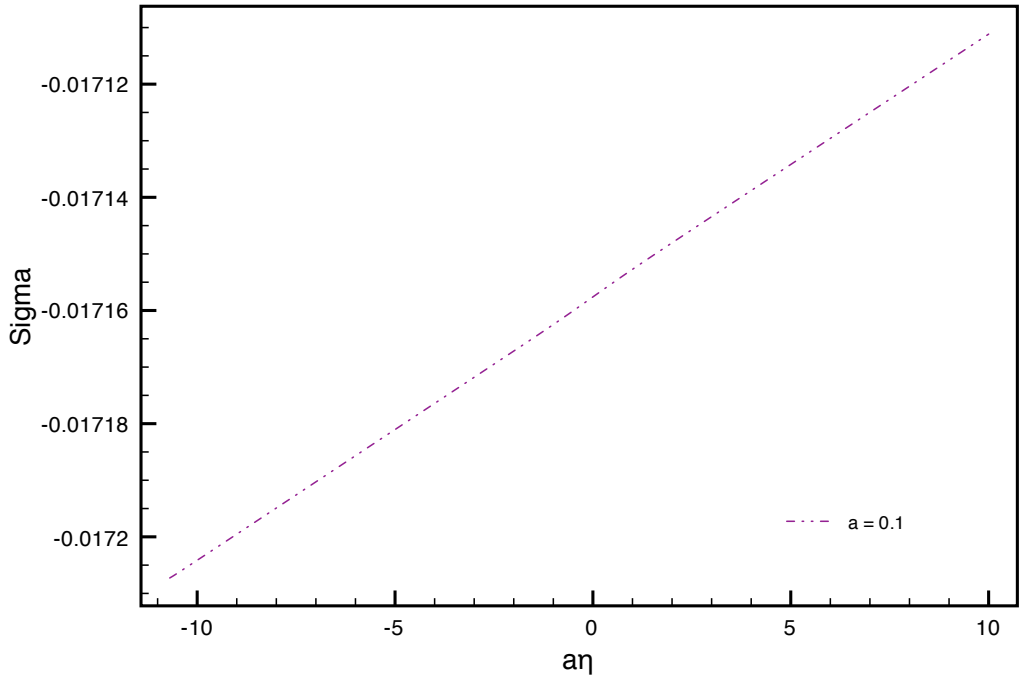

Figure 6.19: Σ in Rindler time slicing for entanglement between a Minkowski and a Rindler detector with $a = 0.1$. The Minkowski detector is located in the right Rindler wedge at $b = 1$.

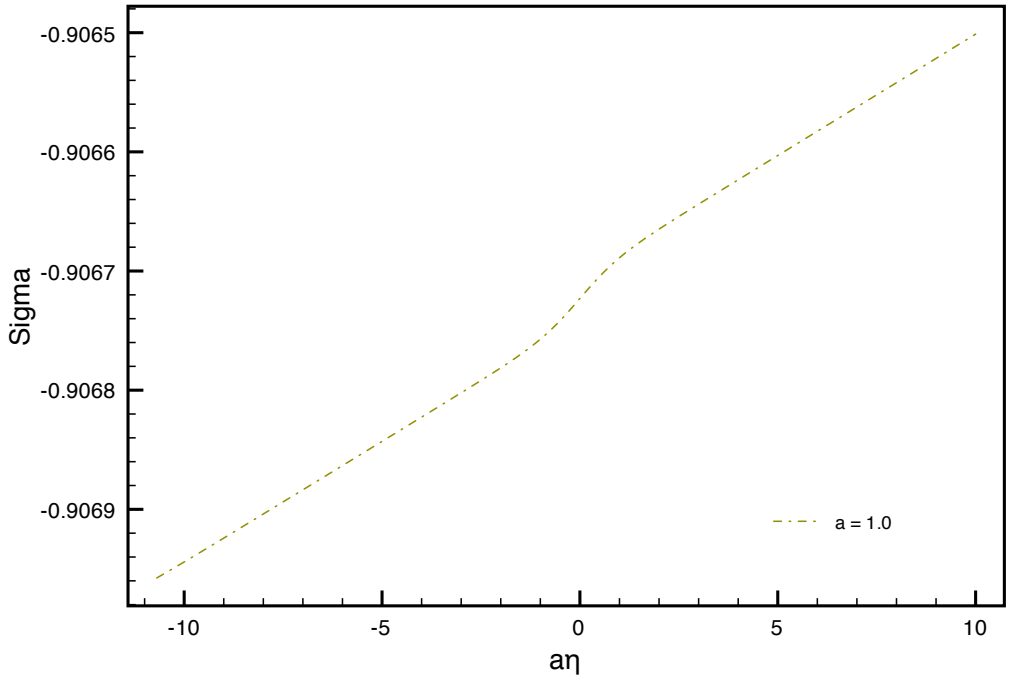

Figure 6.20: Σ in Rindler time slicing for entanglement between a Minkowski and a Rindler detector with $a = 1$. The Minkowski detector is located in the right Rindler wedge at $b = 1$.

6.3.3 Comparisons

This section compares the cases of two Minkowski detectors (obtained analytically), one Minkowski and one Rindler detector, and one Minkowski detector and one Costa-Villalba detector. These comparisons are made in Minkowski time slicing as that is the only time slicing common to all three cases.

As can be seen in Figures 6.21 and 6.22, the dynamics of the entanglement for the Costa-Villalba case are almost identical to that of two Minkowski detectors until near $t = 0$. This is expected since the acceleration of the Costa-Villalba detector is changing very rapidly near this time. The difference between the two cases is more pronounced with larger accelerations (compare Figure 6.21 to Figure 6.22) and it is anticipated that this trend will continue.

For the parameters considered, the entanglement between a Minkowski and a Costa-Villalba detector decreases more rapidly than for the Rindler case, which showed the least degradation of entanglement throughout the interaction. The two Minkowski detectors lost their entanglement the most rapidly. It would be interesting to see if this behavior is generic over a wider range of parameters and when the next order corrections are taken into account.

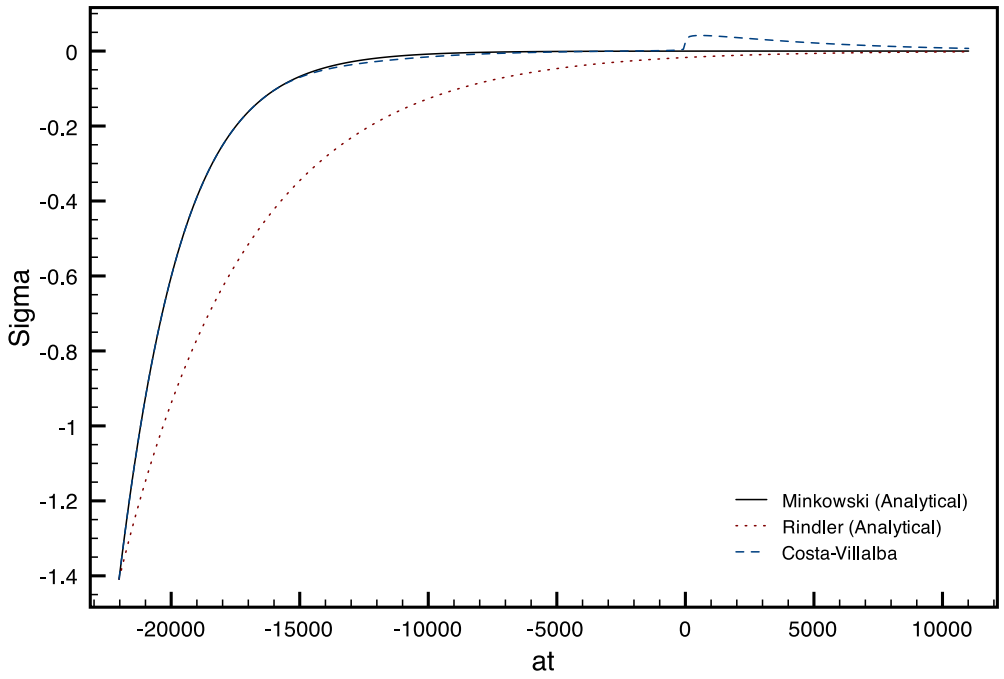

Figure 6.21: Comparison of the dynamics of Σ in Minkowski time slicing for entanglement between two Minkowski detectors; a Minkowski and a Costa-Villalba detector; and a Minkowski and a Rindler detector. The asymptotic acceleration of the Costa-Villalba detector is $a = 0.1$, which is also the acceleration of the Rindler detector.

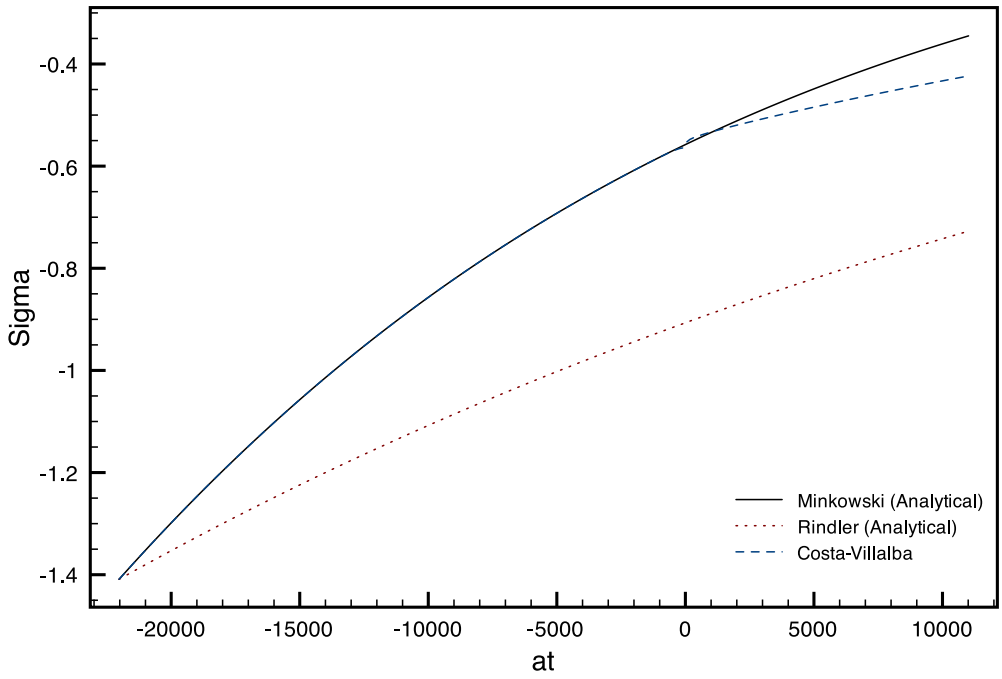

Figure 6.22: Comparison of the dynamics of Σ in Minkowski time slicing for entanglement between two Minkowski detectors; a Minkowski and a Costa-Villalba detector; and a Minkowski and a Rindler detector. The asymptotic acceleration of the Costa-Villalba detector is $a = 1$, which is also the acceleration of the Rindler detector.

Chapter 7

Conclusion and Future Work

The goal of this thesis was to study entanglement in non-inertial frames. It was shown in Chapter 5 that entanglement can be extracted from the Minkowski vacuum of a Dirac spinor field by projective measurements performed by a uniformly accelerating observer. The physical mechanism at work is the Davies-Unruh effect. The produced state is always entangled and its entanglement increases as a function of the acceleration, reaching maximal entanglement in the asymptotic limit of infinite acceleration.

This entanglement is between the occupation number of two modes, which is a plane wave state that is not physically realizable. Any realistic implementation of this effect would require the use of wave packets and it would be interesting to extend the analysis to that case. Squeezed states are a natural choice since the Bogoliubov transform is a squeezing operation.

Another related problem would be to see if the acceleration of the Rindler observer can be deduced by the Minkowski observer from the entangled state produced. While this wouldn't make for a very practical accelerometer, since the observers need to communicate in order to utilize the entanglement (why not just communicate the acceleration?), it would still be interesting to see how the parameters of the dynamics can be extracted from the particle production. This is analogous to the work in [40] where they found that the entanglement between the particles produced by an expanding Robertson-Walker universe encodes the parameters of the spacetime.

Chapter 6 studied the dynamics of two entangled Unruh-DeWitt detectors interacting with a massless Klein-Gordon field. One detector was taken to be stationary while the other was undergoing non-uniform acceleration. The trajectory of the moving detector was initially inertial and smoothly transitions

to a uniform acceleration. In the parameter range considered, entanglement decreased more rapidly in Minkowski time slicing for the case where one detector had non-uniform acceleration than if it had had uniform acceleration. However, it was not as rapid as two inertial detectors.

The dynamics of entanglement were also described in the time slicings associated with each observer. It was found that in the ultraweak coupling limit, the entanglement decreased as a function of time for all parameters considered. In the case where one observer was detector was moving with uniform acceleration, it was found that there was a qualitative difference in the dynamics of the entanglement depending on the separation of the detectors. For the parameters considered, entanglement decreased as a function of time when the inertial detector was in the right Rindler wedge but increased as a function of time when the detector was in the left wedge. This increase in entanglement warrants further study. It would be interesting to know whether it is a generic feature over a wide parameter range and what role the distance dependence (and the associated time reversal for the Minkowski observer) plays.

It would also be interesting to study the dynamics of entanglement over a larger parameter range. In particular, higher accelerations are expected to bring about more of a difference between the Costa-Villalba and Minkowski cases. It would be interesting to see if the case of two Minkowski detectors always loses entanglement faster than the Costa-Villalba case in Minkowski time slicing.

Finally, it would be interesting to go beyond the ultraweak coupling limit. This would involve evaluating the entire two point correlation matrix. For the Costa-Villalba observer, this is a considerable computational task especially since the mutual influences can no longer be ignored.

While there is still much to be learned about relativistic quantum information, this thesis, along with similar research, has demonstrated that relativity adds a new layer of possibilities for both practical and fundamental insights into quantum information and nature.

Appendices

Appendix A

Rindler Coordinates

Uniform acceleration is most conveniently described in the Rindler coordinate system [41]. They are named after Rindler not because he discovered them, but rather because he most thoroughly examined their physical properties. The Rindler coordinates (η, ξ) are defined in terms of the Minkowski coordinates (t, x) as

$$t = \frac{1}{a} e^{a\xi} \sinh(a\eta), \tag{A.1}$$

$$x = \frac{1}{a} e^{a\xi} \cosh(a\eta), \tag{A.2}$$

as can be seen in Figure A.1. These coordinates take values $-\infty < \eta, \xi < \infty$ and cover the region $x > |t|$, which is called the *right Rindler wedge* and is denoted I. The inverse transformation is

$$\eta = \frac{1}{a} \operatorname{arctanh}(t/x),$$
$$\xi = \frac{1}{2a} \ln[a^2(x^2 - t^2)].$$

Another Rindler coordinate system is needed to cover the region $-x > |t|$ (the *left Rindler wedge*, which is denoted *II*). The definition of these coordinates differ from Equations (A.1) and (A.2) by an overall minus sign. Note that this means that η is a decreasing function of t — time "flows backwards" in this wedge. Both coordinate systems give rise to the line element

$$ds^2 = e^{-2a\xi}(d\xi^2 - d\eta^2).$$

The left Rindler wedge is casually disconnected from the right Rindler wedge. However, they can both be influenced by events in the region $-t > |x|$,

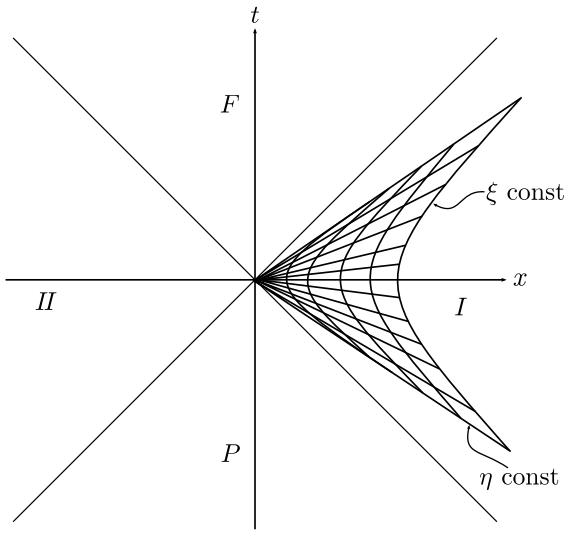

Figure A.1: The Rindler coordinate system in the right Rindler wedge (I). The lines of constant ξ are the worldlines of uniformly accelerating observers. Also shown are the left Rindler wedge (II), the future wedge (F), and the past wedge (P).

which is called the *past wedge*, denoted P. Similarly, both wedges are causally connected to the *future wedge*, which is the region $t > |x|$ and is denoted F.

A.1 Rindler Observers

Observers whose worldline is a line of constant ξ are called *Rindler observers*. In particular, the trajectory an observer with $\xi = \xi_0$ is given in terms of Minkowski coordinates as

$$z^\mu(\eta) = \frac{1}{a} e^{a\xi_0} \left[\sinh(a\eta), \cosh(a\eta)\right].$$

This observer is confined to the right Rindler wedge with the lines $t = x$ and $t = -x$ as communication horizons. This observer's proper time is $e^{a\xi_0}\eta$, from which the proper velocity is found to be

$$v^\mu(\eta) = e^{-a\xi_0} \frac{\partial z^\mu}{\partial \eta} = \left[\cosh(a\eta), \sinh(a\eta)\right].$$

The proper acceleration is

$$a^\mu(\eta) = e^{-a\xi_0} \frac{\partial v^\mu}{\partial \eta} = \frac{1}{a} e^{-a\xi_0} \left[\sinh(a\eta), \cosh(a\eta)\right],$$

which has a constant magnitude squared of

$$a_\mu a^\mu = \frac{1}{a^2} e^{-2a\xi_0}.$$

Therefore, the Rindler observers are moving with a uniform acceleration of $ae^{-a\xi_0}$. In particular, the line $\xi = 0$ is the worldline of an observer who measures proper time η and is moving with uniform acceleration a. This observer crosses the $t = 0$ line at $\eta = 0$ and $x = 1/a$. This is why the Rindler coordinates are ideal for describing uniform motion. In addition to observers in the right wedge, there are analogous observers in the left wedge, whose trajectories are the lines of constant ξ in that wedge.

Appendix B

Costa-Villalba Coordinates

The Costa-Villalba coordinates (υ, ζ) are related to the Minkowski coordinates (t, x) by

$$t + x = \frac{2}{w}\sinh\big(w(\upsilon + \zeta)\big), \tag{B.1}$$

$$t - x = -\frac{1}{w}\exp\big(-w(\upsilon - \zeta)\big), \tag{B.2}$$

as can be seen in Figure B.1. They take values $-\infty < \upsilon, \zeta < \infty$ and cover the region $x > t$. These coordinates give rise to the line element

$$ds^2 = (e^{-2w\upsilon} + e^{2w\zeta})(d\zeta^2 - d\upsilon^2).$$

The inverse transformations are given by

$$\upsilon + \zeta = \frac{1}{w}\operatorname{arcsinh}\left(\frac{w}{2}(t + x)\right),$$
$$\upsilon - \zeta = -\frac{2}{w}\ln\big(-w(t - x)\big),$$

or equivalently,

$$\upsilon = \frac{1}{2w}\operatorname{arcsinh}\left(\frac{w}{2}(t + x)\right) - \frac{1}{2w}\ln\big(-w(t - x)\big),$$
$$\zeta = \frac{1}{2w}\operatorname{arcsinh}\left(\frac{w}{2}(t + x)\right) + \frac{1}{2w}\ln\big(-w(t - x)\big).$$

An alternate form of Equations (B.1) and (B.2) is

$$t = \frac{1}{w}e^{w\zeta}\sinh(w\upsilon) - \frac{1}{2w}\exp\big(-w(\upsilon + \zeta)\big),$$
$$x = \frac{1}{w}e^{w\zeta}\cosh(w\upsilon) - \frac{1}{2w}\exp\big(-w(\upsilon + \zeta)\big),$$

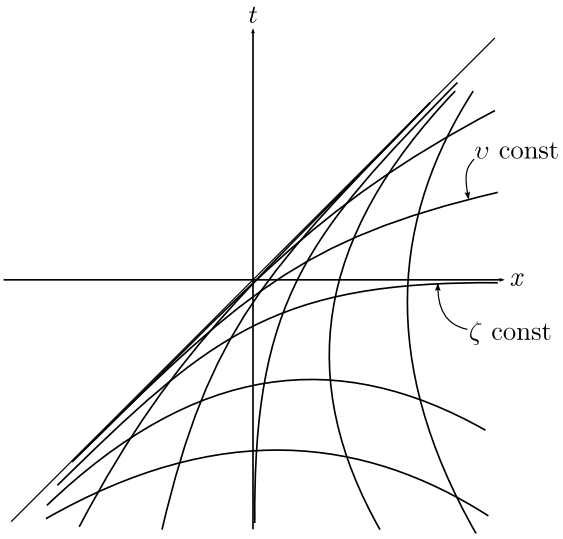

Figure B.1: The Costa-Villalba coordinate system, which covers the region $x > t$. The lines of constant ζ are the wordlines of observers who start inertial and smoothly transition to uniform acceleration.

which allows these coordinates to be viewed as Rindler coordinates with a correction. The rest of Minkowski space can be covered by introducing another coordinate system that is the reflection of the above about the null line $t = x$.

The author refers to these coordinates Costa-Villalba coordinates since Costa and Villalba studied them in the context of particle creation due to non-inertial motion. They were first introduced by Kalnins in his study of the separability of the Laplace equation in two and three dimensional Minkowski space (i.e., the Klein Gordon equation) [42]. Costa further studied them in a series of papers about separable coordinates and particle creation. In the first, he reproduced the coordinate systems of Kalnins by a different method, concentrating on their kinematical properties [43]. In the second, he constructs two vacua of a massive Klein Gordon field corresponding to the asymptotes of a the motion of Costa-Villalba observers [44], introduced in the next section. By calculating the Bogoliubov coefficients linking these vacua to the Minkowski vacuum, he finds that in the asymptotic future, the observer perceives a thermal distribution at the Unruh temperature. In the third, Costa and Svaiter consider the Bogoliubov transformations to the Milne and Rindler vacua [45], which are the true limiting cases of the motion.

Building on [44], Percoco and Villalba found the vacua associated with

these observers for massless Klein-Gordon fields as well as both massive and massless Dirac fields [46]. Villalba and Mateu also used these coordinates to study massive Klein-Gordon and Dirac fields in the presence of a magnetic field [47].

B.1 Costa-Villalba Observers

An observer whose worldline is $\zeta = \zeta_0$ for some constant ζ_0, is called a *Costa-Villalba observer*. Their trajectory, given in Minkowski coordinates, is

$$z^\mu(\upsilon) = \left[\frac{1}{w}e^{w\zeta_0}\sinh(w\upsilon) - \frac{1}{2w}\exp\big(-w(\upsilon+\zeta_0)\big),\right.$$
$$\left.\frac{1}{w}e^{w\zeta_0}\cosh(w\upsilon) - \frac{1}{2w}\exp\big(-w(\upsilon+\zeta_0)\big)\right],$$

where υ is the evolution parameter. The observer's proper time τ is obtained from the line element on the trajectory

$$ds^2 = -d\tau^2 = -\left(e^{-2w\upsilon} + e^{2w\zeta_0}\right)d\upsilon^2.$$

This implies

$$\frac{d\tau}{d\upsilon} = \sqrt{e^{-2w\upsilon} + e^{2w\zeta_0}},$$

which can be integrated to obtain[1]

$$\tau = \frac{1}{w}e^{w\zeta_0}\operatorname{arcsinh}\left(e^{w(\upsilon+\zeta_0)}\right) - \frac{1}{w}\sqrt{e^{-2w\upsilon} + e^{2w\zeta_0}}. \tag{B.3}$$

The observer's proper velocity is then

$$v^\mu = \frac{dz^\mu}{d\tau}$$
$$= \frac{1}{\sqrt{e^{-2w\upsilon} + e^{2e\zeta_0}}}\left[e^{w\zeta_0}\cosh(w\upsilon) + \frac{1}{2}\exp\big(-w(\upsilon+\zeta_0)\big),\right.$$
$$\left.e^{w\zeta_0}\sinh(w\upsilon) + \frac{1}{2}\exp\big(-w(\upsilon+\zeta_0)\big)\right],$$

[1]Note that the expressions for the proper time in [44] and [47] are incorrect. In both, the second term is mistakenly positive, while in Villalba and Mateu there is also a missing square root.

and the proper acceleration is

$$\begin{aligned} a^\mu &= \frac{dv^\mu}{d\tau} \\ &= \frac{w}{e^{-2w\upsilon}+e^{2w\zeta_0}}\left[\frac{e^{-2w\upsilon}}{e^{-2w\upsilon}+e^{2w\zeta_0}}e^{w\zeta_0}\cosh(w\upsilon)+e^{w\zeta_0}\sinh(w\upsilon)\right. \\ &\qquad + \frac{1}{2}\exp\big(-w(\upsilon+\zeta_0)\big)\left(\frac{e^{-2w\upsilon}}{e^{-2w\upsilon}+e^{2w\zeta_0}}-1\right), \\ &\qquad + \frac{e^{-2w\upsilon}}{e^{-2w\upsilon}+e^{2w\zeta_0}}e^{w\zeta_0}\sinh(w\upsilon)+e^{w\zeta_0}\cosh(w\upsilon) \\ &\qquad \left. +\frac{1}{2}\exp\big(-w(\upsilon+\zeta_0)\big)\left(\frac{e^{-2w\upsilon}}{e^{-2w\upsilon}+e^{2w\zeta_0}}-1\right)\right]. \end{aligned}$$

Its magnitude is

$$\sqrt{a_\mu a^\mu} = \frac{we^{2w\zeta_0}}{(e^{-2w\upsilon}+e^{2w\zeta_0})^{3/2}}$$

from which it can be seen that the observer is inertial in the asymptotic past and has uniform acceleration in the asymptotic future. In particular,

$$\lim_{t\to-\infty}\sqrt{a_\mu a^\mu} = 0 \qquad\qquad \lim_{t\to\infty}\sqrt{a_\mu a^\mu} = we^{-w\zeta_0}.$$

This is the only orthogonal coordinate system that has this interpretation and allows the Klein-Gordon (and Dirac) equations to separate [43].

These observers have a horizon at the line $t = x$. An observer on the worldline $\zeta_0 = 0$ starts at $x = 0$ in the infinite past and crosses the $t = 0$ line at $\upsilon = \frac{1}{2w}\ln(2)$ where $x = \frac{1}{w\sqrt{2}}$. This observer's asymptotic acceleration is w.

Appendix C

Unruh-DeWitt Detector Theory

A simple model of a "particle detector" is the Unruh-DeWitt detector [11, 17]. It consists of a point charge with an internal degree of freedom coupled to a quantum field via a monopole interaction. If the internal degree of freedom becomes excited from its ground state, a particle is said to have been detected. Often, the internal degree of freedom is taken to be a two-level system. In this thesis, it is taken to be a harmonic oscillator and can be thought of as a simplified version of an atom. The treatment here will consider the detector coupled to a massless Klein-Gordon field in Minkowski space. This appendix will derive the regularized equations of motion for the mode functions, which completely describe the dynamics of the detector. These derivations reproduce the results of §II and §III of [48]. However, they are generalized to an arbitrary initial time and expressed in terms of the time slicing of the field, as opposed to that of the detector.

C.1 Lagrangian and Equations of Motion

The Lagrange density for a massless Klein-Gordon field $\Phi(x)$ is

$$\mathcal{L}_F(x) = -\frac{1}{2}\partial_\mu\Phi(x)\partial^\mu\Phi(x),$$

which gives rise to the action

$$S_F = \int d^4x\, \mathcal{L}_F(x) = -\frac{1}{2}\int d^4x\, \partial_\mu\Phi(x)\partial^\mu\Phi(x),$$

and consequently, the equation of motion (free Klein-Gordon equation)

$$\begin{aligned} 0 &= \frac{\partial \mathcal{L}_F(x)}{\partial \Phi(x)} - \partial_\mu \left(\frac{\partial \mathcal{L}_F(x)}{\partial\big(\partial_\mu \Phi(x)\big)} \right) \\ &= \partial_\mu \partial^\mu \Phi(x). \end{aligned} \tag{C.1}$$

The conjugate momentum to the field is given by

$$\Pi(x) = \frac{\partial \mathcal{L}_F(x)}{\partial\big(\partial_t \Phi(x)\big)} = \partial_t \Phi(x).$$

The detector's internal degree of freedom Q is taken to be a harmonic oscillator with mass m_0, bare natural frequency Ω_0, and proper time τ_Q. The Lagrangian is

$$L_Q = \frac{m_0}{2} \left((\partial_{\tau_Q} Q)^2 - \Omega_0^2 Q^2 \right),$$

and the resulting action

$$S_Q = \int d\tau_Q \, L_Q = \int d\tau_Q \, \frac{m_0}{2} \left((\partial_{\tau_Q} Q)^2 - \Omega_0^2 Q^2 \right),$$

gives rise to the equation of motion

$$\begin{aligned} 0 &= \frac{\partial L_Q}{\partial Q} - \partial_{\tau_Q} \left(\frac{\partial L_Q}{\partial\big(\partial_{\tau_Q} Q(\tau_Q)\big)} \right) \\ &= -m_0 \partial_{\tau_Q}^2 Q - m_0 \Omega_0^2 Q. \end{aligned}$$

The detector's conjugate momentum is

$$P_Q(\tau_Q) = \frac{\partial L_Q(\tau_Q)}{\partial\big(\partial_{\tau_Q} Q(\tau_Q)\big)} = m_0 \partial_{\tau_Q} Q(\tau_Q).$$

The Lagrange density that describes the interaction of the detector with the field is

$$\mathcal{L}_I = \lambda_0 Q(\tau_Q) \Phi(x) \delta^4\big(x^\mu - z^\mu(\tau_Q)\big), \tag{C.2}$$

where $z^\mu(\tau_Q)$ is the trajectory of the detector. Note that $z^\mu(\tau_Q)$ is not treated as a dynamical variable in this model. That is, the back reaction of the field on the trajectory is ignored. The coupling strength λ_0 is taken to be constant. In general, it is a smooth function that can be used to turn the interaction on and off (say, adiabatically). The corresponding action is then

$$S_I = \int d\tau_Q \int d^4x \, \mathcal{L}_I = \lambda_0 \int d\tau_Q \int d^4x \, Q(\tau_Q) \Phi(x^\mu) \delta^4\big(x^\mu - z^\mu(\tau_Q)\big).$$

C.1.1 Quantum Theory In The Heisenberg Picture

The quantum theory is constructed by promoting the dynamical variables $\Phi(x)$, $\Pi(x)$, $Q(\tau_Q)$, and $P_Q(\tau_Q)$ to be Hermitian operators on a Hilbert space and enforcing the equal time commutation relations

$$\begin{aligned}\big[\hat{\Phi}(t,\boldsymbol{x}),\hat{\Pi}(t,\boldsymbol{x}')\big] &= i\delta^3(\boldsymbol{x}-\boldsymbol{x}'),\\ \big[\hat{Q}(\tau_Q),\hat{P}_Q(\tau_Q)\big] &= i.\end{aligned} \tag{C.3}$$

In the Heisenberg picture, the equations of motion are the operator valued analogies of the classical equations of motion

$$\partial_\mu\partial^\mu\hat{\Phi}(x) = -\lambda_0\int_{\tau_0}^{\infty} d\tau_Q\,\hat{Q}(\tau_Q)\delta^4\big(x-z(\tau_Q)\big), \tag{C.4}$$

$$\partial_{\tau_Q}^2\hat{Q}(\tau_Q)+\Omega_0^2\hat{Q}(\tau_Q) = \frac{\lambda_0}{m_0}\hat{\Phi}\big(\tau_Q,\boldsymbol{z}(\tau_Q)\big). \tag{C.5}$$

The detector is a point source for the field while it is driven by the field amplitude at its current position.

C.2 Mode Decomposition

Since the system is linear, the evolution will be a linear transformation in the phase space of the operators. If the coupling is turned on at time t_0, the field operator can be represented as

$$\begin{aligned}\hat{\Phi}(t,\boldsymbol{x}) = \int d^3x'\,\Big(&f^{\Phi}(t,\boldsymbol{x},\boldsymbol{x}')\hat{\Phi}(t_0,\boldsymbol{x}')+f^{\Pi}(t,\boldsymbol{x},\boldsymbol{x}')\hat{\Pi}(t_0,\boldsymbol{x}')\Big)\\ &+f^{Q}(x)\hat{Q}\big(\tau_Q(t_0)\big)+f^{P_Q}(x)\hat{P}_Q\big(\tau_Q(t_0)\big).\end{aligned} \tag{C.6}$$

Similarly, $\hat{Q}$ can be represented as

$$\begin{aligned}\hat{Q}(\tau_Q) = \int d^3x'\,\Big(&q^{\Phi}(\tau_Q,\boldsymbol{x}')\hat{\Phi}(t_0,\boldsymbol{x}')+q^{\Pi}(\tau_Q,\boldsymbol{x}')\hat{\Pi}(t_0,\boldsymbol{x}')\Big)\\ &+q^{Q}(\tau_Q)\hat{Q}\big(\tau_Q(t_0)\big)+q^{P_Q}(\tau_Q)\hat{P}_Q\big(\tau_Q(t_0)\big).\end{aligned} \tag{C.7}$$

At the initial time t_0, the field is free giving

$$\begin{aligned}\hat{\Phi}(t_0,\boldsymbol{x}) &= \hat{\Phi}_0(\boldsymbol{x}), & \hat{Q}\big(\tau_Q(t_0)\big) &= \hat{Q}_0,\\ \hat{\Pi}(t_0,\boldsymbol{x}) &= \hat{\Pi}_0(\boldsymbol{x}), & \hat{P}_Q\big(\tau_Q(t_0)\big) &= \hat{P}_0.\end{aligned}$$

The free field $\hat{\Phi}_0(\boldsymbol{x})$ can be expanded in the modes

$$\hat{\Phi}_0(\boldsymbol{x}) = \frac{1}{(2\pi)^{3/2}} \int d^3k \sqrt{\frac{1}{2\omega}} \left(e^{i\boldsymbol{k}\cdot\boldsymbol{x} - i\omega t_0} \, \hat{b}_{\boldsymbol{k}} + e^{-i\boldsymbol{k}\cdot\boldsymbol{x} + i\omega t_0} \, \hat{b}^\dagger_{\boldsymbol{k}} \right) \tag{C.8}$$

and consequently, the initial conjugate momentum to field is given by

$$\hat{\Pi}_0(x) = \partial_t \hat{\Phi}(t_0, \boldsymbol{x}) = \frac{1}{(2\pi)^{3/2}} \int d^3k \, (-i\omega) \sqrt{\frac{1}{2\omega}} \left(e^{i\boldsymbol{k}\cdot\boldsymbol{x} - i\omega t_0} \, \hat{b}_{\boldsymbol{k}} - e^{-i\boldsymbol{k}\cdot\boldsymbol{x} + i\omega t_0} \, \hat{b}^\dagger_{\boldsymbol{k}} \right).$$

To satisfy Equation (C.3), the mode operators must satisfy

$$\left[\hat{b}_{\boldsymbol{k}}, \hat{b}^\dagger_{\boldsymbol{k}'} \right] = \delta^3(\boldsymbol{k} - \boldsymbol{k}').$$

Since the mode operators are independent of time, Equation (C.1) requires the dispersion relation

$$\omega = |\boldsymbol{k}|.$$

Similarly, ladder operators can be defined for the detector as

$$\hat{Q}_0 = \sqrt{\frac{1}{2\Omega_r m_0}} \left(e^{-i\Omega_r \tau_Q(t_0)} \, \hat{a} + e^{i\Omega_r \tau_Q(t_0)} \, \hat{a}^\dagger \right), \tag{C.9}$$

and so

$$\hat{P}_0 = m_0 \partial_\tau Q(\tau_Q(t_0)) = -i \sqrt{\frac{\Omega_r m_0}{2}} \left(e^{-i\Omega_r \tau_Q(t_0)} \, \hat{a} - e^{i\Omega_r \tau_Q(t_0)} \, \hat{a}^\dagger \right).$$

The canonical commutation relation on $\hat{Q}$ and $\hat{P}$ impose

$$\left[a, a^\dagger \right] = 1.$$

In anticipation of the regularization to come, the renormalized frequency Ω_r (to be defined in Section C.3.1) has been used in the above definitions instead of the bare natural frequency Ω_0.

Combining Equations (C.6) and (C.8) results in

$$\hat{\Phi}(x) = \hat{\Phi}_a(x) + \hat{\Phi}_b(x), \tag{C.10}$$

where

$$\hat{\Phi}_a(x) = \sqrt{\frac{1}{2\Omega_r m_0}} \left(f^a(t, \boldsymbol{x}) \hat{a} + f^{a*}(t, \boldsymbol{x}) \hat{a}^\dagger \right),$$

$$\hat{\Phi}_b(x) = \frac{1}{(2\pi)^{3/2}} \int d^3k \sqrt{\frac{1}{2\omega}} \left(f^{(+)}(t, \boldsymbol{x}, \boldsymbol{k}) \hat{b}_{\boldsymbol{k}} + f^{(-)}(t, \boldsymbol{x}, \boldsymbol{k}) \hat{b}^\dagger_{\boldsymbol{k}} \right),$$

and

$$
\begin{aligned}
f^{a}(t,\boldsymbol{x}) &= \left(f^{Q}(x) - i\Omega_r m_0 f^{P_Q}(x)\right) e^{-i\Omega_r \tau_Q(t_0)},\\
f^{(+)}(t,\boldsymbol{x},\boldsymbol{k}) &= \int d^3x' \left(f^{\Phi}(t,\boldsymbol{x},\boldsymbol{x'}) - i\omega f^{\Pi}(t,\boldsymbol{x},\boldsymbol{x'})\right) e^{i\boldsymbol{k}\cdot\boldsymbol{x'} - i\omega t_0},\\
f^{(-)}(t,\boldsymbol{x},\boldsymbol{k}) &= \int d^3x' \left(f^{\Phi}(t,\boldsymbol{x},\boldsymbol{x'}) + i\omega f^{\Pi}(t,\boldsymbol{x},\boldsymbol{x'})\right) e^{-i\boldsymbol{k}\cdot\boldsymbol{x'} + i\omega t_0}.
\end{aligned}
$$

Note that Hermiticity of $\hat{\Phi}(x)$ requires

$$
f^{(+)}(t,\boldsymbol{x},\boldsymbol{k}) = f^{(-)^*}(t,\boldsymbol{x},\boldsymbol{k}).
$$

This means that $f^{\Phi}(x,\boldsymbol{x'})$ and $f^{\Pi}(x,\boldsymbol{x'})$ must be real functions. Due to the Hermiticity of $\hat{Q}(\tau_Q)$, $f^{Q}(x)$ and $f^{P_Q}(x)$ are also real functions. Combining Equations (C.7) and (C.9) results in

$$
\hat{Q}(\tau_Q) = \hat{Q}_a + \hat{Q}_b, \tag{C.11}
$$

where

$$
\hat{Q}_a(\tau_Q) = \sqrt{\frac{1}{2\Omega_r m_0}} \left(q^{a}(\tau_Q)\hat{a} + q^{a*}(\tau_Q)\hat{a}^{\dagger}\right),
$$

$$
\hat{Q}_b(\tau_Q) = \frac{1}{(2\pi)^{3/2}} \int d^3k \sqrt{\frac{1}{2\omega}} \left(q^{(+)}(\tau_Q,\boldsymbol{k})\hat{b}_{\boldsymbol{k}} + q^{(-)}(\tau_Q,\boldsymbol{k})\hat{b}^{\dagger}_{\boldsymbol{k}}\right),
$$

and

$$
\begin{aligned}
q^{a}(\tau_Q) &= \left(q^{Q}(\tau_Q) - i\Omega_r m_0 q^{P}(\tau_Q)\right) e^{-i\Omega_r \tau_Q(t_0)},\\
q^{(+)}(\tau_Q,\boldsymbol{k}) &= \int d^3x' \left(q^{\Phi}(\tau_Q,\boldsymbol{x'}) - i\omega q^{\Pi}(\tau_Q,\boldsymbol{x'})\right) e^{i\boldsymbol{k}\cdot\boldsymbol{x'} - i\omega t_0},\\
q^{(-)}(\tau_Q,\boldsymbol{k}) &= \int d^3x' \left(q^{\Phi}(\tau_Q,\boldsymbol{x'}) + i\omega q^{\Pi}(\tau_Q,\boldsymbol{x'})\right) e^{-i\boldsymbol{k}\cdot\boldsymbol{x'} + i\omega t_0}.
\end{aligned}
$$

Again, Hermiticity of $\hat{\Phi}(x)$ requires

$$
q^{(+)}(\tau_Q,\boldsymbol{k}) = q^{(-)^*}(\tau_Q,\boldsymbol{k})
$$

and as a result, $q^{\Phi}(\tau_Q,\boldsymbol{x'})$ and $q^{\Pi}(\tau_Q,\boldsymbol{x'})$ must be real functions. The Hermiticity of $\hat{Q}(\tau_Q)$ imposes that $q^{Q}(\tau_Q)$ and $q^{P_Q}(\tau_Q)$ must also be real.

C.3 Equations of Motion for the Modes

It is sufficient to solve for $f^a(x)$, $f^{(+)}(x, \boldsymbol{k})$, $q^a(\tau_Q)$, and $q^{(+)}(\tau_Q, \boldsymbol{k})$ due to the Hermiticity of $\hat{\Phi}(x)$ and $\hat{Q}(\tau_Q)$. Inserting Equations (C.10) and (C.11) into Equations (C.4) and using the linear independence of $\hat{b}_{\boldsymbol{k}}$, $\hat{b}^\dagger_{\boldsymbol{k}}$, $\hat{a}$, and $\hat{a}^\dagger$ yields

$$(\partial_t^2 - \nabla^2) f^a(x) = \lambda_0 \int d\tau_Q \, q^{(+)}(\tau_Q, \boldsymbol{k}) \delta^4\big(x - z(\tau_Q)\big), \tag{C.12}$$

$$(\partial_t^2 - \nabla^2) f^{(+)}(x, \boldsymbol{k}) = \lambda_0 \int d\tau_Q \, q^a(\tau_Q) \delta^4\big(x - z(\tau_Q)\big). \tag{C.13}$$

Similarly, linear independence as well as Equations (C.10), (C.11), and (C.5) results in

$$(\partial_{\tau_Q}^2 + \Omega_0^2) q^a(\tau_Q) = \frac{\lambda_0}{m_0} f^a\big(z(\tau_Q)\big), \tag{C.14}$$

$$(\partial_{\tau_Q}^2 + \Omega_0^2) q^{(+)}(\tau_Q, \boldsymbol{k}) = \frac{\lambda_0}{m_0} f^{(+)}\big(z(\tau_Q), \boldsymbol{k}\big). \tag{C.15}$$

Prior to the interaction the field and the detectors were free, which leads to the following initial conditions

$$\begin{aligned}
q^a\big(\tau_0(t_0)\big) &= e^{-i\Omega_r \tau_Q(t_0)}, \\
\partial_{\tau_Q} q^a(\tau_0(t_0)) &= -i\Omega_r e^{-i\Omega_r \tau_Q(t_0)}, && \text{(C.16)} \\
f^{(+)}(t_0, \boldsymbol{x}, \boldsymbol{k}) &= e^{i\boldsymbol{k}\cdot\boldsymbol{x} - i\omega t_0}, && \text{(C.17)} \\
\partial_t f^{(+)}(t_0, \boldsymbol{x}, \boldsymbol{k}) &= -i\omega e^{i\boldsymbol{k}\cdot\boldsymbol{x} - i\omega t_0}, \\
q^{(+)}\big(\tau_Q(t_0)\big), \boldsymbol{k}) &= \partial_{\tau_Q}(\tau_Q(t_0), \boldsymbol{k}) = 0, \\
f^a(t_0, \boldsymbol{x}) &= \partial_t f^a(t_0, \boldsymbol{x}) = 0. && \text{(C.18)}
\end{aligned}$$

The equations of motion for the operators $\hat{Q}(\tau_Q)$ and $\hat{\Phi}(x)$ have been reduced to equations of motion for the complex-valued modes, which look analogous to classical fields.

C.3.1 Regularized Equations Of Motion

Equations (C.12) and (C.13) can be solved using the retarded Green's function for the massless Klein-Gordon equation

$$G_{\text{ret}}(x, x') = \frac{1}{4\pi} \theta(t - t') \delta(\sigma),$$

where $\theta(t)$ is the Heaviside step function and

$$\sigma = -\frac{1}{2}(x_\mu - x'_\mu)(x^\mu - x'^\mu).$$

The solution to Equation (C.13) is given by

$$f^{(+)}(x, \boldsymbol{k}) = f_0^{(+)}(x, \boldsymbol{k}) + f_1^{(+)}(x, \boldsymbol{k}), \tag{C.19}$$

where $f_0^{(+)}(x, \boldsymbol{k})$ is the free field solution and $f_1^{(+)}(x, \boldsymbol{k})$ is the retarded solution. In accordance with boundary condition (C.17), the free field solution is

$$f_0^{(+)}(x, \boldsymbol{k}) = e^{i\boldsymbol{k}\cdot\boldsymbol{x} - i\omega t}.$$

The retarded solution can be further evaluated formally as

$$\begin{aligned}
f_1^{(+)}(x, \boldsymbol{k}) &= \lambda_0 \int_{-\infty}^{\infty} d^4x' \int_{-\infty}^{\infty} d\tau_Q \, G_{\text{ret}}(x, x') q^{(+)}(\tau_Q, \boldsymbol{k}) \delta^4\big(x' - z(\tau_Q)\big) \\
&= \lambda_0 \int_{-\infty}^{\infty} d\tau_Q \, G_{\text{ret}}\big(x, z(\tau_Q)\big) q^{(+)}(\tau_Q, \boldsymbol{k}) \\
&= \frac{\lambda_0}{4\pi} \int_{\infty}^{\infty} d\tau_Q \, \theta\big(t - z^0(\tau_Q)\big) \delta(\sigma) q^{(+)}(\tau_Q, \boldsymbol{k}) \\
&= \frac{\lambda_0}{4\pi} \int_{\tau_Q(t_0)}^{\infty} d\tau_Q \, \delta(\sigma) q^{(+)}(\tau_Q, \boldsymbol{k}) \\
&= \frac{\lambda_0}{4\pi} \theta\big(\tau_Q^{\text{ret}}(x) - \tau_Q(t_0)\big) q^{(+)}\big(\tau_Q^{\text{ret}}(x), \boldsymbol{k}\big) \left[\left| \frac{\partial \sigma}{\partial \tau_Q} \right|_{\tau_Q^{\text{ret}}} \right]^{-1}.
\end{aligned}$$

The function $\tau_Q^{\text{ret}}(x)$ is the retarded time and depends on the details of the trajectory. It is the solution to $\sigma = 0$. Similarly, $\left| \frac{\partial \sigma}{\partial \tau_Q} \right|_{\tau_Q^{\text{ret}}}$ is the retarded distance, which is the spatial distance between the field point and the detector at the retarded time. This will cause the field $f^{(+)}(x, \boldsymbol{k})$ to diverge at the location of the detector. This complicates solving Equation (C.15) since the field amplitude at the position of the detector is the driving force for $q^{(+)}(\tau_Q, \boldsymbol{k})$.

To handle this divergence the following regularization scheme [49, 50] is used. Note that the system under consideration is a detector moving along a prescribed trajectory and, by construction, there will be only one detector. Therefore, at the energy scales of detector pair productions there is a natural cutoff on frequency Λ. This is equivalent to giving the detector a finite width $O(\Lambda^{-1})$. This will limit the spatial resolution of the theory.

The effective field theory is constructed by replacing the retarded Green's function with

$$G^{\Lambda}_{\rm ret}(x,x') = \frac{1}{4\pi}\theta(t-t')\left(\sqrt{\frac{8}{\pi}}\Lambda^2 e^{-2\Lambda^4\sigma^2}\right),$$

where the delta function has been replaced by a Gaussian function that has a very small standard deviation. This reduces to the usual Green's function in the limit of no cutoff, as required for consistency. That is,

$$\lim_{\Lambda\to\infty} G^{\Lambda}_{\rm ret}(x,x') = G_{\rm ret}(x,x').$$

The retarded solution is then

$$\begin{aligned} f_1^{(+)}(x,\boldsymbol{k}) &\approx \lambda_0 \int d\tau'_Q\, G^{\Lambda}_{\rm ret}\big(x, z(\tau'_Q)\big) q^{(+)}(\tau'_Q,\boldsymbol{k}) \\ &= \lambda_0 \frac{\Lambda^2}{4\pi}\sqrt{\frac{8}{\pi}} \int_{\tau_Q(t_0)}^{\tau_Q} d\tau'_Q\, q^{(+)}(\tau'_Q,\boldsymbol{k}) e^{-2\Lambda^4\sigma^2}. \end{aligned}$$

Near the trajectory, $x = z_\mu(\tau_Q)$ so the following expansion can be made

$$z_\mu(\tau'_Q) = z_\mu(\tau_Q) + s v_\mu(\tau_Q) + \frac{s^2}{2}a_\mu(\tau_Q) + \frac{s^3}{3!}\dot{a}_\mu(\tau_Q) + \cdots,$$

where $s = \tau'_Q - \tau_Q$, $v_\mu(\tau_Q) = \dot{z}_\mu(\tau_Q)$, $a_\mu(\tau_Q) = \dot{v}_\mu(\tau_Q)$, and overdot denotes differentiation with respect to τ_Q. Inserting this into the definition of σ results in

$$\begin{aligned} \sigma &= -\frac{1}{2}\big(z_\mu(\tau_Q) - z_\mu(\tau'_Q)\big)\big(z^\mu(\tau_Q) - z^\mu(\tau'_Q)\big) \\ &\approx -\frac{1}{2}\big(s v_\mu(\tau_Q) + \frac{s^2}{2}a_\mu(\tau_Q) + \frac{s^3}{3!}\dot{a}_\mu(\tau_Q)\big)\big(s v^\mu(\tau_Q) + \frac{s^2}{2}a^\mu(\tau_Q) + \frac{s^3}{3!}\dot{a}^\mu(\tau_Q)\big). \end{aligned}$$

This can be simplified to

$$\sigma = s^2 + \frac{s^4}{24}a_\mu a^\mu + \frac{s^5}{6}\dot{a}_\mu a^\mu + \frac{s^6}{36}\dot{a}_\mu\dot{a}^\mu$$

by using the following relations

$$v_\mu v^\mu = -1, \qquad a_\mu v^\mu = \frac{1}{2}\frac{\partial(v_\mu v^\mu)}{\partial\tau_Q} = 0, \qquad v_\mu \dot{a}^\mu = -a_\mu a^\mu.$$

Taylor expanding

$$q^{(+)}(\tau'_Q,\boldsymbol{k}) = q^{(+)}(\tau_Q,\boldsymbol{k}) + s\dot{q}^{(+)}(\tau_Q,\boldsymbol{k}) + \frac{s^2}{2}\ddot{q}^{(+)}(\tau_Q,\boldsymbol{k}) + \cdots,$$

the retarded solution near the trajectory becomes

$$f_1^{(+)}(z_\mu(\tau_Q),\boldsymbol{k}) \approx \lambda_0 \frac{\Lambda^2}{4\pi}\sqrt{\frac{8}{\pi}} \int_{\tau_Q(t_0)}^{\tau_Q} d\tau_Q'\, e^{-2\Lambda^4(s^2/2+s^4 a_\mu a^\mu/24)^2} \\ \times \left(q^{(+)}(\tau_Q,\boldsymbol{k}) + s\dot{q}^{(+)}(\tau_Q,\boldsymbol{k}) + \frac{s^2}{2}\ddot{q}^{(+)}(\tau_Q,\boldsymbol{k})\right).$$

It is now assumed that $\Lambda^4 s^4 \gg 1$ but $\Lambda^4 s^6 a_\mu a^\mu \ll 1$ so that

$$f_1^{(+)}(z_\mu(\tau_Q),\boldsymbol{k}) \approx \lambda_0 \frac{\Lambda^2}{4\pi}\sqrt{\frac{8}{\pi}} \left\{ q^{(+)}(\tau_Q,\boldsymbol{k}) \int_{\tau_Q(t_0)-\tau_Q}^{0} ds\, e^{-\frac{\Lambda^4 s^4}{2}} \right. \\ + \dot{q}^{(+)}(\tau_Q,\boldsymbol{k}) \int_{\tau_Q(t_0)-\tau_Q}^{0} ds\, s e^{-\frac{\Lambda^4 s^4}{2}} \\ \left. + \frac{1}{2}\ddot{q}^{(+)}(\tau_Q,\boldsymbol{k}) \int_{\tau_Q(t_0)-\tau_Q}^{0} ds\, s^2 e^{-\frac{\Lambda^4 s^4}{2}} \right\}.$$

Since Λ is very large, the standard deviation of the Gaussian is very small. As a result, the integration can be extended to infinity with negligible difference. Letting $s \to -s$ results in

$$f_1^{(+)}(z_\mu(\tau_Q),\boldsymbol{k}) \approx \lambda_0 \frac{\Lambda^2}{4\pi}\sqrt{\frac{8}{\pi}} \left\{ q^{(+)}(\tau_Q,\boldsymbol{k}) \int_0^{\infty} ds\, e^{-\frac{\Lambda^4 s^4}{2}} \right. \\ + \dot{q}^{(+)}(\tau_Q,\boldsymbol{k})(\tau_q,\boldsymbol{k}) \int_0^{\infty} ds\, s e^{-\frac{\Lambda^4 s^4}{2}} \\ \left. + \frac{1}{2}\ddot{q}^{(+)}(\tau_Q,\boldsymbol{k}) \int_0^{\infty} ds\, s^2 e^{-\frac{\Lambda^4 s^4}{2}} \right\}.$$

Further letting $x = \Lambda^4 s^4/2$ yields

$$f_1^{(+)}(z_\mu(\tau_Q),\boldsymbol{k}) = \lambda_0 \frac{\Lambda^2}{4\pi}\sqrt{\frac{8}{\pi}} \left\{ \frac{1}{\Lambda}\frac{1}{2^{7/4}} q^{(+)}(\tau_Q,\boldsymbol{k}) \int_0^{\infty} dx\, x^{-3/4} e^{-x} \right. \\ - \frac{1}{\Lambda^2}\frac{1}{2\sqrt{2}} \dot{q}^{(+)}(\tau_Q,\boldsymbol{k}) \int_0^{\infty} dx\, x^{-1/2} e^{-x} \\ \left. + \frac{1}{\Lambda^3}\frac{1}{2^{13/4}} \int_0^{\infty} dx\, x^{-1/4} e^{-x} \right\}$$

$$
\begin{aligned}
&= \lambda_0 \frac{\Lambda^2}{4\pi}\sqrt{\frac{8}{\pi}}\left\{ q^{(+)}(\tau_Q,\boldsymbol{k})\frac{1}{\Lambda}\frac{1}{2^{7/4}}\Gamma(1/4)\right.\\
&\quad - \dot{q}^{(+)}(\tau_Q,\boldsymbol{k})\frac{1}{\Lambda^2}\frac{1}{2\sqrt{2}}\Gamma(1/2)\\
&\quad \left. +\ddot{q}^{(+)}(\tau_Q,\boldsymbol{k})\frac{1}{\Lambda^3}\frac{1}{2^{5/4}}\Gamma(3/4)\right\}.
\end{aligned}
$$

Dropping the term $O(\Lambda^{-1})$, the mode near the trajectory becomes

$$
f_1^{(+)}(z_\mu(\tau_Q),\boldsymbol{k}) \approx \frac{\lambda_0}{4\pi}\big(\Lambda\kappa q^{(+)}(\tau_q,\boldsymbol{k}) - \dot{q}^{(+)}(\tau_Q,\boldsymbol{k})\big),
$$

where $\kappa = \dfrac{2^{7/4}\Gamma(5/4)}{\sqrt{\pi}}$. Finally, inserting this into Equation (C.15) results in the regularized equation of motion for $q^{(+)}$

$$
(\partial_{\tau_Q}^2 + 2\gamma\partial_{\tau_Q} + \Omega_r^2)q^{(+)}(\tau_Q,\boldsymbol{k}) = \frac{\lambda_0}{m_0}f_0^{(+)}(z_\mu(\tau_Q),\boldsymbol{k}). \tag{C.20}
$$

Now the mode behaves like a damped harmonic oscillator with

$$
\gamma = \frac{\lambda_0^2}{8\pi m_0}, \qquad \text{and} \qquad \Omega_r^2 = \Omega_0^2 - \frac{\lambda_0^2\Lambda^2\kappa}{4\pi m_0},
$$

driven by the vacuum fluctuations of the field.

The same procedure is used to regularize Equation (C.14). However, in this case $f_0^a(x) = 0$ by boundary condition (C.18) so that

$$
(\partial_{\tau_Q}^2 + 2\gamma\partial_{\tau_Q} + \Omega_r^2)q^a(\tau_Q) = 0. \tag{C.21}
$$

The dynamics of the Unruh-DeWitt detector are contained in the mode functions $q^{(+)}(\tau_Q,\boldsymbol{k})$ and $q^a(\tau_Q)$. These are described as damped harmonic oscillators governed by Equations (C.20) and (C.21). The dynamics of the field are contained in the mode functions $f^{(+)}(x,\boldsymbol{k})$ and $f^a(x)$, which are governed by Equations (C.13) and (C.12). To proceed further requires specialization to a trajectory.

Appendix D

Numerical Techniques

This appendix introduces the numerical techniques employed in the calculations for Chapter 6. Numerical integration was carried out using *Simpson's rule* while numerically solving equations, such as the transcendental Costa-Villalba proper time, was achieved using *Newton's method*.

D.1 Simpson's Rule

Simpson's rule is a method to approximate the value of a definite integral. It achieves this by approximating the integrand as a second order polynomial, which is fit to the function at the endpoints of integration x_1 and x_3 as well as the midpoint x_2. Integrating this polynomial results in

$$\int_{x_1}^{x_3} dx\, f(x) \approx \frac{h}{3}\big(f(x_1) + 4f(x_2) + f(x_3)\big),$$

where $h = (x_3 - x_1)/2$. It is exact for polynomials of degree up to and including three.

Dividing the integration region up into smaller, equally spaced intervals and applying Simpson's rule to each results in the *extended Simpson's rule*

$$\int_{x_1}^{x_n} dx\, f(x) \approx \frac{x_n - x_1}{3(n-1)} \left[f(x_1) + 4 \sum_{i=1}^{(n+1)/2} f(x_{2i}) + 2 \sum_{i=1}^{(n-1)/2} f(x_{2i-1}) + f(x_n) \right],$$

where n is the number of times the function is sampled. It can be shown that the error in the approximation is of order $O(1/n^4)$ [51]. The more function samples, the better the approximation.

D.2 Newton's Method

Newton's method is a numerical technique to approximate the root of a function [51]. Given an initial estimate of the root x_0, the function is approximated by the Taylor series

$$f(x) \approx f(x_0) + f'(x_0)(x - x_0),$$

where prime denotes differentiation with respect to x. The root of this approximation is often a better estimate to the actual root. The estimate can then be further refined by repeating the procedure

$$x_{n+1} = x_n - \frac{f(x_n)}{f'(x_n)}.$$

Since Newton's method relies on a Taylor series, the initial guess must be close to the actual root for it to be effective.

Appendix E

Free Field Mode Summation

This appendix will prove the result

$$\frac{1}{2\pi}\int \frac{d^3k}{2\omega}\, f_0^{(+)}(z^\mu(\tau),\boldsymbol{k}) f_0^{(-)}(z^\mu(\tau'),\boldsymbol{k}) = \left(\frac{1}{\Delta x^2 - \Delta t^2}\right), \qquad \text{(E.1)}$$

where $\Delta x = z^i(\tau) - z^i(\tau')$ and $\Delta t = z^0(\tau) - z^0(\tau')$. The free field mode is

$$f_0^{(+)}\big(z(\tau),\boldsymbol{k}\big) = e^{-i\omega z^0(\tau) + i\boldsymbol{k}\cdot\boldsymbol{z}(\tau')}$$

and $f_0^{(-)} = f_0^{(+)^*}$. Inserting these into the integral results in

$$\frac{1}{2\pi}\int \frac{d^3k}{2\omega}\, f_0^{(+)}(z^\mu(\tau),\boldsymbol{k}) f_0^{(-)}(z^\mu(\tau'),\boldsymbol{k}) = \frac{1}{2\pi}\int \frac{d^3k}{2\omega} e^{-i\omega\Delta t} e^{i\boldsymbol{k}\cdot\Delta\boldsymbol{x}}.$$

Switching to spherical coordinates and performing the ϕ and θ integrations results in

$$\frac{1}{2\pi}\int \frac{d^3k}{2\omega} e^{-i\omega\Delta t} e^{i\boldsymbol{k}\cdot\Delta\boldsymbol{x}} = -\int_0^\infty d\omega\, \frac{1}{\Delta x}\left(e^{-i\omega(\Delta t - \Delta x)} - e^{-i\omega(\Delta t + \Delta x)}\right).$$

Since the integrand oscillates, a cutoff must be introduced in order to perform the integration. Letting $\Delta t \to \Delta t - i\epsilon$ where ϵ is a small positive constant and performing the remaining integration yields

$$-\int_0^\infty d\omega\, \frac{1}{\Delta x}\left(e^{-i\omega(\Delta t - i\epsilon - \Delta x)} - e^{-i\omega(\Delta t - i\epsilon + \Delta x)}\right) = \left(\frac{1}{\Delta x^2 - (\Delta t - i\epsilon)^2}\right).$$

The desired result is obtained by taking the limit $\epsilon \to 0$.

Bibliography

[1] Rolf Landauer. Information is physical. *Physics Today*, 44(5):23–29, May 1991. (Cited on page 1.)

[2] Peter W. Shor. Algorithms for quantum computation: discrete logarithms and factoring. In *Proceedings of the 35th Annual Symposium on Foundations of Computer Science*, pages 124–134, Santa Fe, New Mexico, November 20–22, 1994. IEEE Computer Society Technical Committee on Mathematical Foundations of Computing, IEEE Computer Society Press, Los Alamitos, CA. (Cited on page 1.)

[3] Michael A. Nielsen and Isaac L. Chuang. *Quantum Computation and Quantum Information*. Cambridge University Press, Cambridge, 2000. (Cited on pages 1 and 14.)

[4] Lov K. Grover. Quantum mechanics helps in searching for a needle in a haystack. *Phys. Rev. Lett.*, 79(2):325–328, July 1997, arXiv:quant-ph/9706033. (Cited on page 1.)

[5] Michele Mosca. Quantum algorithms. To appear in *Encyclopedia of Complexity and Systems Science*. Springer. arXiv:0808.0369 [quant-ph], August 2008. (Cited on page 1.)

[6] Paul. M. Alsing and Gerard J. Milburn. Teleportation with a uniformly accelerated partner. *Phys. Rev. Lett.*, 91(18):180404, October 2003, arXiv:quant-ph/0302179. (Cited on pages 2, 17, and 22.)

[7] Paul. M. Alsing, David McMahon, and Gerard J. Milburn. Teleportation in a non-inertial frame. *J. Opt. B: Quantum Semiclass.*, 6(8):S834–S843, August 2004, arXiv:quant-ph/0311096. (Cited on pages 2, 17, and 22.)

[8] Ivette Fuentes-Schuller and Robert. B. Mann. Alice falls into a black hole: Entanglement in non-inertial frames. *Phys. Rev. Lett.*, 95(12):120404, September 2005, arXiv:quant-ph/0410172. (Cited on pages 2 and 17.)

[9] Paul. M. Alsing, Ivette Fuentes-Schuller, Robert. B. Mann, and Tracey. E. Tessier. Entanglement of Dirac fields in non-inertial frames. *Phys. Rev. A*, 74(3):32326, September 2006, arXiv:quant-ph/0603269. (Cited on pages 2, 17, 22, and 23.)

[10] Paul C. W. Davies. Scalar particle production in Schwarzchild and Rindler metrics. *J. Phys. A: Math. Gen.*, 8(4):609–616, April 1975. (Cited on pages 2, 9, and 20.)

[11] William G. Unruh. Notes on black-hole evaporation. *Phys. Rev. D.*, 14(4):870–892, August 1976. (Cited on pages 2, 9, 20, and 77.)

[12] Muxin Han, Jay S. Olson, and Jonathan P. Dowling. Generating entangled photons from the vacuum by accelerated measurements: Quantum-information theory and the Unruh-Davies effect. *Phys. Rev. A*, 78(2):022302, August 2008, arXiv:0705.1350 [quant-ph]. (Cited on pages 2, 19, and 20.)

[13] Shih-Yuin Lin, Chung-Hsien Chou, and Bei-Lok Hu. Disentanglement of two harmonic oscillators in relativistic motion. arXiv:0803.3995 [gr-qc], May 2008. (Cited on pages 2, 16, 29, 37, 43, 45, 52, and 54.)

[14] Nicholas David Birrell and Paul C. W. Davies. *Quantum Fields In Curved Space*. Cambridge monographs on mathematical physics. Cambridge University Press, Cambridge, 1982. (Cited on pages 3, 8, and 10.)

[15] Stephen A. Fulling. Nonuniqueness of canonical field quantization in Riemannian space-time. *Phys. Rev. D.*, 7(10):2850–2862, May 1973. (Cited on pages 8, 20, and 22.)

[16] Luís C. B. Crispino, Atsushi Higuchi, and George E. A. Matsas. The Unruh effect and its applications. *Rev. Mod. Phys.*, 80(3):787–838, July 2008, arXiv:0710.5373 [gr-qc]. (Cited on page 9.)

[17] Bryce S. DeWitt. Quantum gravity: the new synthesis. In Stephen W. Hawking and Werner Israel, editors, *General relativity: an Einstein centenary survey*, pages 680–745. Cambridge University Press, Cambridge, 1979. (Cited on pages 9 and 77.)

[18] Michael E. Peskin and Daniel V. Schroeder. *An Introduction to Quantum Field Theory*. Addison-Wesley, Reading, Massachusetts, 1995. (Cited on page 11.)

[19] R. Simon. Peres-Horodecki separability criterion for continuous variable systems. *Phys. Rev. Lett.*, 84(12):2726–2729, March 2000, arXiv:quant-ph/9909044. (Cited on page 16.)

[20] Asher Peres. Separability criterion for density matrices. *Phys. Rev. Lett.*, 77(8):1413, August 1996, arXiv:quant-ph/9604005. (Cited on page 16.)

[21] Michał Horodecki, Paweł Horodecki, and Ryszard Horodecki. Separability of mixed states: necessary and sufficient conditions. *Phys. Lett. A*, 223(1–2):1–8, November 1996, arXiv:quant-ph/9605038. (Cited on page 16.)

[22] Guifre Vidal and Reinhard F. Werner. Computable measure of entanglement. *Phys. Rev. A*, 65(3):032314, March 2002, arXiv:quant-ph/0102117. (Cited on page 16.)

[23] Martin B. Plenio. Logarithmic negativity: A full entanglement monotone that is not convex. *Phys. Rev. Lett.*, 95(9):090503, August 2005, arXiv:quant-ph/0505071. (Cited on page 16.)

[24] Asher Peres and Daniel R. Terno. Quantum information and relativity theory. *Rev. Mod. Phys.*, 76(1):93–123, January 2004, arXiv:quant-ph/0212023. (Cited on page 17.)

[25] Asher Peres, Petra F. Scudo, and Daniel R. Terno. Quantum entropy and special relativity. *Phys. Rev. Lett.*, 88(23):230402, June 2002, arXiv:quant-ph/0203033. (Cited on page 17.)

[26] Marek Czachor. Comment on "Quantum entropy and special relativity". *Phys. Rev. Lett.*, 94(7):078901, February 2005, arXiv:quant-ph/0312040. (Cited on page 17.)

[27] Asher Peres, Petra F. Scudo, and Daniel R. Terno. Reply to "Comment on 'Quantum entropy and special relativity' ". *Phys. Rev. Lett.*, 94(7):078902, February 2005. (Cited on page 17.)

[28] Robert M. Gingrich and Christoph Adami. Quantum entanglement of moving bodies. *Phys. Rev. Lett.*, 89(27):270402, December 2002, arXiv:quant-ph/0205179. (Cited on page 17.)

[29] Robert M. Gingrich, Attila J. Bergou, and Christoph Adami. Entangled light in moving frames. *Phys. Rev. A*, 68(4):042102, October 2003, arXiv:quant-ph/0302095. (Cited on page 17.)

[30] Paul. M. Alsing and Gerard J. Milburn. Lorentz invariance of entanglement. *Quant. Inf. Comput.*, 2(6):487–512, October 2002, arXiv:quant-ph/0203051. (Cited on page 17.)

[31] Ralf Schützhold and William G. Unruh. Comment on "Teleportation with a uniformly accelerated partner". arXiv:quant-ph/0506028, June 2005. (Cited on page 17.)

[32] Gerardo Adesso, Ivette Fuentes-Schuller, and Marie Ericsson. Continuous-variable entanglement sharing in noninertial frames. *Phys. Rev. A*, 76(6):062112, December 2007, arXiv:quant-ph/0701074. (Cited on page 18.)

[33] Ting Yu and J. H. Eberly. Finite-time disentanglement via spontaneous emission. *Phys. Rev. Lett.*, 93(14):140404, October 2004, arXiv:quant-ph/0404161. (Cited on page 18.)

[34] Benni Reznik. Entanglement from the vacuum. *Found. Phys.*, 33(1):167–176, January 2003, arXiv:quant-ph/0212044. (Cited on pages 18 and 56.)

[35] Jonathan Silman and Benni Reznik. Long-range entanglement in the Dirac vacuum. *Phys. Rev. A*, 75(5):052307, May 2007, arXiv:quant-ph/0609212. (Cited on pages 18 and 56.)

[36] S. J. van Enk and Terry Rudolph. Quantum communication protocols using the vacuum. *Quant. Inf. Comput.*, 3(5):423–430, September 2003, arXiv:quant-ph/0302091. (Cited on page 18.)

[37] Ralf Schützhold, Gernot Schaller, and Dietrich Habs. Tabletop creation of entangled multi-keV photon pairs via the Unruh effect. *Phys. Rev. Lett.*, 100(9):091301, March 2008, arXiv:0705.4385 [quant-ph]. (Cited on page 19.)

[38] D. F. Walls and Gerard J. Milburn. *Quantum Optics*. Springer-Verlag, New York, 1994. (Cited on page 23.)

[39] Shih-Yuin Lin and Bei-Lok Hu. Backreaction and the Unruh effect: New insights from exact solutions of uniformly accelerated detectors. *Phys. Rev. D.*, 76(6):064008, September 2007, arXiv:gr-qc/0611062. (Cited on page 41.)

[40] John L. Ball, Ivette Fuentes-Schuller, and Frederic P. Schuller. Entanglement in an expanding spacetime. *Phys. Lett. A*, 359(6):550–554, December 2006, arXiv:quant-ph/0506113. (Cited on page 67.)

[41] W. Rindler. Kruskal space and the uniformly accelerated frame. *Am. J. Phys.*, 34(12):1174–1178, December 1966. (Cited on page 70.)

[42] E. G. Kalnins. On the separation of variables for the Laplace equation $\Delta\psi + K^2\psi = 0$ in two- and three-dimensional Minkowski space. *SIAM J. Math. Anal.*, 6(2):340–374, April 1975. (Cited on page 74.)

[43] Isaias Costa. Separable coordinates and particle creation I: the Klein-Gordon equation. *Rev. Bras. Fis.*, 17(4):585–600, 1987. (Cited on pages 74 and 76.)

[44] Isaias Costa. Separable coordinates and particle creation. II: Two new vacua related to accelerating observers. *J. Math. Phys.*, 30(4):888–891, April 1989. (Cited on pages 74 and 75.)

[45] Isaias Costa and N. F. Svaiter. Separable coordinates and particle creation III: Accelerating, Rindler, and Milne vacua. *Rev. Bras. Fis.*, 19(2):271–280, 1989. (Cited on page 74.)

[46] Umberto Percoco and Victor M. Villalba. Particle creation in an asymptotically uniformly accelerated frame. *Class. Quantum Grav.*, 9(1):307–316, January 1992. (Cited on page 75.)

[47] Victor M. Villalba and Juan Mateu. Vacuum effects in an asymptotically uniformly accelerated frame with a constant magnetic field. *Phys. Rev. D.*, 61(2):025007, December 1999, arXiv:hep-th/9910072. (Cited on page 75.)

[48] Shih-Yuin Lin and Bei-Lok Hu. Accelerated detector-quantum field correlations: From vacuum fluctuations to radiation flux. *Phys. Rev. D.*, 73(12):124018, June 2006, arXiv:gr-qc/0507054. (Cited on page 77.)

[49] Philip R. Johnson and Bei-Lok Hu. Stochastic theory of relativistic particles moving in a quantum field: Scalar Abraham-Lorentz-Dirac-Langevin equation, radiation reaction, and vacuum fluctuations. *Phys. Rev. D.*, 65(6):065015, March 2002, arXiv:quant-ph/0101001. (Cited on page 83.)

[50] Chad R. Galley, Bei-Lok Hu, and Shih-Yuin Lin. Electromagnetic and gravitational self-force on a relativistic particle from quantum fields in curved space. *Phys. Rev. D.*, 74(2):024017, July 2006, arXiv:gr-qc/0603099. (Cited on page 83.)

[51] William H. Press, Saul A. Teukolsky, William T. Vetterling, and Brian P. Flannery. *Numerical Recipes in C: The Art of Scientific Computing*. Cambridge University Press, Cambridge, second edition, 1992. (Cited on pages 87 and 88.)